CANADIAN THESES

THÈSES CANADIENNES

NOTICE

The quality of this microfiche is heavily dependent upon the quality of the original thesis submitted for microfilming. Every effort has been made to ensure the highest quality of reproduction possible.

If pages are missing, contact the university which granted the degree.

Some pages may have indistinct print especially if the original pages were typed with a poor typewriter ribbon or if the university sent us an inferior photocopy.

Previously copyrighted materials (journal articles, published tests, etc.) are not filmed.

Reproduction in full or in part of this film is governed by the Canadian Copyright Act, R.S.C. 1970, c. C-30.

AVIS

La qualité de cette microfiche dépend grandement de la qualité de la thèse soumise au microfilmage. Nous avons tout fait pour assurer une qualité supérieure de reproduction.

S'il manque des pages, veuillez communiquer avec l'université qui a conféré le grade.

La qualité d'impression de certaines pages peut laisser à désirer, surtout si les pages originales ont été dactylographiées à l'aide d'un ruban usé ou si l'université nous a fait parvenir une photocopie de qualité inférieure.

Les documents qui font déjà l'objet d'un droit d'auteur (articles de revue, examens publiés, etc.) ne sont pas microfilmés.

La reproduction, même partielle, de ce microfilm est soumise à la Loi canadienne sur le droit d'auteur, SRC 1970, c. C-30.

THIS DISSERTATION
HAS BEEN MICROFILMED
EXACTLY AS RECEIVED

LA THÈSE A ÉTÉ
MICROFILMÉE TELLE QUE
NOUS L'AVONS REÇUE

Experimental Determination of Residual Stresses in Filament Wound Composite Rings

by

CHRIS J. ALEONG

A thesis
presented to the University of Ottawa
in fulfillment of the
thesis requirement for the degree of
Master of Applied Science
in
Mechanical Engineering

ISBN 0-315-33268-9

UNIVERSITÉ D'OTTAWA
UNIVERSITY OF OTTAWA

ABSTRACT

Composite rings ranging from 26 cm. to 44 cm. outer diameter were manufactured by combining S2-glass, E/XAS carbon and Kevlar 49 fibres with an elevated cure resin system in a filament winding process. These rings were to be utilized in high speed composite flywheels for which the radial stresses were of extreme importance. Experimental determination of the residual stresses, with emphasis on the radial component, were carried out on thin, radially thick and axially/radially thick composite rings employing the 'radial cut with strain gauge' method. For radially thick S2-glass and E/XAS carbon composite rings the manufacturing variables of cure schedule, winding tension and radial thickness were investigated. It was found that in the radially thick composite rings, an increasing winding tension decreased the residual stresses. With E/XAS carbon composite rings the cure schedule affected the residual stress and with both fibre types an increasing radial thickness produced increased residual stresses. For the E/XAS carbon composite rings, in particular, the radial residual stress showed a linear profile with respect to the radial thickness of the composite rings with the same inner diameters.

ACKNOWLEDGMENT

The author would like to express his sincere gratitude and appreciation to Dr. Michael Munro for his invaluable guidance, encouragement and advice throughout the course of this work.

Also, the author wishes to thank the staff of the Department of Mechanical Engineering Machine Shop for the substantial contribution to this project.

In addition, he wishes to thank the National Research Council of Canada for their financial support under contracts OSU80-00043, OSU82-0042 OST84-00459 and the Natural Sciences and Engineering Research Council under grant A1663. The teaching assistantships from the Department of Mechanical Engineering, University of Ottawa is also gratefully acknowledged.

The author also wishes to thank the other members of the University of Ottawa Flywheel Team for their help and support in this work.

And finally, last but not least, the author would like to specially thank his wife, Rosanne, for her unending understanding, support and encouragement throughout the course of this work.

TABLE OF CONTENTS

Abstract ii

Acknowledgment iii

Nomenclature vii

List of Figures ix

List of Tables xiii

Chapter I: Composite Flywheel Program 1

1.1 Introduction 1
1.2 Problem definition 5

Chapter II: Experimental methods of residual stress measurement 8

2.1 Introduction 8
2.2 Residual stresses in composites 9
2.2.1 Residual stress determination by radial cut with dimensional measurement 9
2.2.2 Residual stress determination by radial cut with circumferential strain gauges 14
2.2.3 Residual stress determination by icremental machining 20
2.2.4 Residual stress determination by orthotropic photoelastic analysis 25
2.3 Theoretical evaluation of factors affecting residual stress 27

Chapter III: Filament winding of fibre composite rings 33

3.1 Introduction 33
3.2 Filament winding materials 34
3.2.1 Fibres 34
3.2.2 Resin system 35
3.3 Filament winding equipment and the winding process 36
3.3.1 Mandrels 36
3.3.2 Filament winder 38
3.3.2.1 Fibre delivery 39

3.3.2.2 Resin bath. 40
3.3.2.3 Tensioning of the rovings 43
3.3.2.4 Filament winder modifications and control. 45
3.3.3 Curing of the manufactured rings. 51

Chapter IV: Residual stress measurement in fibre composite rings. 54

4.1 Introduction. 54
4.2 Strain measurement on composite materials. 54
4.2.1 Errors due to strain gauge misalignment . . . 55
4.2.2 Errors due to transverse sensitivity in strain gauges. 56
4.3 Residual stress measurement in thin rings. 58
4.3.1 Residual stress measurement in thin rings by dimensional change. 58
4.3.2 Residual stress measurement in thin rings with strain gauges. 64
4.3.3 Evaluation of factors affecting residual stress 68
4.3.3.1 Introduction. 68
4.3.3.2 Ring thermal expansion coefficients . . 68
4.3.3.3 Thermal residual stresses 74
4.3.3.4 Residual stress due to winding tension. 75
4.3.3.5 Total experimental residual stress. . . 76
4.3.3.6 Residual stress due to resin shrinkage and resin flow/fibre migration 78
4.4 Residual stress measurement in thick composite rings. 88
4.4.1 Residual strain measurement in radially thick composite rings. 88
4.4.2 Theoretical determination of transverse sensitivity on radially thick composite rings 102
4.4.3 Comparison of experimental and predicted radial residual strains. 105
4.4.4 Residual strain measurement in axially/radially thick rings 110
4.4.5 Radial residual stress versus radial thickness. 115

Chapter V: Discussion 118

5.1 Introduction. 118
5.2 Experimental techniques 118
5.3 Experimental verification 126
5.4 Effect of variables on the residual stress. . 129

Chapter VI: Conclusions and Recommendations. 140

Bibliography 143

Appendix A: Filament winding program for thick ring winding 150

Appendix B: Data program for filament winder program 153

Appendix C: Determination of fibre volume fraction in filament wound fibre composite rings . . . 155

Appendix D: Figures for thermal expansion coefficient determination. 158

Appendix E: Listing of computer program 'THEMOCOE' . . 169

Appendix F: Listing of computer program 'THEMOSUP' . . 173

Appendix G: Listing of computer program 'FTENSION' . . 177

Appendix H: Listing of computer program 'OVERLAP'. . . 186

Appendix I: Transverse sensitivity calculations. . . . 189

F.1 Radially thick S2-glass and E/XAS carbon composite rings 189
F.2 S2-glass-E/XAS carbon biannular composite ring. . 190

NOMENCLATURE

a, R_i - inside radius of composite ring

b, R_o - outside radius of composite ring

c - radius ratio of a ring, a/b

D_B, D_A - inner diameter before and after radial cut

$E_{\theta\theta}, E_\theta$ - Young's Modulus in the circumferential direction

E_r - Young's Modulus in the radial direction

E_f - Young's Modulus of E-Glass fibre

E_m - Young's Modulus of mandrel

k - spring back factor, (R_o/R_f)

K - Modulus ratio, $\sqrt{E_\theta/E_r}$

K' - filament to mandrel stiffness ratio, $(E_f t_f/E_m t_m)$

n - number of hoop layers

P_a, P_b - internal, external pressure on a single ring

r - radial position

R_f - final radius of composite after cut

R - mean radius, $(a+b)/2$

r_m, R_m - mean radius of E-Glass fibres

R^* - location of neutral surface

t - ring thickness

t_f - E-Glass composite thickness

t_m - mandrel thickness

T - change of temperature

T' - winding tension per unit width of fibre

$T(r)$ - winding tension function

V_f - fibre volume fraction

V_v - void volume fraction

V_{fA} - apparent fibre volume fraction

V_{fD} - volume fraction from matrix dissolution method

V_{fR} - real fibre volume fraction

W_f - weight fraction of fibre

W_m - weight fraction of matrix

z - overlap of transversely sectioned ring

α_θ, α_r - thermal coefficients of expansion in the circumferential, radial directions

$\epsilon_\theta, \epsilon_r$ - strains in the circumferential, radial direction

$\epsilon_{\theta_I}, \epsilon_{\theta_O}$ - circumferential strains on the inside and outside surface

ν_c - Poisson's ratio of composite

ν_θ, ν_r - Poisson's ratios in the circumferential, radial directions

ρ_c - calculated density from matrix dissolution method

ρ_f - fibre density

ρ_m - matrix density

ρ_M - measured density of composite

σ_o - residual stress, outer surface

σ_i - residual stress, inner surface

σ_θ, σ_r - stresses in the circumferential, radial directions

$\sigma_{\theta R}, \sigma_{rR}$ - residual stresses in the circumferential, radial directions

$\sigma_{\theta T}, \sigma_{rT}$ - thermal residual stresses in the circumferential, radial directions

LIST OF FIGURES

1.1 Flywheel design number 1 3

1.2 Flywheel design number 2 3

1.3 Flywheel design number 3 4

1.4 Flywheel design number 4 4

2.1 Glass fibre ring 10

2.2 Location of strain gauges on Fourney's rings . . . 16

2.3 Incremental machining residual stress analysis model 24

3.1 S2-glass, E/XAS carbon and Kevlar 49 fibre spools 35

3.2 Steel mandrels used in producing the composite rings 37

3.3 Original metal lathe used to wind thin rings . . . 38

3.4 Modified lathe used to manufacture full scale rings 39

3.5 Spool holders shown with E/XAS carbon mounted . . 40

3.6 Epoxy resin temperature controlled water bath . . . 41

3.7 Finger arrangement used to spread fibres in resin bath 42

3.8 Assembly showing rubber squeezers removing excess resin 42

3.9 Tensioning system 44

3.10 Magnetic brake monitor/controller 45

3.11 Aluminum channel with resin bath and tensioning device 46

3.12 Control cabinet for filament winder 49

3.13 Axially/radially thick ring being manufactured . . 50

3.14 Fume hood over winding area 51

3.15 Gruenberg Electric Company oven used in curing the composite rings 52

4.1 Percentage error due to gauge misalignment[23] . . 56

4.2 Water cooled diamond saw used to cut thin rings. 60

4.3 Average circumferential residual stress in thin E-glass rings. 63

4.4 Springs used to position pads on mandrel. 66

4.5 Locations of measurements on pad area. 66

4.6 Pads used to produce a smooth outer surface . . . 67

4.7 Side view of the thin rings 67

4.8 Typical moulded surface with strain gauge attached. 70

4.9 Strain indicator with switch and balance unit. . . 70

4.10 Circumferential residual stress components as a function of winding tension 82

4.11 Circumferential residual stress components as a function of winding tension 83

4.12 Circumferential residual stress components as a function of winding tension 84

4.13 Radial residual stress components as a function of winding tension 85

4.14 Radial residual stress components as a function of winding tension 86

4.15 Radial residual stress components as a function of winding tension 87

4.16 Circumferential residual stress as a function of ring thickness & constant winding tension. . 92

4.17 Radial residual stress as a function of ring thickness and constant winding tension. 93

4.18 Circumferential residual stress as a function of ring thickness & variable winding tension. . 94

4.19 Radial residual stress as a function of ring thickness and variable winding tension. 95

4.20 Circumferential residual stress as a function of ring thickness & constant winding tension. . 96

4.21 Radial residual stress as a function of ring thickness and constant winding tension. 97

4.22 Circumferential residual stress as a function of ring thickness and cure schedule 98

4.23 Radial residual stress as a function of ring thickness and cure schedule 99

4.24 Circumferential residual stress as a function of ring thickness & constant winding tension. 100

4.25 Radial residual stress as a function of ring thickness and constant winding tension. . . . 101

4.26 Typical circumferential strain profile generated by computer. 103

4.27 Typical radial strain profile generated by computer. 104

4.28 Typical gauge attachment on the radially thick composite rings. 105

4.29 Strain profile generated by the computer 107

4.30 Comparison of predicted and experimental residual strains 109

4.31 Axially radially thick ring (XAS-ATK-1-25) with gauges mounted. 111

4.32 Ring XAS-ATK-3-25 with gauges mounted. 113

4.33 Comparison of predicted and experimental residual strains 114

4.34 Radial residual stress as a function of ring thickness 116

4.35 Overlap produced as a function of ring thickness. 117

5.1 Comparison of methods to determine radial residual stress 122

5.2 Comparison of methods to determine radial residual stress 125

D.1 Thermal strain as a function of temperature change 159

D.2 Thermal strain as a function of temperature change 160

D.3 Thermal strain as a function of temperature change 161

D.4 Thermal strain as a function of temperature change 162

D.5 Thermal strain as a function of temperature change 163

D.6 Thermal strain as a function of temperature change 164

D.7 Thermal strain as a function of temperature change 165

D.8 Thermal strain as a function of temperature change 166

D.9 Thermal strain as a function of temperature change 167

D.10 Thermal strain as a function of temperature change 168

I.1 Location and orientaion of rosette gauges. . . . 190

LIST OF TABLES

1.1 Typical Circumferential and Radial Strengths for Fibre Composites. 6

1.2 Typical Maximum Stresses at Operating Speed. . . . 6

2.1 Experimental and Theoretical Strains [7]. 16

2.2 Dewey and Knight's Experimental and Theoretical Strains [8]. 17

4.1 Winding Tension Parameters for E-glass Rings. . . 59

4.2 Average Circumferential Residual Stress Results for Thin S2-glass Composite Rings. . . 62

4.3 Thermal Expansion Coefficients for Thin Composite Rings. 73

4.4 Total (Experimental) Residual Stresses in Thin Composite Rings. 77

4.5 Residual Stresses in Thin E/XAS Carbon Composite Rings. 79

4.6 Residual Stresses in Thin S2-glass Composite Rings. 80

4.7 Residual Stresses in Thin Kevlar 49 Composite Rings. 81

4.8 Manufacturing Parameters for Radially Thick Rings. 89

4.9 Data Used for 'OVERLAP' Program. 91

4.10 Transverse Sensitivity Effects on S2-glass and E/XAS Carbon Composite Rings. 102

4.11 Comparison of Predicted and Experimental Residual Transverse Strains in Radially Thick Composite Rings. 108

4.12 Dimensions for Axially/Radially Thick Rings. . . 110

4.13 Strain Readings for Ring XAS-ATK-1-25. 111

4.14 Strain Readings for Ring XAS-ATK-3-25. 112

4.15 Residual Strain Profile from Transverse Gauges. 113

4.16 Radial Residual Stress in E/XAS Carbon Rings as a Function of Radial Thickness. 115

5.1 Radial Residual Stress Comparison for Thick Composite Rings. 124

5.2 Comparison of Predicted and Experimental Strains. 127

5.3 E/XAS Carbon Composite Radially Thick Ring Transverse Tensile Test Results. 136

5.4 Dimensions and Radial Residual Stress Comparisons for E/XAS Carbon Composite Rings. 138

C.1 Variables Used in Volume Fraction Equations. . . 156

I.1 Inputs for Transverse Sensitivity Equations. . . 189

I.2 Strain Readings from Biannular Ring. 191

Chapter I

COMPOSITE FLYWHEEL PROGRAM.

1.1 Introduction.

In 1979, a research team at the Department of Mechanical Engineering, University of Ottawa, undertook a study of fibre composite flywheels. A project was initially carried out to appraise the latest flywheel technology available as well as to provide recommendations for an R & D program [1].

Decision analysis techniques were extensively used throughout the appraisal. In fact, a series of twenty flywheel design concepts were identified and assessed relative to each other [1]. These concepts were then set against fourteen impact parameters; namely, integrity, ease of containment, rigidity, radial compatability, material costs, manufacturing costs, assembly costs, industrial implementation, quality control, inspection, state-of-the art, technology level required, and technical risk. From those designs, three were selected, namely: Single Material Multi- Ring-on-Ring, Multi-Material Multi-Ring with Overwrap or Bandwrap and Multi-Material Multi-Ring-on-Ring [1]. For the ring type flywheels selected, nine hub designs were identified and similar to the flywheel design concepts, decision analysis ratings were utilized. The outcome of

those ratings indicated that a manufactured metallic (aluminum) hub appeared to be the most suitable with composite material equivalent hubs also appearing attractive. However, after extensive material and dynamic testing on both the rings and hub components from 1981 to 1984, final designs were realized. Four different designs were to be considered for full-size flywheels:

1. E/XAS carbon single ring with sheet moulding compound (SMC) hub with metallic shaft attachment (Figure 1.1).
2. E/XAS carbon single ring with S2-glass laminate hub with metallic shaft attachment (Figure 1.2).
3. S2-glass-E/XAS carbon biannular ring with aluminum hub (Figure 1.3).
4. S2-glass-E/XAS carbon biannular ring with metallic spoke hub (Figure 1.4).

In terms of dimensions, all the above flywheels had outer diameters of 60.96 cm with the first two flywheel designs having axial thicknesses of 7.62 cm and 6.35 cm, respectively. The two biannular flywheels both have axial thicknesses of 8.89 cm.

Due to the large size of the composite rings for the flywheels, much preliminary work was necessary since no one had previously manufactured such large components. Initially, small rings, on the order of 26.0 cm inner diameter, 2.54 cm width and 0.6 cm thickness were manufactured. Larger rings were subsequently wound with the

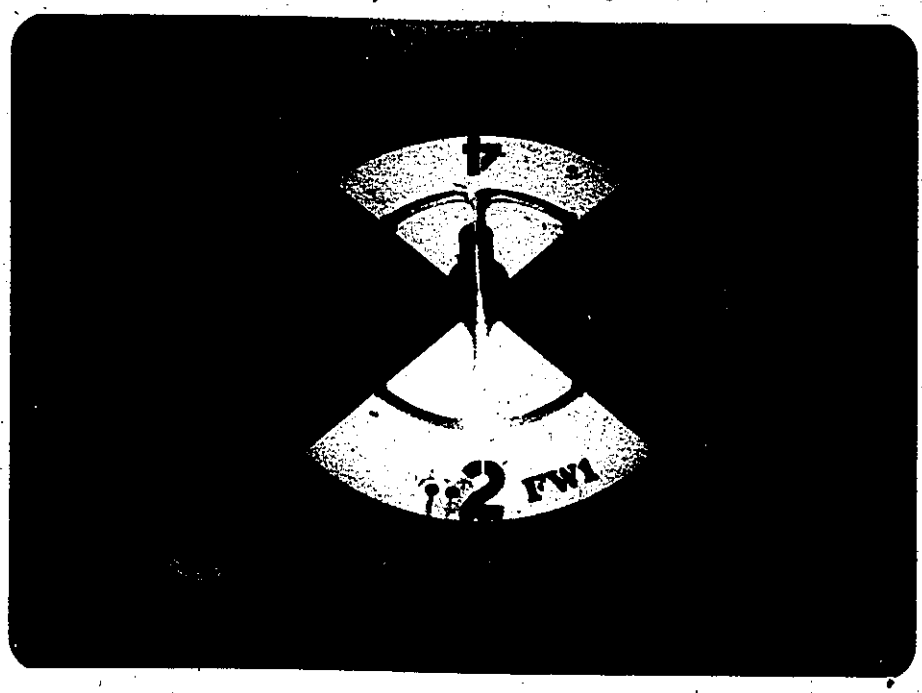

Figure 1.1: Flywheel design number 1. E/XAS carbon outer ring, SMC hub and aluminum attachment.

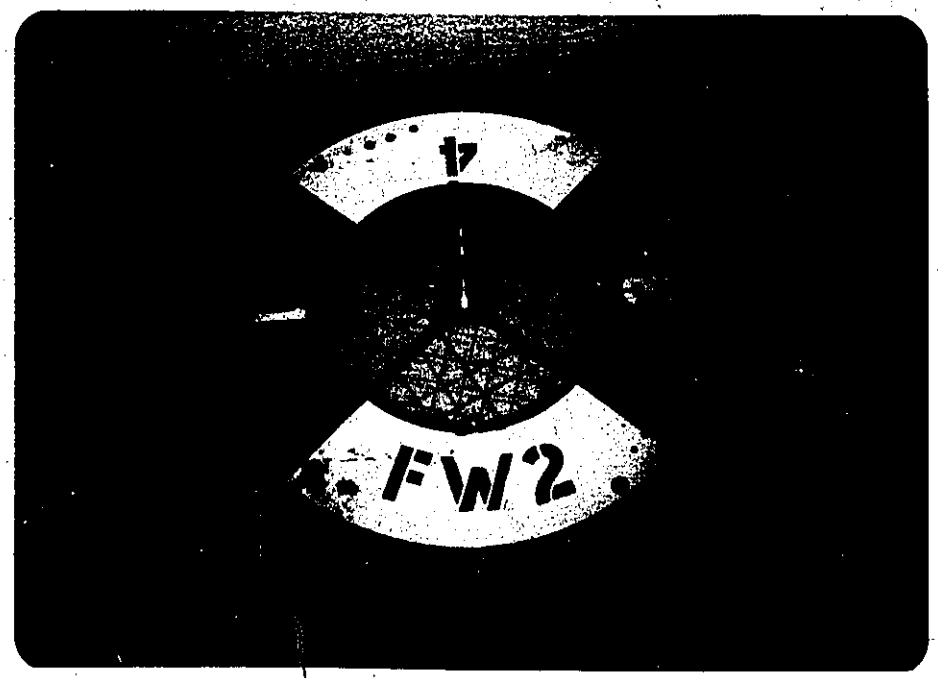

Figure 1.2: Flywheel design number 2.. E/XAS carbon outer ring, S2-glass laminate hub and steel attachment.

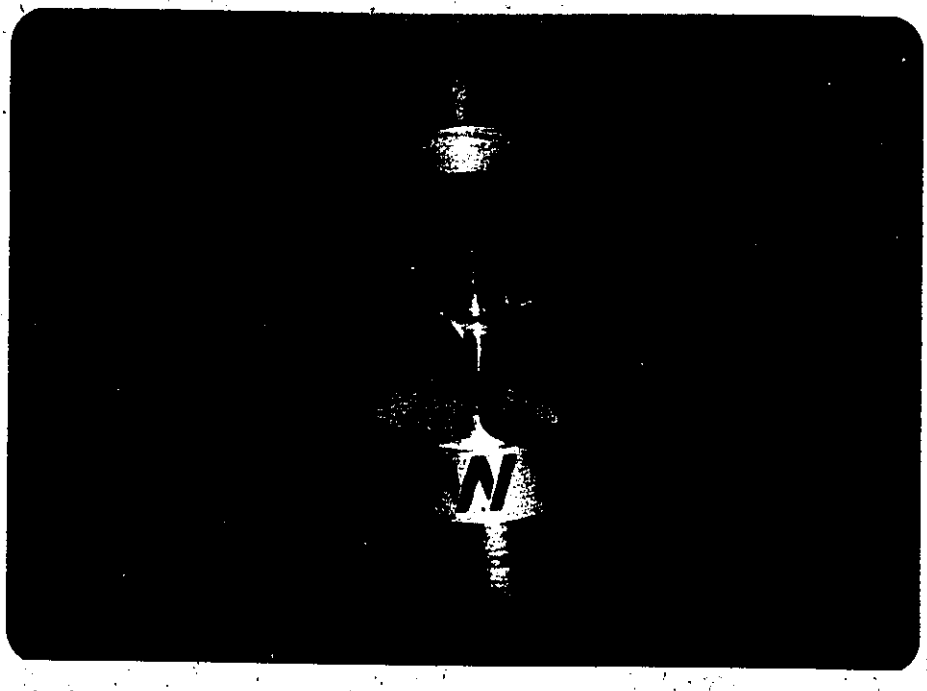

Figure 1.3: Flywheel design number 3. E/XAS carbon outer ring, S2-glass inner ring and aluminum hub.

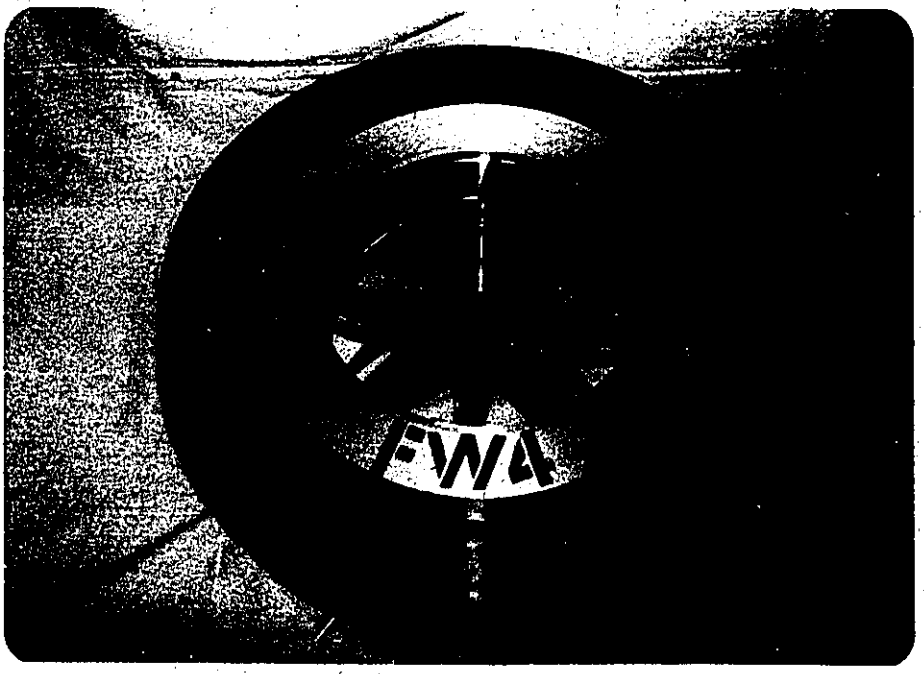

Figure 1.4: Flywheel design number 4. E/XAS carbon outer ring, S2-glass inner ring, aluminum insert and steel spring spoke hub.

same inner diameter and width but with an axial thickness of approximately 5 cm. The major manufacturing concern with increasing the radial thickness was the problem of fibre buckling during filament winding. From the results with the radially thick rings (2.54 cm wide X 5 cm thick), full scale ring winding was deemed possible. The full scale rings, mentioned above, were manufactured and destructively tested in order to verify strength and integrity of these components and evaluate residual stresses. Details of these investigations are to be found in Chapters 3 and 4 of this thesis.

1.2 Problem definition.

The design of a flywheel for high speed applications necessarily involves many engineering aspects. For a fibre composite flywheel, not only are centrifugal stresses developed during spinning but interfacial pressures are produced during assembly and locked-in stresses occur due to the materials used and method of manufacture [2].

For the University of Ottawa Flywheel Program, the ring components of the fibre composite flywheels were fabricated by wet filament winding with the fibres under tension. This tension becomes locked-in after the structure has fully cured and along with the chemical setting and thermal curing of the matrix produce part of the residual stresses. These residual stresses occur both in the circumferential as well

as the radial directions. In thick rim flywheels, the circumferential residual stress can be the cause of outer layer failure [2], however, not to be forgotten and of equal importance is the radial component. Generally, uni-directional fibre composites have high longitudinal (circumferential) strengths but very low transverse (radial) strengths (Table 1.1).

Table 1.1: Typical Circumferential and Radial Strengths for Fibre Composites.

Fibre Type	Radial Strength* (MPa.)	Circumferential Strength* (MPa.)
S2-glass	34.7	1900
E/XAS carbon	35.5	1700
Kevlar 49	8.8	1658
* - in-house experiments on filament wound rings.		

The radial residual stress is tensile in nature and is superimposed onto the radial tensile stress due to centrifugal loading [3]. Table 1.2 shows some typical values for flywheel design number [illegible] (Figure 1.2 on page 3).

Table 1.2: Typical Maximum Stresses at Operating Speed.

Direction	Stress		Percentage Residual/Total
	Residual (MPa.)	Total (MPa.)	
Circumferential	89	565	16
Radial	7	19	37

The figures show that the radial residual component is a larger percentage of the total radial stress as compared to that for the circumferential case.

In order to gain some insight into these residual stresses, a portion of the overall Flywheel Program was initiated to look specifically at these stresses and by so doing forestall any unforeseen problems at a later date. The available literature was reviewed in order to determine what had been done by others in the composite flywheel field. From such an approach an appropriate method was utilized in experimentally determining the magnitudes of the residual stresses in the composite rings. The literature review also indicated what manufacturing variables were responsible for the residual stresses. Furthermore, the results were correlated with the theoretical predictions, developed by the designer in the program, J. Wong, for the composite rings. This ensured that the final set of designs would encompass all factors necessary for safe operation of the full scale flywheels.

Chapter II

EXPERIMENTAL METHODS OF RESIDUAL STRESS MEASUREMENT.

2.1 Introduction

The procedure of determining the state of stress at a point, by means of experimentally acquired quantities, is referred to as experimental stress analysis. However, experimental stress analysis almost never involves the measurement of stress, per se. Instead, it involves the measurement of some quantity which in turn can be related to stress. This is accomplished by the use of computations based on theory with strain being the quantity most often measured. The stress analysis involves experimentally determining the state of strain at a point and deducing the state of stress at the same point.

A fibre composite component experiences stresses due to the loading but, in most cases, prior to this load being applied, there exist in the structure locked in stresses due in part to the manufacturing process. Since the fibres are embedded in a matrix, tension on the strand, thermal cooldown and resin cure shrinkage introduce stresses which are retained when the whole structure is fully cured. These stresses are commonly known as residual stresses. In this

chapter, various experimental methods of determining these stresses will be examined and discussed. In addition, the literature on the theoretical evaluation of factors affecting residual stress in fibre composite rings is reviewed.

2.2 Residual stresses in composites.

2.2.1 Residual stress determination by radial cut with dimensional measurement.

The earliest tests, to determine residual stresses in filament wound materials, were performed in 1963 by S.P. Prosen et al [4], at the U.S. Naval Ordnance Laboratory (NOL). They were concerned with the magnitude of the locked-in stresses in their filament wound glass fibre rings brought about during winding and cure. The residual stress measurements were only a part of their overall test program as they also looked at compressive and fatigue properties of the rings.

The manufacture of their rings was carried out by pulling the resin-impregnated strands of glass fibres under tension onto a rotating mandrel until the desired thickness was achieved. They suggested that as the thickness of the ring built up, the strands compacted and resin was displaced or squeezed out. This compaction or migration of the strands was thought to change the tension in the fibres during the winding process. Additional fibre migration was believed to

occur during the curing of the ring. When the curing was complete, the stresses due to these changes were "locked-in" inside the ring. The cured ring was then removed from the mandrel and cut radially.

It was found experimentally that the ends sprung together thus relieving the "locked-in" stresses as shown in Figure 2.1.

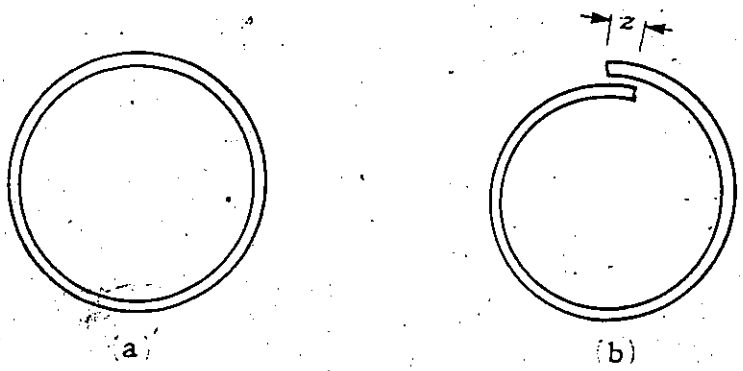

Figure 2.1: Glass fibre ring. a)before radial cut, b)after radial cut, z = overlap.

The researchers developed an equation from thin ring theory, for a unidirectional composite material, which calculated the circumferential residual stress in terms of the ring overlap, thickness and radial dimension as:

$$\sigma_\theta = \frac{Ezt}{4\pi r^2} \tag{2.1}$$

These researchers manufactured a series of rings approximately 15 cm inner diameter and 0.305 cm thick. From each ring a 2.54 cm length was cut from the circumference.

Each ring demonstrated the "closing mode" (i.e. the ends overlaped when cut) and the distance z that the ends overlaped was measured. The circumferential residual stress results showed considerable variation having a mean value of 12.05 MPa. with a standard deviation of 3.29 MPa.

They postulated that the stresses obtained represented the net stress of the many stress levels in the cross-section of the ring, i.e. an average value. They also stated that the technique is a tedious one, since for each measurement a ring has to be destructively tested. They recommended that an alternative technique be used such as photo-stress analysis. This other method is discussed in Section 2.2.4.

In 1980, R. Nimmer, K. Torossian and N. Wilkening [5], from General Electric, became aware of the presence of residual stresses in filament wound rings during sectioning of rings for test specimens. They observed that as the rings were cut they snapped closed on the blade.

As previously mentioned, Prosen and his associates basically used a dimensional change in terms of end overlap. Nimmer et al also used a dimensional measurement but in terms of the displacement necessary to restore the original uncut geometry of the ring. Starting with thin ring theory they developed the necessary equations resulting in an expression for the maximum residual circumferential stress at the inside diameter as:

$$\sigma_R = \frac{D_B - D_A}{4} \frac{Et}{R_m^2} \qquad (2.2)$$

Nimmer et al stated that this equation only gives a first approximation to the residual bending stresses in a ring.

Experimentally, they only performed measurements on two graphite epoxy rings. One ring (TS No.12) had a mean radius of 17.09 cm and an annular thickness, t, of 6.12 cm, while the other (TS No.25) had a mean radius of 20.47 cm and an annular thickness of 4.01 cm.

The circumferential residual stress results at the inside diameter were tensile in nature and yielded 72.56 MPa. and 54.0 MPa. for TS No.12 and TS No.25, respectively. Nimmer et al's investigation of the residual stress was due to their concern during centrifugal loading of the rings which produces a maximum stress at the inside diameter. They considered the residual stress significant enough to be used in future design analysis for General Electric's Flywheel Program.

In 1983, H.A. Al-Qureshi [6], at the Institute of Aeronautical Technology in Brazil, also used the diameter change method to measure the residual stress. He evaluated the residual stresses in pressure vessels by examining filament wound fiberglass rings. His rings were wound on a plaster mandrel of 29.97 cm outside diameter and an inside diameter of 12.19 cm. During the winding the Type "E" fibreglass, impregnated with an elevated temperature epoxy

resin, was tensioned using a brake arrangement with different cylinders being wound varying the number of layers from 2 to 18. The rings were cut from the central part of the cylinders to avoid tension changes and filament turn-around at the ends.

Al-Qureshi used what he calls the spring-back factor for which he reported the following equation :

$$k = \frac{R_o}{R_f} = 1 - \frac{2R_o T'(1-\nu_c^2)}{n.E_f.t_f^2}\left|1 - \frac{1}{n}\sum_{i-1}^{n}\frac{1}{1+(i-1)K'}\right| \qquad (2.3)$$

From his experiments all of the rings were observed to be of the "opening-mode" (i.e. ends spring apart when cut). The results showed that increasing the number of hoop layers increases the amount of the spring-back factor. This "opening-mode" was directly opposed to what was observed by Nimmer et al and Prosen et al with their rings, but, it must be remembered that they both used steel mandrels while Al-Qureshi used a plaster one. Al-Qureshi does mention, however, that the analysis is only good for the "opening-mode" type of results and not the "closing-mode". He also mentioned that the residual stresses on a filament wound structure cured on a mandrel does depend on the mandrel material. Al-Qureshi made no mention of the magnitude of the residual stresses, but, basically associated the spring-back factor to the residual stress

indicating that a reduced factor produces a reduced residual stress.

2.2.2 Residual stress determination by radial cut with circumferential strain gauges.

The previous section dealt with residual stress determination using dimensional measurement techniques. These were of limited scope and accuracy and as a means of improving the results researchers looked at other ways of determining the residual stress.

In 1968, W. L. Fourney [7] investigated the residual stress state in an axially symmetric filament wound orthropic ring. He developed the necessary elasticity equations in order to obtain an analytical prediction of the stresses in the rings and was able to define the residual stress at the outer surface as:

$$\sigma_o = C_1 - C_2 K R_o^{-(K+1)} + C_3 K R_o^{(K-1)} \tag{2.4}$$

and at the inner surface as:

$$\sigma_i = C_1 - C_2 K R_i^{-(K+1)} + C_3 K R_i^{(K-1)} \tag{2.5}$$

where,

$$C_1 = -\frac{C_3}{2}\left[\frac{(-R_o^{K-1} - R_i^{K-1})}{R_o^{-(K+1)} - R_i^{-(K+1)}}(R_o^{-(K+1)} + R_i^{-(K+1)}) + R_o^{(K-1)} + R_i^{(K-1)}\right]$$

and

$$C_2 = -\frac{R_o^{(K-1)} - R_i^{(K-1)}}{R_o^{-(K+1)} - R_i^{-(K+1)}} C_3$$

The variable C_3 was evaluated using equation 2.5 and the stress—strain relationship below:

$$\epsilon_r = \frac{\sigma_r}{E_r} - \nu\frac{\sigma_\theta}{E_\theta}; \quad \epsilon_\theta = \frac{\sigma_\theta}{E_\theta} - \nu\frac{\sigma_r}{E_r} \tag{2.6}$$

With the above equation the strain relief at the inner surface could be used as input for equation 2.5.

Experimentally, Fourney manufactured a series of rings using glass fibre pre-preg tape wound onto a mandrel under tension. After cure, the rings were instrumented with eight strain gauges as shown in Figure 2.2. The rings were then cut radially and the strain relief at the inner and outer surfaces measured when the ends deflected.

Fourney compared his experimental results with analytical predictions at the outer surface and obtained a difference ranging from 2.06 to 9.70% as shown in Table 2.1. It must be noted that he made no mention of the circumferential residual stress magnitude at the inner and outer surfaces, but only the strain magnitudes.

The following year, in 1969, B.R. Dewey and C.E. Knight, Jr. [8], developed an analysis for the state of residual strain in an axially symmetric multilayered filament wound ring. Their analysis assumes that the residual strain is

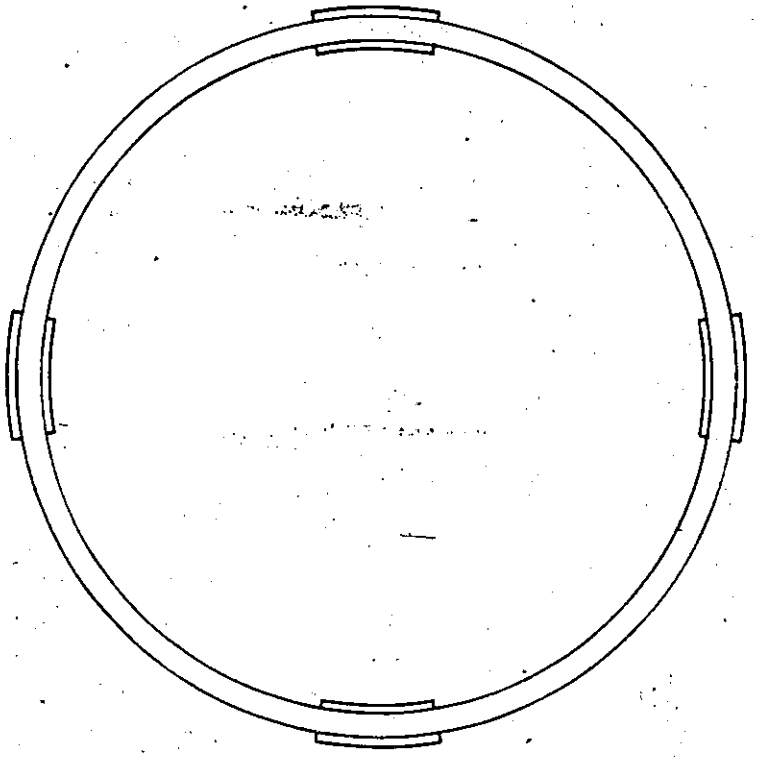

Figure 2.2: Location of strain gauges on Fourney's rings.

Table 2.1: Experimental and Theoretical Strains [7].

Inner Radius (in.)	Average Thickness (in.)	Average Exp. Strain Inner Surface ($x10^{-6}$)	Average Exp. Strain Outer Surface ($x10^{-6}$)	Theor. Strain Outer Surface ($x10^{-6}$)	Difference (%)
2.68	0.2372	180	-158	-170.0	7.31
2.65	0.1646	140	-146	-134.5	8.23
2.65	0.1837	128	-119	-122.6	2.98
2.65	0.2218	126	-108	-119.0	9.70
2.65	0.2210	152	-147	-144.0	2.06

equal to the strain produced by restoring a ring with a radial cut to its original state, by means of pure bending moments applied at the cut ends. They also take into account the variation of the circumferential modulus with

radial change. The equation they developed relies on the location of the neutral surface at radius R in conjunction with the strain released.

The equation was expressed as:

$$R^* = \frac{\sum_{j=1}^{n} E_j t_j}{\sum_{j=1}^{n} E_j log(b_j/a_j)} \tag{2.7}$$

where b_j and a_j are the outer and inner radii of layer j.

In order to verify their equations, six rings were manufactured with varied winding tensions. Strain gauges were mounted on the inner and outer surfaces in a similar fashion to Fourney (Figure 2.2 on page 16). Strain data was obtained from the strain gauges after radial cuts were made in the rings.

Dewey and Knight compared their experimental outer strain results with theoretical predictions in a similar manner to Fourney as shown in Table 2.2.

Table 2.2: Dewey and Knight's Experimental and Theoretical Strains [8].

Inner Radius (in.)	Average Thickness (in.)	Exp. Inner Strain ($x10^{-6}$)	Exp. Outer Strain ($x10^{-6}$)	Theor. Outer Strain ($x10^{-6}$)	Difference (%)
3.006	0.310	639	-570	-598.1	4.81
3.005	0.313	-478	413	447.4	7.99
3.005	0.313	-555	509	519.5	2.04
3.003	0.319	294	-287	-274.9	-4.31
3.005	0.308	410	-384	-384.2	0.05
3.004	0.315	723	-687	-676.5	-1.54

They commented that their results showed better correlation when the elastic modulus variation with thickness was considered, however, if Table 2.1 on page 16 is compared with Table 2.2 on page 17 the difference does not appear that significant. One must admit, though, some improvement was evident and they, like Fourney, made no mention of the residual stress in the rings.

In 1970, C.E. Knight Jr. [9], again used this 'radial-cut/strain gauge' method to determine the residual stress of filament wound rings. This time he used only two gauges mounted on each of the inner and outer surfaces of the ring located 180 degrees apart. The results obtained when the ring was cut were used as a comparison with two other methods he was experimenting with at the time, photoelastic analysis and incremental machining . The data produced only gave an inner surface stress magnitude and an outer surface value. No stress distribution across the ring profile was carried out but, he did state that the technique only gave an approximate distribution of the residual stresses in the ring.

In 1981, J. Wong [3], at the University of Ottawa, developed equations to determine the residual stresses in filament wound composite rings as part of the University of Ottawa Flywheel Program. His equations were derived from elasticity theory and are valid for orthotropic filament wound composite rings. Utilizing the radial cut method the

equations determine the circumferential and radial residual stresses in terms of the ring overlap, ring properties and dimensions.

The circumferential component was defined as:

$$\sigma_\theta = \frac{E_{\theta\theta} z}{2\pi(1-K^2)R}\left[1 - \frac{1-c^{(K+1)}}{1-c^{(2K)}} K \left(\frac{r}{b}\right)^{(K-1)} + \frac{1-c^{(K-1)}}{1-c^{(2K)}} K c^{(K+1)} \left(\frac{b}{r}\right)^{(K+1)}\right] \quad (2.8)$$

while the radial component would be expressed as:

$$\sigma_r = \frac{E_{\theta\theta} z}{2\pi(1-K^2)R}\left[1 - \frac{1-c^{(K+1)}}{1-c^{(2K)}} \left(\frac{r}{b}\right)^{(K-1)} - \frac{1-c^{(K-1)}}{1-c^{(2K)}} \left(\frac{b}{r}\right)^{(K+1)} c^{(K+1)}\right] \quad (2.9)$$

The term z is the ring overlap as depicted in Figure 2.1 on page 10 and could be a measured value from the inner diameter change or calculated from the circumferential strain reading at the inner surface, ϵ_{θ_i} when the ring was cut:

$$z = \frac{2\pi(1-K^2)R\epsilon_{\theta_i}}{(1 - KC_2 + KC_3) - \nu_\theta(1 - C_2 - C_3)} \quad (2.10)$$

where,

$$C_2 = \frac{1-c^{K+1}}{1-c^{2K}} c^{K-1}$$

$$C_3 = \frac{1-c^{K-1}}{1-c^{2K}}$$

As mentioned above, the stresses could be determined by substituting an overlap directly into both equations. As a comparison, strain readings taken on the inside surface of a ring were substituted into equation No. 2.10, representing the overlap produced by the released strain. This overlap was then substituted into equations Nos. 2.8 and 2.9 and the stresses calculated. By so doing, two sets of results were obtained, one produced by the strain gauges and another by the diameter change in the ring. This process was the method finally chosen to be used in calculating the residual stresses in the rings. These results are further elaborated on in Chapter 5 of this thesis.

2.2.3 Residual stress determination by incremental machining.

C.E. Knight, Jr. [9], was one of the few researchers working with the new composite materials in the early 70's. One of the many and varied investigations he carried out was that of residual stresses in the manufactured composites. In his filament wound rings, incremental machining was one of the techniques investigated.

Knight manufactured four rings of W-1 clear fibreglass with Maraglas 655 epoxy. All rings were 15.24 cm inside diameter with various thicknesses and winding tension of 7.4 Newtons. Rings 1 and 4 were single rings of 0.424 cm and 1.158 cm thickness respectively. Rings 2 and 3 were multiple rings, the former being two layers of 0.381 cm thickness, while the latter consisted of three layers, one

0.356 cm. thick and two 0.417 cm thick. Each ring was 2.54 cm in width with three test specimens machined from each one, 0.635 cm wide. He instrumented these rings with two circumferential strain gauges attached 180 degrees apart on the inner surface. Each ring in turn was put onto a lathe and material removed from the outer surface with a diamond coated grinding wheel. After each cut, the ring was removed and the strain reading recorded.

Using equations presented by other researchers, namely, W. Olson and C. Bert [10], Knight was able to convert the strain data to residual stress. He plotted the incremental machining data versus nondimensional thickness and was able to show the variation of the residual stresses across the ring profile.

He concluded that the method was difficult to perform and required two specimens for both inside and outside machining. Theoretically, strain gauges could be put on the outside and material machined from the inside.

In 1977, along with a research team at Union Carbide Corporation, Knight [11] again evaluated the residual stress by means of incremental machining. Several test rings with Kevlar 49 fibres were manufactured by filament winding. A wet-winding process was utilized with a room temperature curing epoxy resin system (Dow Chemical DER 322/Jefferson Chemical Jeffamine T403). Two rings had 15.24 cm inner diameter, 2.54 cm wide and 3.81 cm thickness. A third ring

had 33.02 cm inner diameter with 6.35 cm thickness while a fourth had 38.1 cm inner diameter with 6.35 cm wall thickness. The rings were then instrumented with strain gauges as before and the strain change measured as thin layers of material were machined away. A schematic of the process is shown in Figure 2.3 after removal of the i^{th} layer. The radial residual stress was calculated from the equation for the tangential stresses in a thick-wall orthotropic ring subjected to an external pressure and the total strain change from the initial reading [11]. With the strain gauges located on the inside, the tangential stress change on the inside radius produced by the strain change during machining was determined from the equation [11] below:

$$\Delta\sigma_\theta = \Delta\epsilon_\theta E_\sigma = \frac{2Ka^{(K-1)}r^{(K+1)}}{r^{(2K)} - a^{(2K)}}\sigma_{r_i} \tag{2.11}$$

Rearranging the equation gives:

$$\sigma_{r_i} = \frac{r^{(2K)} - a^{(2K)}}{2Ka^{(K-1)}r^{(K+1)}}\Delta\epsilon_\theta E_\theta \tag{2.12}$$

The circumferential stress in any layer i was found utilizing the differential pressure, therefore,

$$\sigma_{\theta_i} = \left(\sigma_{r_{(i-1)}} - \sigma_{r-i}\right)\frac{r}{\Delta r} \tag{2.13}$$

These series of rings were used as test rings, however, in full size rings(38.1 cm ID X 50.8 cm OD)the strain gauge was

attached on the side face and in this way, machining of the layers could be conducted both from the outside and inside surfaces in increments using the same ring. Knight reduced the data in a manner similar to the method previously described but he did not give any equations for this new method. He does state though, that the strain increments that result from layer removal depends on both the radial and tangential stress components at the strain gauge location.

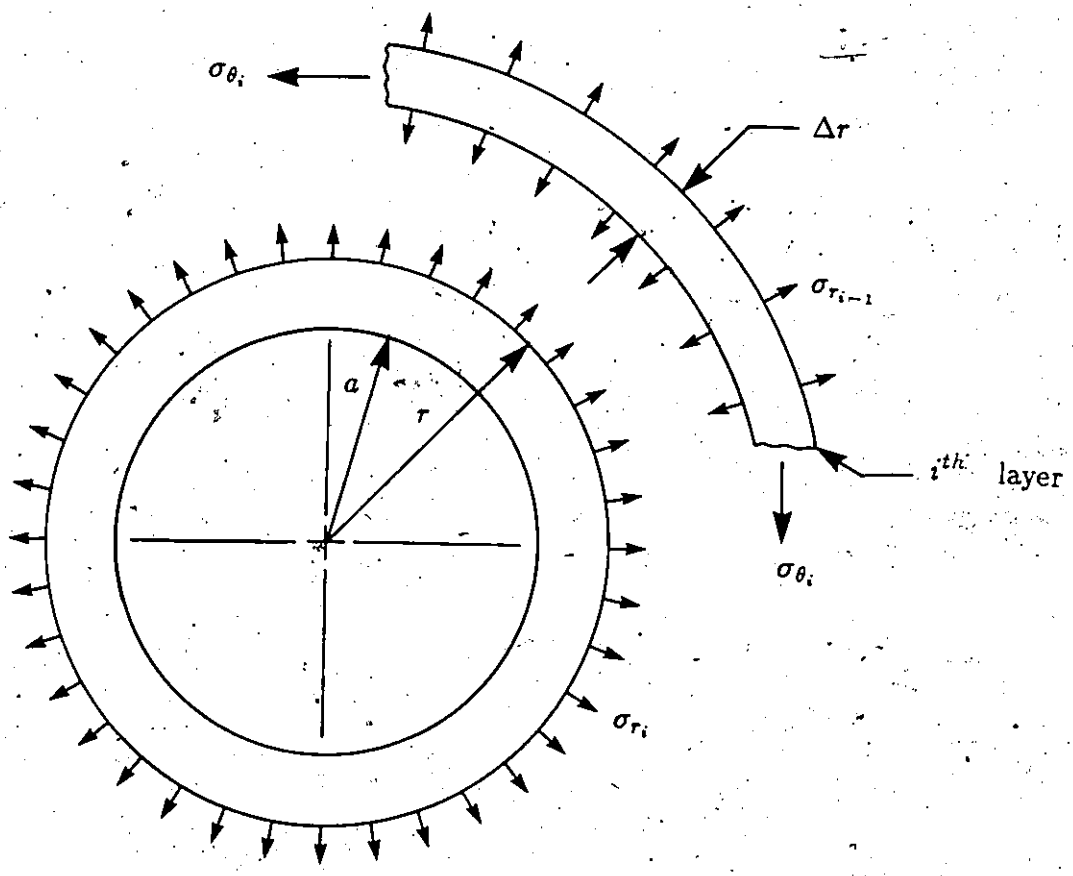

Figure 2.3: Incremental machining residual stress analysis model [11].

2.2.4 Residual stress determination by orthotropic photoelastic analysis.

The photoelastic effect was first noted by Sir David Brewester in the early 1800's [12], but its application to stress analysis was not made until the early 1900's. E.G. Coker and L.N. Filon [13] published the first extensive analysis of photoelasticity as a method of experimental stress analysis in 1931.

With the rapid development of composite materials as structural components, phototelastic techniques of stress analysis were investigated. In 1970, C.E. Knight, Jr. [9], in particular, looked at the photoelastic method for the analysis of residual stress distributions in filament wound rings.

For photoelastic analysis, the obvious requirement for the material is that it must be transparent. For fibre composites clear fibreglass and epoxy resin were selected by Knight. In order for the completed structure to be transparent, it must be void free and the index of refraction of fibre and matrix must be equal.

Knight manufactured four sets of rings as described in the previous section. Microdensitometer scanning of photographic negatives and photography were used to gather the necessary photoelastic data. Fringe values across the ring section were obtained at the dark and light-field polariscope settings. Fringe order magnitudes were obtained

with an epoxy resin tensile bar placed in series with the ring in the polariscope and observing the location of the black fringes as the bar was loaded.

Knight established a true zero order which comes from the fact that a residual fringe order exists in a straight, unidirectional composite material due to microstresses between the fibre/matrix elements. The fibre and matrix have a large difference in their thermal expansion coefficients, thus, he believes that this residual to be thermal cool-down stresses after curing.

Due to the orientation of the fibres in the rings, only two material fringe values are needed - axial and transverse. Knight obtained these values by winding flat plates using the same fibre/resin combination. These tensile bars were wound and clamped between flat steel plates to obtain 0.318 cm thickness and cured.

He separated the principle stresses, using the photoelastic data to obtain the actual residual stress distribution. The tangential and radial residual stress distributions for his four rings were plotted with all the rings giving inner surface tension with outer surface compression. He concluded that this method of residual stress determination provides a nondestructive whole-field view of the distribution but the main problems are fabricating a suitable material (match of refractive indices) and accurately determining the fringe order. In

terms of the flywheel Project, this method was not even considered due to the requirements of transparent fibres and the match of refractive indices.

2.3 Theoretical evaluation of factors affecting residual stress.

In 1973, R.C. Reuter, Jr.[14], at Sandia Laboratories, determined theoretically the macroscopic residual stresses in hoop wound fibre glass rings. He accomplished this by analytically modelling each phase of the fabrication process. His method gave a prediction of the final residual stress profile without destructive testing but the theory is restricted to "thin" shells. "Thin" shells being defined as having a minimum R/t ratio of 20. Reuter separated the fabrication into distinctive phases being:

a) filament winding,

b) application of autoclave pressure,

c) temperature increase to cure temperature,

d) layer migration,

e) cooling to room temperature,

f) pressure removal,

g) removal of the mandrel.

For each phase, constitutive relationships for the mandrel and each layer were written in terms of total radial load per unit axial length and radial displacement. To check his equations numerically, Reuter presented his results with curves based on the properties, geometry and

environmental parameters for the winding. Those results showed that by varying the winding tension, the final radial load intensity and thus, the residual stress profile could be significantly reduced.

To illustrate the effect of variable winding tension on the residual stresses, Reuter manufactured and tested six ring specimens. Two had constant tension, two with an increasing tension and two had a decreasing tension profile. These rings were cut from hoop wound cylinders fabricated by winding pre-preg tapes onto a 15.24 cm diameter solid aluminum mandrel. The two 1.27 cm wide test rings were cut from the central portion of the cylinder to avoid the end regions. Strain gauges were positioned on the inside and outside surfaces at four equally spaced polar positions and the ring was then cut. The strain data obtained was simply plotted as circumferential strain at the inner and outer surfaces. Reuter used his theoretical predictions to obtain the strain profiles across the rings but the residual stress profile was not elaborated on. His analysis, however, does show that the most dramatic change in the stress profile is due to the migration phase.

Two years after Reuter's work, in 1975, a Japanese research team, consisting of E. Shiratori, K. Ikegami, T. Hattori and K. Shimazu [15,16], were experimenting with fibre reinforced composites applied to rotating discs. It was found that circumferential cracks occurred in the discs

with uniform thickness and uniform fibre volume when the inner to outer radius ratio became larger than a certain value. On examination, the cause was found to be due to residual stresses in the disc. They believed that these stresses developed due to anisotropic shrinkage in the unidirectional fibre reinforced plastics during the setting and cooling processes. It was also noticed that the cracks occured at almost the same places in the same size discs.

Shiratori et al, investigated this anisotropic shrinkage and determined that it consisted of two components. Firstly, the chemical shrinkage when the resin sets and secondly, the thermal shrinkage when the disc is cooled from the moulding temperature to room temperature.

The radial and circumferential residual stresses were determined from equations 2.14 and 2.15 below,

$$\sigma_r = \frac{(\epsilon_{ro} - \epsilon_{\theta o}) E_r}{1 - \frac{1}{K^2}} \left[\left(\frac{\gamma_1^{K+1} - 1}{\gamma_1^{2K} - 1} \right) \gamma^{K-1} + \left(\frac{\gamma_1^{(-K+1)}}{\gamma_1^{(-2K)} - 1} \right) \gamma^{(-K-1)} - 1 \right] \qquad (2.14)$$

$$\sigma_\theta = \frac{(\epsilon_{ro} - \epsilon_{\theta o}) K E_r}{1 - \frac{1}{K^2}} \left[\left(\frac{\gamma_1^{K+1} - 1}{\gamma_1^{2K} - 1} \right) \gamma^{K-1} - \left(\frac{\gamma_1^{(-K+1)} - 1}{\gamma_1^{(-2K)} - 1} \right) \gamma^{(-K-1)} - \frac{1}{K} \right] \qquad (2.15)$$

where $\gamma = r/r_1$ and $\gamma_1 = r_2/r_1$, with the practical total strains given in equations 2.16 and 2.17 below,

$$\epsilon_r = \frac{(\epsilon_{ro} - \epsilon_{\theta o})}{1 - \frac{1}{K^2}} \left[\left(1 - \sqrt{\nu_{\theta r}\nu_{r\theta}} \right) \left(\frac{\gamma_1^{K+1} - 1}{\gamma_1^{2K} - 1} \right) \gamma^{K-1} + \left(1 + \sqrt{\nu_{\theta r}\nu_{r\theta}} \right) \left(\frac{\gamma_1^{-K+1} - 1}{\gamma_1^{2K} - 1} \right) \gamma^{-K-1} + (\nu_{r\theta} - 1) \right] + \epsilon_{ro} \qquad (2.16)$$

$$\epsilon_\theta = \frac{(\epsilon_{ro} - \epsilon_{\theta o})}{1 - \frac{1}{K^2}} \left[\left(\frac{1}{K} - \nu_{r\theta} \right) \left(\frac{\gamma_1^{K+1} - 1}{\gamma_1^{2K} - 1} \right) \gamma^{K-1} - \left(\frac{1}{K} + \nu_{r\theta} \right) \left(\frac{\gamma_1^{-K+1} - 1}{\gamma_1^{-2K} - 1} \right) \gamma^{-K-1} + \nu_{r\theta} - 1 \right] + \epsilon_{ro} \qquad (2.17)$$

The residual strains, ϵ_{rR} and $\epsilon_{\theta R}$ were obtained by subtracting free shrinkage strains, ϵ_{ro} and $\epsilon_{\theta o}$, from the total practical strains ϵ_r and ϵ_θ of equations 2.16 and 2.17 respectively yielding equations 2.18 and 2.19 below,

$$\epsilon_{rR} = \epsilon_r - \epsilon_{ro} = \frac{(\epsilon_{ro} - \epsilon_{\theta o})}{1 - \frac{1}{K^2}} \left\{ \left(1 - \sqrt{\nu_{\theta r}\nu_{r\theta}} \right) \left(\frac{\gamma_1^{K+1}}{\gamma_1^{2K} - 1} \right) \gamma^{K-1} + \left(1 + \sqrt{\nu_{\theta r}\nu_{r\theta}} \right) \left(\frac{\gamma_1^{-K+1} - 1}{\gamma_1^{-2K} - 1} \right) \gamma^{-K-1} + (\nu_{r\theta} - 1) \right\} \qquad (2.18)$$

$$\epsilon_{\theta R} = \epsilon_\theta - \epsilon_{\theta o}$$
$$= \frac{(\epsilon_{ro} - \epsilon_{\theta o})}{1 - \frac{1}{K^2}} \left\{ \left(\frac{1}{K} - \nu_{r\theta} \right) \left(\frac{\gamma_1^{K+1} - 1}{\gamma_1^{2K} - 1} \right) \gamma^{K-1} \right.$$
$$\left. - \left(\frac{1}{K} + \nu_{r\theta} \right) \left(\frac{\gamma_1^{-K+1} - 1}{\gamma_1^{-2K} - 1} \right) \gamma^{-K-1} + \left(\nu_{r\theta} - \frac{1}{K^2} \right) \right\} \qquad (2.19)$$

Shiratori determined that the maximum values σ_r and σ_θ, are along the inner surface and near the middle radius circle of the disc, respectively. Thus, the crack in the disc should occur at the position where the magnitude of residual stresses satisfies the failure condition of the unidirectional fibre reinforced plastics. He was also able to develop the equation for the maximum value of radial residual stress as:

$$\sigma_{rRmax} = \frac{(\epsilon_{ro} - \epsilon_{\theta o}) E_r}{1 - \frac{1}{K^2}} \left[\left(\frac{\gamma_1^{K+1} - 1}{\gamma_1^{2K} - 1} \right)^{\frac{1+(1+K)}{2}} \left\{ \frac{(K+1)(\gamma_1^{-K+1} - 1)}{(K-1)(\gamma_1^{-2K} - 1)} \right\}^{\frac{1-(1/K)}{2}} \right.$$
$$\left. + \left(\frac{\gamma_1^{-K+1} - 1}{\gamma_1^{-2K} - 1} \right)^{\frac{1-(1/K)}{2}} \left\{ \frac{(K-1)(\gamma_1^{K+1} - 1)}{(K+1)(\gamma_1^{2K} - 1)} \right\}^{\frac{1+(1/K)}{2}} - 1 \right] \qquad (2.20)$$

Experimentally, Shiratori et al measured the residual strains in the moulded discs by cutting the discs after strain gauges were installed in the circumferential and radial direction at various points along a diametrically opposed line. They were able to measure the free shrinkage strains and with them calculate the residual stresses existing in the ring. While Reuter basically said that the

migration of the fibres causes the most change in the stress profile, Shiratori et al showed that the resin and thermal shrinkages were the cause of the residual stresses. Reuter did include temperature changes in his investigations but made no mention of the chemical shrinkage aspect of the manufacturing process.

Chapter III

FILAMENT WINDING OF FIBRE COMPOSITE RINGS.

3.1 Introduction.

The process of filament winding a structure basically involves the laying down onto a rotating mandrel, continuous unidirectional reinforcements of either wet impregnated bare fibres or pre-pregs. The pre-pregs are fibres preimpregnated with a thermosetting resin system in a B-staged (i.e. partially cured) format. Bare fibres on the other hand are typically wet wound with the resin system being applied during the manufacturing stage. For high performance composites curing in both cases is usually carried out at an elevated temperature.

The basic process is subject to a broad spectrum of design features, material combinations and equipment. In this chapter, the chosen fibres, matrix system and equipment involved as well as the winding process, for this study, are described in detail.

It should be noted that this study was part of the overall University of Ottawa Flywheel Program and as such a number of the details presented in the chapter were the results of substantial collaborative efforts of other members of the group (J. Wong [17], A. Miyase [18] and D. Lindstrom [19]).

3.2. Filament winding materials.

3.2.1 Fibres.

As per decisions made in the Flywheel Program[20], the two fibres chosen for the final flywheels were S2-glass 449AA-750 (666.7 Tex.) roving and Grafil 12K E/XAS carbon (800 Tex.) tow (Figure 3.1). The term Tex refers to the weight of the fibre in grams for 1000 metres of the roving or tow. Kevlar 49 was also evaluated in the earlier part of the study the results of which are presented in Chapter 4 of this thesis. This fibre was deemed unsuitable since a suitable flywheel design with this fibre could not be accomplished within the limitations of the design parameters [3].

For the full scale prototype carbon and S2-glass composite rings, two rovings were used. This decision resulted from material tests on rings fabricated with two, three and four rovings. The outcome of these experiments provided evidence that a decrease in the transverse tensile strength of the rings occured with an increase in the number of strands [20].

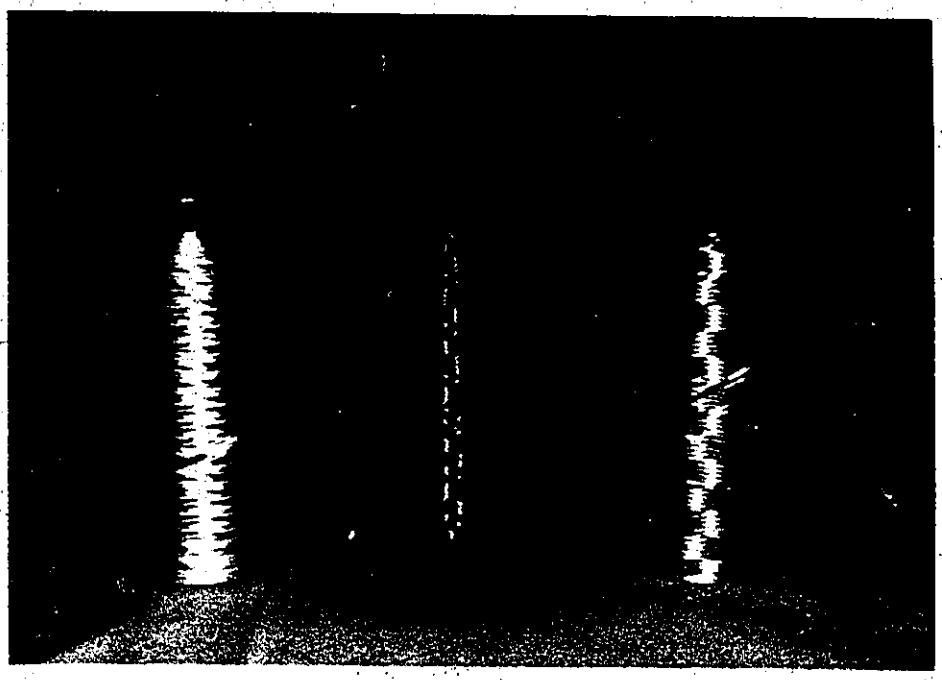

Figure 3.1: S2-glass, E/XAS carbon and Kevlar 49 fibre spools.

3.2.2 Resin system.

After extensive materials testing on six suitable epoxy matrices [21], Shell Epon 825 epoxy resin with Pacific Anchor Ancamine 1482 Hardener at 19 parts per hundred parts resin (by weight) was selected. This resin system is a thermosetting type in that an elevated temperature cure is required. At room temperature, the epoxy has a viscosity of 3000-5000cp. with a pot life of 4-5 hours. It is generally recommended that the viscosity of the resin system for wet filament winding be less than 1000cp. To achieve this, a heated resin bath was used as described in Section 3.3.2.2. Viscosity tests on the chosen resin system showed that resin

heated at a constant 55 degrees centigrade resulted in a viscosity of 125cp rising to 2000cp at the end of 3.5 hours [22]. The recommended cure schedule is 1 to 4 hours, depending on the size of the ring, at 100 degrees centigrade.

3.3 Filament winding equipment and the winding process.

3.3.1 Mandrels.

As mentioned before, the wetted rovings are wound onto a rotating mandrel. A variety of mandrels were used to fabricate rings for this study, namely,

1) Thin ring mandrel,
2) Radially thick mandrel,
3) Prototype ring mandrel,
4) Full scale ring mandrels.

Basically, the mild steel mandrels consisted of a central core with two side plates, along with a removable shaft with which it was rotated. The design of the mandrels also allowed for easy removal of the fabricated rings. The various sizes of the mandrels are shown in Figure 3.2.

The surface of the steel has to be coated with a suitable release agent so that the cured rings can be removed. A silicone release agent, Dow Corning No.7, was used for this purpose. After all machining was completed on the mandrels the silicone grease was applied. The coated steel was then placed in an oven at approximately 170 degrees Centigrade

for 12 to 14 hours. After cooling, the excess silicone grease was then removed leaving a thin layer on the steel surfaces. Although commercially available aerosol release agents such as Miller-Stephenson MS-136 dry release agent as well as in-house liquid mixtures were evaluated, the Dow Corning No.7 compound provided the most consistent results from winding to winding. This finish was reapplied after each ring was manufactured to provide consistency from ring to ring.

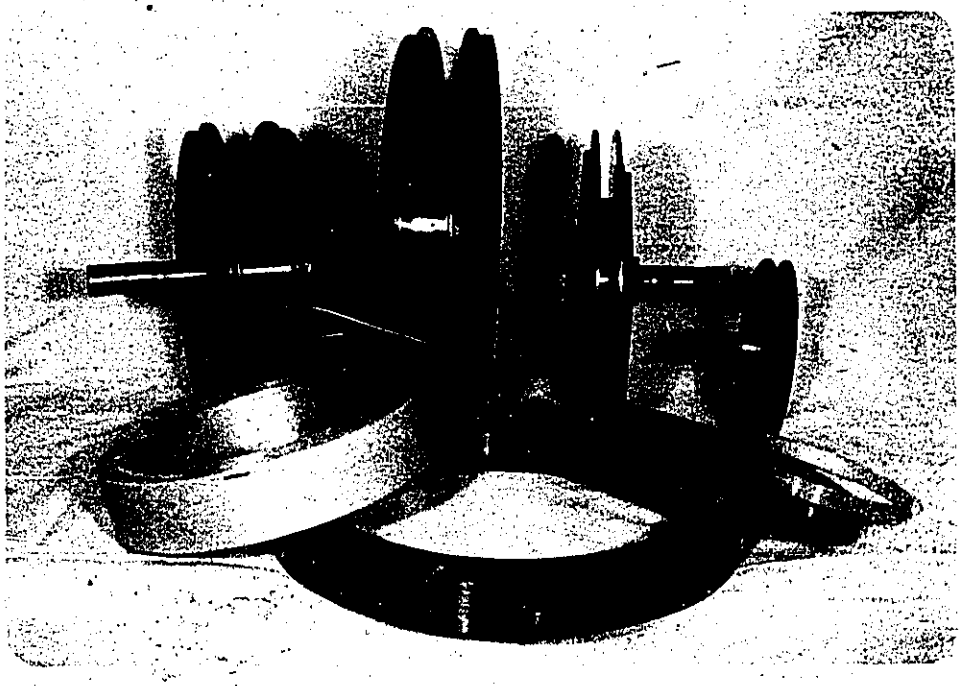

Figure 3.2: Steel mandrels used in producing the composite rings. A sample ring produced by each mandrel is also shown.

3.3.2 Filament winder.

The first series of thin rings were manufactured on a modified metal lathe (Figure 3.3) but the majority of the rings reported in this study were wound on a computer-controlled filament winder (Figure 3.4). The various components of the filament winder, in sequential order, are described in the following sections.

Figure 3.3: Original metal lathe used to wind thin rings.

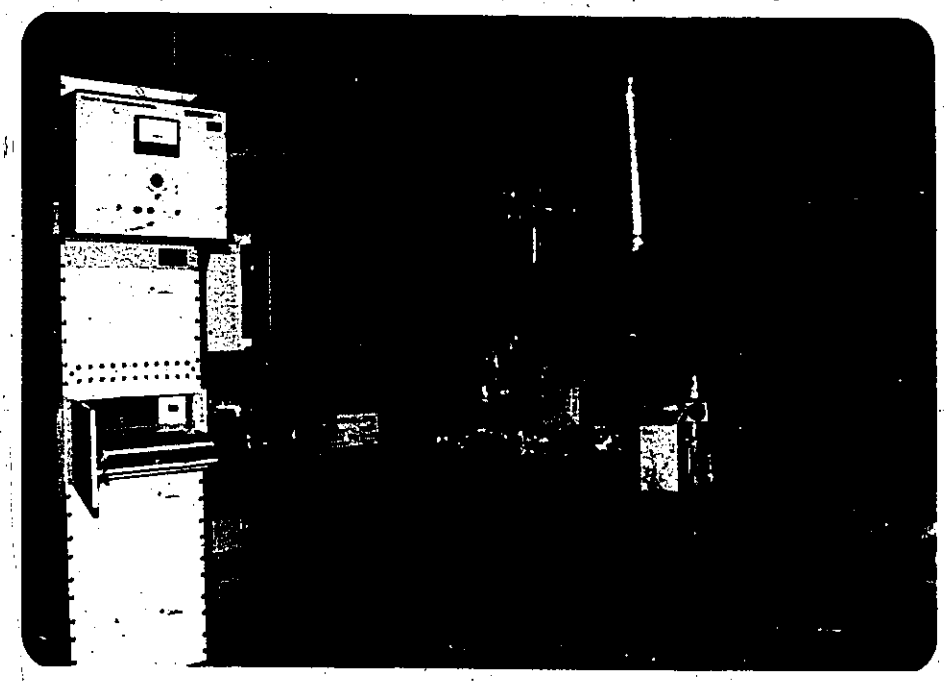

Figure 3.4: Modified lathe used to manufacture full scale rings.

3.3.2.1 Fibre delivery.

The fibre spools were set up on a support stand consisting of spool holders and allowed to rotate in roller bearings (Figure 3.5). The mass of each full spool of S2-glass is 7kg while that for carbon can be 2.5, 1.8 or 0.9 kg. Depending on the size of the ring being wound, a combination of these sizes were used. This was important in the full scale rings in order to position any joints away from a high stress region.

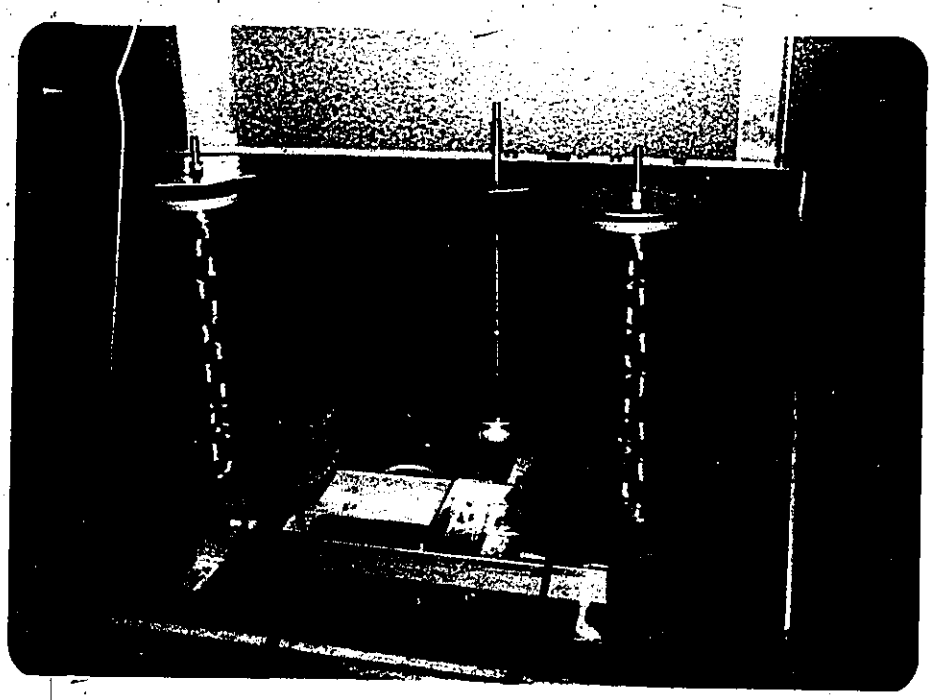

Figure 3.5: Spool holders shown with E/XAS carbon mounted. A similar set up was carried out for S2-glass.

3.3.2.2 Resin bath.

The resin and hardener mixture was kept at a temperature of approximately 55 degrees centigrade using a heated water bath (Figure 3.6), the temperature of which was controlled with a Brinkmann IC-2 recirculator-heater [23]. A finger arrangement spreads and flexes the rovings as they pass through the bath (Figure 3.7) in order to improve the wetting of the fibres. Before the impregnated rovings leave the bath, excess resin was removed by passing the fibres through a set of rubber squeezers (Figure 3.8). This device was useful in providing some control on the fibre

volume fraction as well as returning most of the excess resin to the reservoir. Depending on which fibre was being used, the amount of resin picked up varied. It was observed that the carbon tows picked up substantially more resin passing through the bath/rubber squeezer assembly than did the S2-glass rovings.

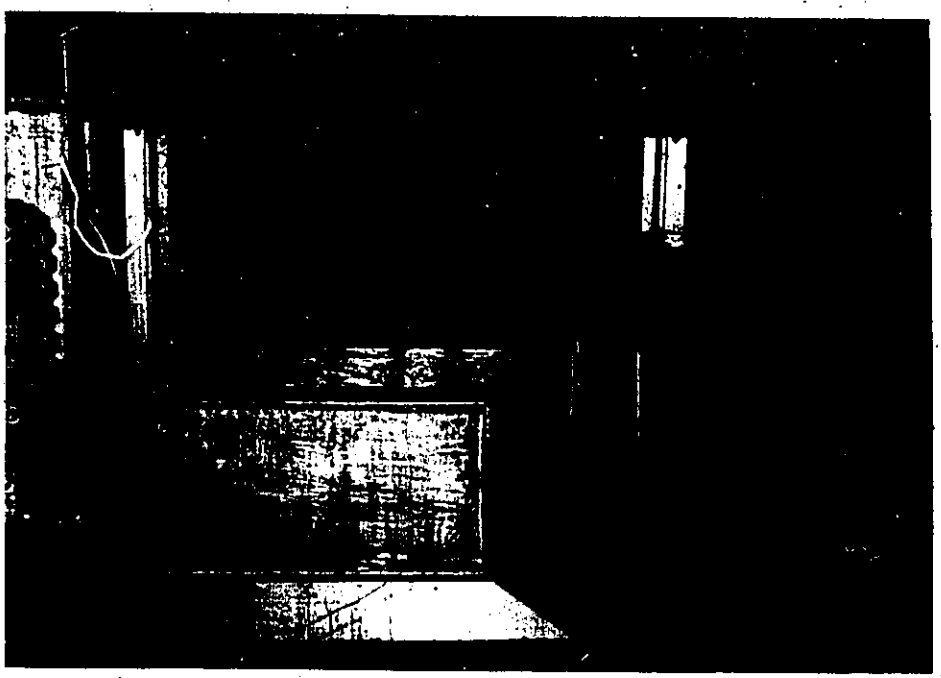

Figure 3.6: Epoxy resin temperature controlled water bath.

Figure 3.7: Finger arrangement used to spread fibres in resin bath.

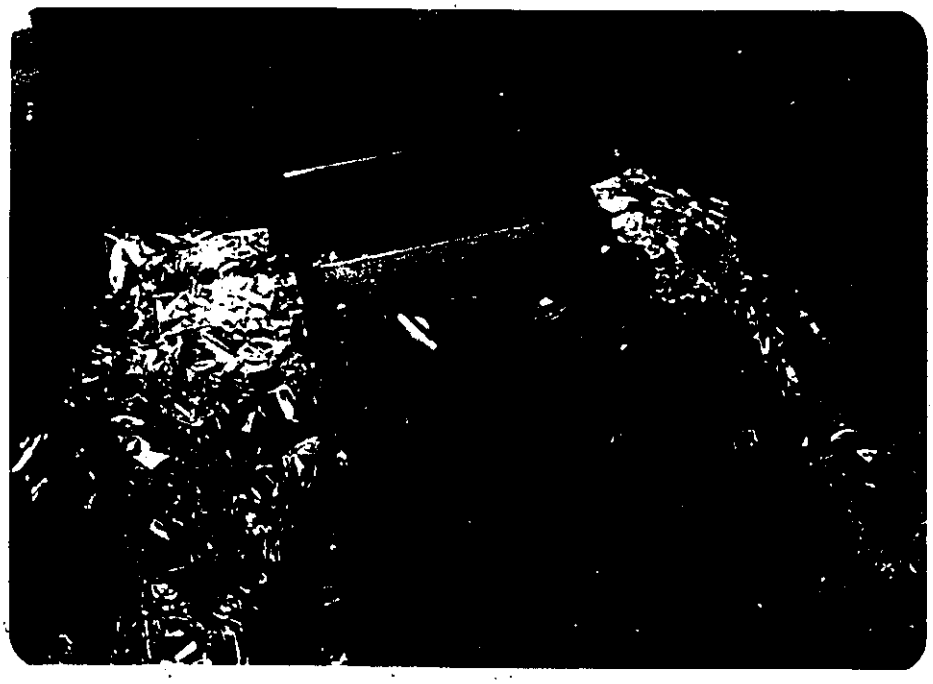

Figure 3.8: Assembly showing rubber squeezers removing excess resin.

3.3.2.3 Tensioning of the rovings.

Unlike industrial practice and other researchers[9] who tensioned their fibres at the spool, tensioning just before laying down onto the mandrel was settled on. By so doing, more control of the tension being applied could be maintained.

The tensioning system consists of a magnetic brake connected to a sensor via a feedback loop (Figure 3.9). The monitor/controller (Figure 3.10) is a Magnetic Power Systems Inc., Magpower TRAC-1 tension readout and controller, with the sensor having a capacity of 450 Newtons. Although originally designed for conveyor belt systems, it has proved to be an accurate and dependable piece of equipment. The controller was calibrated so that 100% on the scale represented 100 Newtons tension. This allowed quick and easy control of the applied winding tension in terms of Newtons per 1000 Tex of fibre roving or tow.

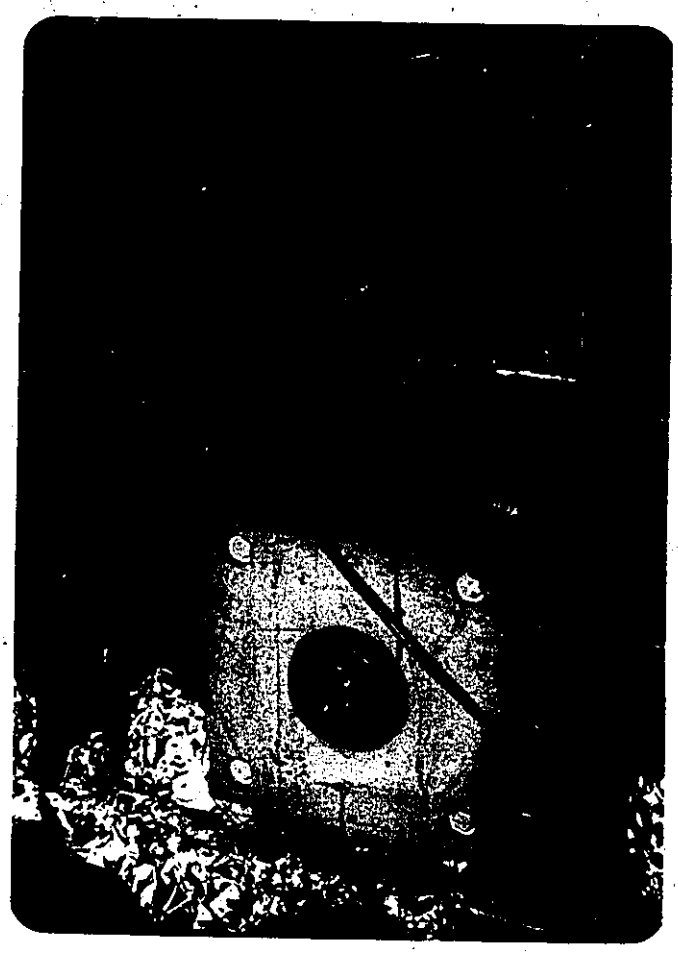

Figure 3.9: Tensioning system. Tension sensor is shown as well as magnetic brake.

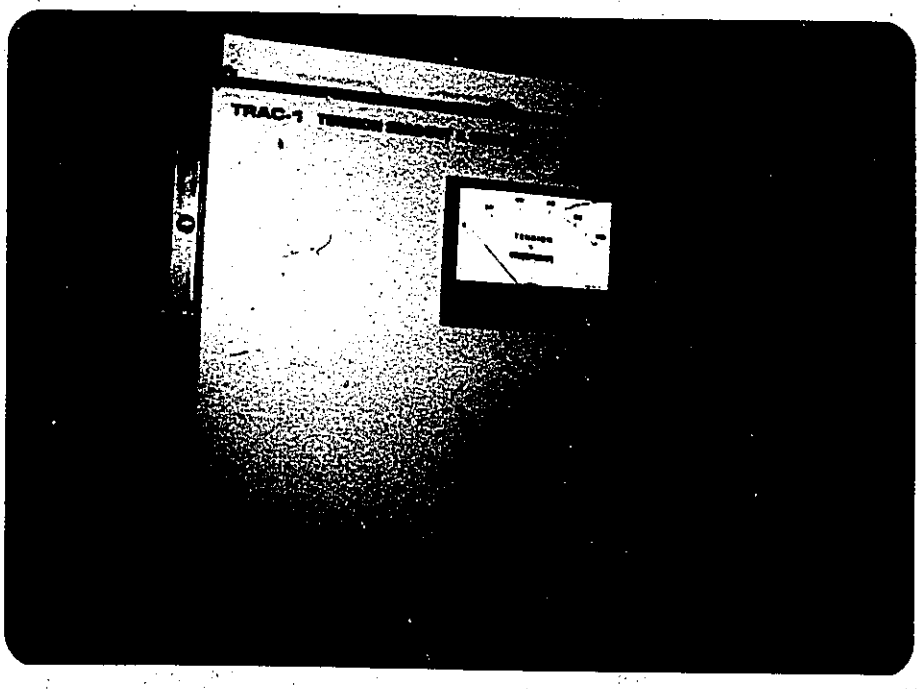

Figure 3.10: Magnetic brake monitor/controller. Scale and associated switches can be clearly seen.

3.3.2.4 Filament winder modifications and control.

The previous sections described the basic aspects of the filament winding process; namely, fibres, resin system, tensioning device and mandrels. These constituents were all merged together with the use of the filament winder.

Although several large companies design and produce custom built filament winders (usually at great cost), modifications to an used metal lathe were carried out in-house. The finished product was essentially converted into a five-axis filament winder[1], with the use of DC stepping motors. Although only two axes were needed for the filament winding of rings, a future requirement necessitated

[1] With Doug Lindstrom [24].

modifying the lathe at that time [24]. The head stock as well as the tail stock were raised to accommodate the larger diameter of the full scale mandrels. Further modifications resulted in the cross slide (support for the cutting tool) being replaced with 15.24 cm aluminium channel bolted to the saddle. The channel itself was 2.13m long and carried all the ancillary equipment, including the resin bath and tensioning device (Figure 3.11).

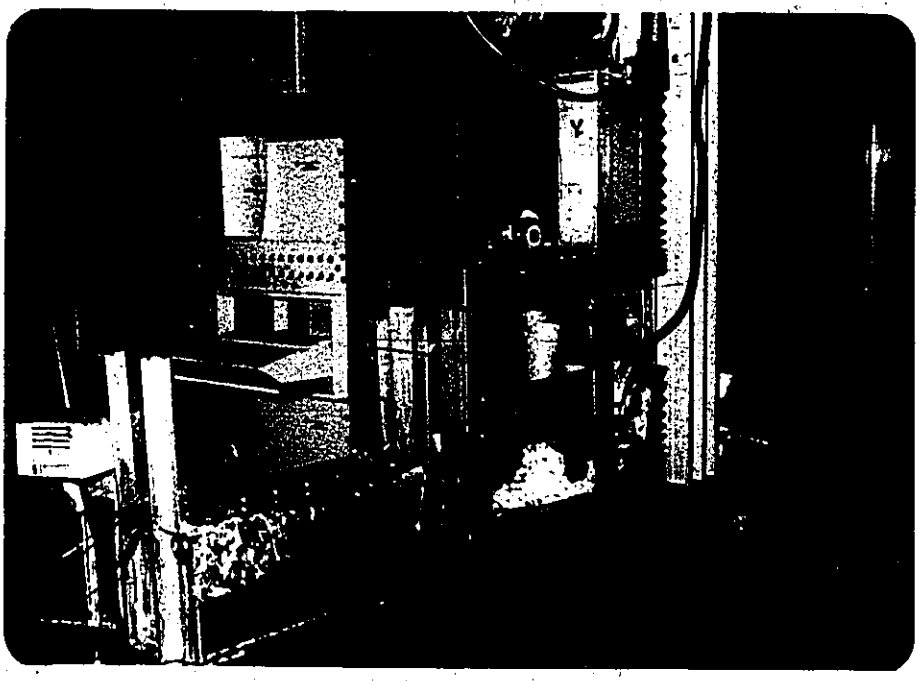

Figure 3.11: Aluminum channel with resin bath and tensioning device.

In the new filament winder, an Apple IIE computer controlled the DC stepper motors via auxiliary hardware with in-house filament winding programs[2] (listings of the

[2] by Doug Lindstrom [19].

programs are given in Appendices A & B). The programs takes into account, the rpm of the mandrel, the type of fibre, the total travel, and the traverse feed rate of the aluminum channel. Added input for the program simply entails the number of double passes (two layers of winding) required for the ring involved.

All controls for the winder motors and tensioning device were centrally located in an instrument cabinet (Figure 3.12). The tensioning device was mounted high on the cabinet, since once set, only monitoring of the readout was required.

During winding, the operator can monitor the location of the fibres, relative to the axial thickness, as well as the current double pass on a monitor mounted on the winder (Figure 3.12). The temperature of the water bath was originally monitored with the aid of a thermometer but, at a later date, a digital display (Analogic AN2572 T type) was installed in the cabinet (Figure 3.12). As mentioned in Section 3.3.2.2, the carbon fibres pick up a substantial amount of resin even with the squeezer at the exit of the bath. As additional assistance in removal of this resin, a secondary scraper was installed during E/XAS carbon winding (Figure 3.13). Initial tests with radially thick, 2.54 cm axial rings showed that desired fibre volume fractions of 60-65% were realized. However, tests on S2-glass rings showed the reverse with a drop in the fibre volume fraction

with the secondary scraper. Thus, during the winding of the carbon rings, this secondary scraper was continually utilized while with the S2-glass rings, scraping was only done when an excessive amount of resin built up on the surface.

Due to physical size of the full scale carbon rings along with the available size of the E/XAS carbon tow spools, joining of the tows was required. To accomplish this, nylon glue was used, dispensed from a Bostic 260 hot-melt glue gun. After trial and error, joints approximately 1.3 cm long were obtained. The main concern here was that the joints may introduce or become a defect in the ring, causing premature failure at design speeds. As an added precaution, no joint was allowed to fall at the point of maximum radial stress (approximately 50% of the radial thickness) but instead was positioned on either side of that location. In manufacturing the thin rings, the length of time involved with actual winding was approximately 15 minutes. However, with the full scale rings, this time increased to 8 hours for the S2-glass and 12-14 hours for the E/XAS carbon. The winding system also had to be constantly monitored to prevent any problems that may introduce flaws into the ring. Since the E/XAS carbon is brittle by nature, loose fibres usually accumulated on the pulleys and to prevent jamming of these pulleys any build-up was quickly removed. The epoxy/hardener mixture produces fumes when heated, thus as a

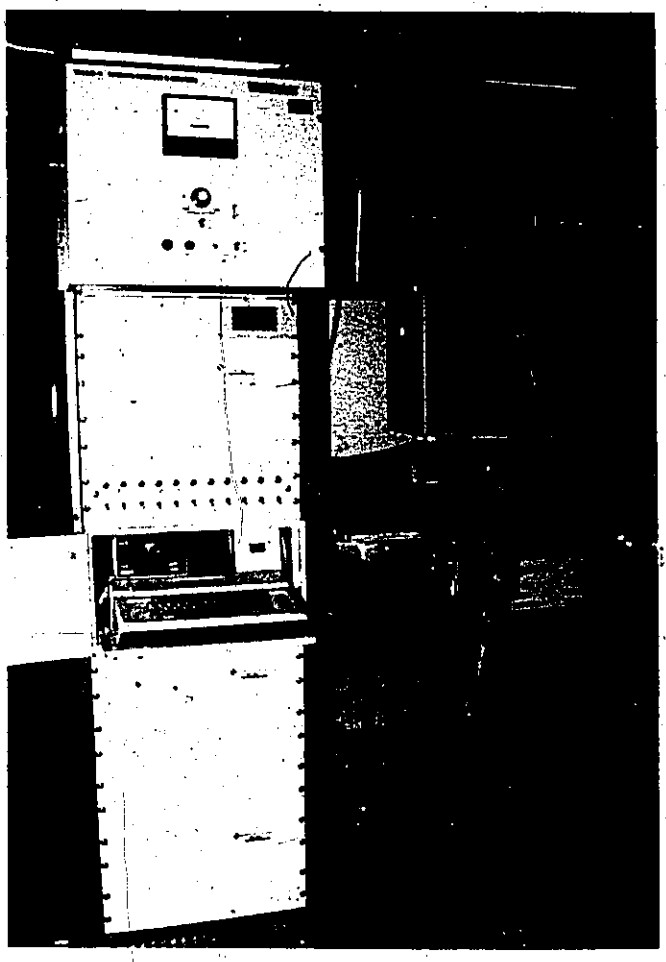

Figure 3.12: Control cabinet for filament winder.

Figure 3.13: Axially/radially thick ring being manufactured. Location of secondary scraper is shown.

safety measure, fume hoods were installed over the winding apparatus as well as over the curing oven (Figure 3.14 and Figure 3.15).

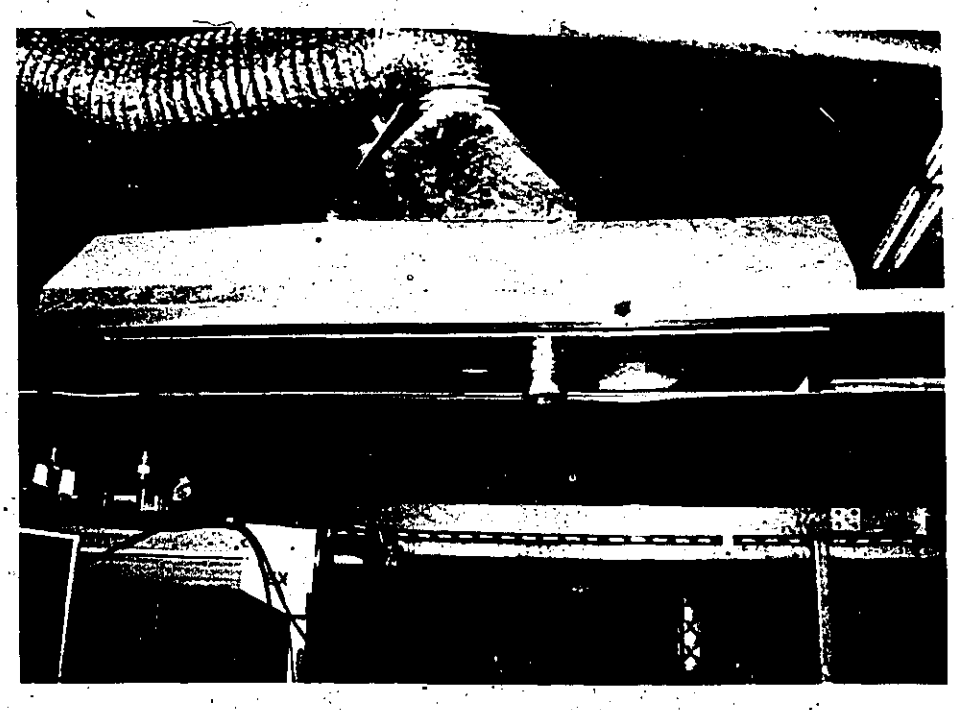

Figure 3.14: Fume hood over winding area.

3.3.3 Curing of the manufactured rings.

After a winding was completed, the whole assembly was removed from the winder and placed in the oven. Owing to the large size of the full scale rings, a suitable oven was required. A Gruenberg Electric Company, Model P2307M oven (Figure 3.15) proved to have the dimensions required, accommodating the largest of the mandrels.

After manufacture, the ring/mandrel assembly was placed in the oven at 120 degrees centigrade and allowed to cure.

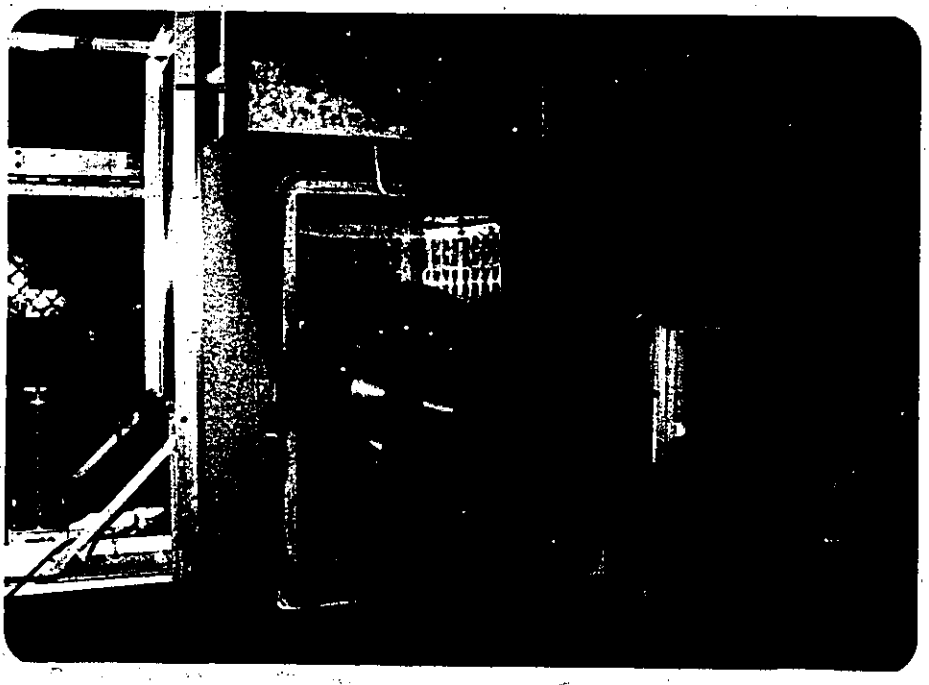

Figure 3.15: Gruenberg Electric Company oven used in curing the composite rings.

This cure schedule is referred to as the standard cure and the length of time spent in the oven depended on the size of the ring. The thin rings were usually in the oven for approximately one hour, while the radially thick rings were cured for approximately twice as long. The full scale rings were cured for approximately four to four and a half hours due to their large size. The first set of carbon thin rings were given this standard cure and at first appeared adequate, however with the radially thick rings, material tests proved that this method of cure was unsuitable in terms of meeting the design requirements. Five different cure schedules were investigated for the carbon rings, low

temperature, controlled heat-up, two-stage, two-stage plus post-cure as well as the standard cure. The low temperature cure involved curing the ring at 68 degrees Centigrade for twenty hours. The controlled heat-up required that the oven start cold and the temperature increased in stages up to 100 degrees Centigrade. In a two-stage cure the manufactured ring is allowed to B-stage at room temperature for approximately forty eight hours with a subsequent cure at 100 degrees Centigrade. The two-stage plus post-cure has the B-stage and 100 degree centigrade stage but also cures the ring at a temperature of 150 degrees centigrade. Depending on the size of the rings the length of time spent in the oven at the final stage was varied. The different cures are further elaborated on in Chapter 4. From material tests carried out on specimens from rings with the different cures, a two stage cure was selected [25]. To prevent any mass shifts of the fibre/resin structure, the rings were rotated while in the oven at 3 rpm during the B-staging and subsequent cure. This procedure also prevented any excessive build up of resin in one particular location. After removal from the oven the rings were quite easy to remove from the mandrels owing to the shrinkage which occured during curing as well as the release coating on the mandrels. The results of the tests carried out on the rings manufactured with the above methods will be presented in the following chapter.

Chapter IV.

RESIDUAL STRESS MEASUREMENT IN FIBRE COMPOSITE RINGS.

4.1 Introduction.

With the rapid advance of technology a myriad of new materials are coming to the forefront. Some of these exotic materials considered are fibre composites. Increasing use of advanced composites are being made in many diverse applications ranging from commercial aircraft, space vehicles to a variety of sporting goods. With the decision to use fibre composites for the Flywheel Program, it was necessary to measure the residual stresses produced in the rings.

4.2 Strain measurement on composite materials.

After examining the available literature (Chapter 2) it was decided that all measurements for determining the residual stresses to be carried out using strain gauges. However because composite materials are normally not isotropic in their mechanical properties standard metallic techniques can not be used ad hoc. Basically it is due to the orthotropic nature of composites that the use of strain gauges should be carefully considered. This is especially

true in terms of gauge misalignment and transverse sensitivity. Some analysis of these factors was carried out and are elaborated on in the following sections.

4.2.1 Errors due to strain gauge misalignment.

With conventional materials, gauge alignment is normally carried out by first marking the surface with alignment marks. These impressions are usually applied with a relatively blunt tipped instrument such as a ballpoint pen or the like. The gauge is then aligned using these marks. Tolerances on the order of plus or minus 1 or 2 degrees can usually be obtained. For most uses, this amount of misalignment would probably produce negligible errors with an isotropic material. However, with the orthotropic nature of these composites, no such generalization can be taken and a search of the available literature was undertaken. One paper [26] was provided by a strain gauge manufacturer but the information therein was quite general in nature. A second paper [27] was specifically composite orientated and is reported here.

M.E. Tuttle and H.F. Brinson [27] investigated the effect of having varying amounts of gauge misalignment on unidirectional composite orthotropic plates. Misalignment errors of -4, -2, 2 and 4 degrees were used along with a constant stress level. They determined that for fibre angles (with respect to the gauge orientation) ranging from about 3 to 40 degrees, the percentage error due to

misalignment was appreciable (Figure 4.1). Their results also showed that at a fibre angle of eight degrees, this error was a maximum.

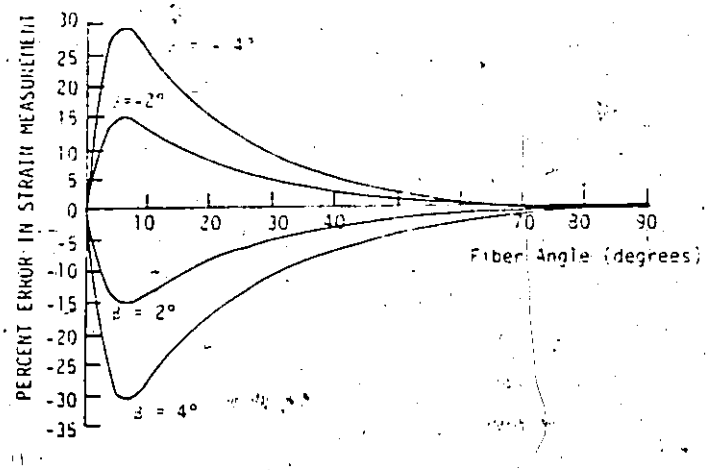

Figure 4.1: Percentage error due to gauge misalignment[23]

4.2.2 Errors due to transverse sensitivity in strain gauges.

The gauge factor for a strain gauge is usually determined with a set method [28]. The manufacturer defines this factor as :

$$S_g = \frac{\Delta R/R}{\epsilon_x} \quad \text{when} \quad \epsilon_y = -0.285\epsilon_x \tag{4.1}$$

It is obtained by mounting a gauge on a steel specimen of Poisson's ratio of 0.285 and then subjecting the specimen to a uniaxial stress of σ_x. Actually, according to Dove and Adams [12], only one manufacturer gives the value of ν as 0.285 that being Baldwin-Lima-Hamilton Corporation [29].

However, it is safe to assume that all manufacturers use metal specimens for which ν is approximately 0.3. If this gauge factor is used for any other material the results would be in error. The magnitude of said error could vary from insignificant to appreciable.

The effect of taking the transverse sensitivity, K, into consideration can now be discussed. Materials other than metals, specifically composite construction, offer a new range of problems regarding transverse sensitivity. Whitney, Daniel and Pipes [28] investigated this phenomenon with regards to composites. They determined that the transverse sensitivity can be used with the 'apparent strains' to obtain the true strains along two mutually perpendicular directions with the equations:

$$\epsilon_r = \frac{1-\nu_o K}{1-K^2}(\epsilon_r' - K\epsilon_\theta') \tag{4.2}$$

$$\epsilon_\theta = \frac{1-\nu_o K}{1-K^2}(\epsilon_\theta' - K\epsilon_r') \tag{4.3}$$

where:

$\epsilon_r, \epsilon_\theta =$ actual strains

$\epsilon_r', \epsilon_\theta' =$ apparent strains

$K =$ transverse sensitivity (%)

$\nu_o =$ Poisson's ratio = 0.285

This same information was also found in a short publication distributed by the Micro-Measurements Corporation [30].

Further information was also gathered regarding this transverse effect with composite materials [31,32]. They determined that the transverse sensitivity correction only becomes considerable if the strain to be measured is small compared to that in the perpendicular direction. Both theoretical and experimental studies were carried out and are reported in Section 4.4.2 and Appendix I.

4.3 Residual stress measurement in thin rings.

4.3.1 Residual stress measurement in thin rings by dimensional change.

One of the simplest methods used to obtain the residual stress in a filament wound composite ring is by the use of a dimensional change. This could either involve measuring a change in diameter or an overlapping of the ends when the ring was radially cut (Figure 2.1 on page 10). As previously discussed in Chapter 2, the method used by the Naval Ordnance Laboratory could be considered a dimensional change method [4]. In the ring both radial and circumferential stresses are developed during manufacture, however, for the Flywheel Program the radial component was of particular interest due to the usually low transverse strength of the composite ring.

As an initial series of tests to obtain some experience with experimental methods, five rings (26.67cm IDx2.54cm widex0.6cm thick), were wound using 1100 Tex E glass fibres

(type 3709) and Shell Epon 825 Epoxy resin with Pacific Anchor Ancamine 1482 Hardener. The fibres and matrix in each of the five cases remained the same while the winding tension was intentionally varied. This data is presented in Table 4.1 in terms of total load on the strand and two normalized values - the Tex value is used for manufacturing while the stress value is used for calculation purposes.

Table 4.1: Winding Tension Parameters for E-glass Rings.

Ring Number	Winding Tension		
	Newtons(N)	N/1000Tex	MPa.
VS-1	4.41	4.01	10.98
VS-2	8.93	8.11	22.22
VS-4	17.85	16.23	44.43
VS-6	26.78	24.35	66.65
VS-8	35.71	32.46	88.87

Using Prosen's [4] method, the circumferential residual stress in these rings was calculated. Due to the very nature of the manufacturing process, i.e. different winding tensions, each ring produced varied in thickness. After the rings were cut with a water-cooled diamond saw (Highland Park Model 10TSB, Figure 4.2), the amount of overlap produced was recorded.

From each ring, a circumferential section approximately 5 cm was removed and used to determine the fibre volume fraction of the rings. The process to determine fibre volume fraction is described in Appendix C.

In the equations previously discussed, the thickness of the composite was required. The method to determine this

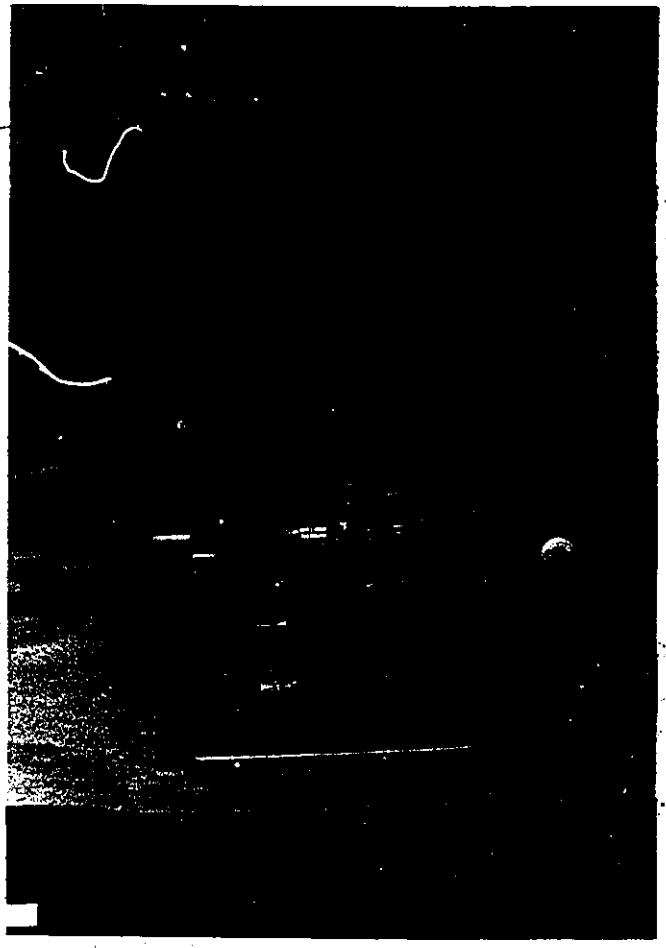

Figure 4.2: Water cooled diamond saw used to cut thin rings.

thickness involved magnifying the cross-section by a factor of 10 using a projection microscope (Photoelastic Inc., Model 051), tracing the magnified image onto a high quality tracing paper. This process was repeated for at least four locations on the ring in order to determine an average for the ring. The tracings were then cut out and weighed. On each tracing, a reference area was drawn, cut out and weighed since this minimizes the effect of there being any density differences at different locations in the paper. Knowing the total weight of the tracing and the weight and area of the reference area, the total area of the tracing was determined. The length of the tracing was known thus with the area calculated before the ring thickness was resolved.

With the volume fraction known, the composite's circumferential Young's modulus was calculated from in-house experiments [18] and the average circumferential residual stress over the cross section was determined. Final experimental results are shown tabulated in Table 4.2. As can be seen, results for VS-1 (Table 4.1 on page 59), were not included as it was very difficult to control the tension on the strand during manufacture at this 4.4 Newton setting. This is due to the fact that the minimum tension that can be applied is 8 Newtons.

Varying the winding tension for each ring was done to determine if any relationship exists between the resulting

Table 4.2: Average Circumferential Residual Stress Results for Thin S2-glass Composite Rings.

RING No.	MEAN THICKNESS (mm)		WINDING TENSION (MPa.)	OVERLAP z (mm)	FIBRE VOLUME FRACTION (%)	YOUNG'S MODULUS E_θ (MPa.)	AVERAGE RESIDUAL STRESS (MPa.)
VS-2	2.54	0.14	22.22	26.51	62.2	46.51	18.96
VS-4	2.48	0.19	44.43	46.04	65.4	48.00	24.12
VS-6	2.29	0.10	66.65	44.45	67.7	49.61	23.19
VS-8	2.29	0.19	88.87	55.56	68.0	49.81	29.07

residual stress and the winding tension. This result is shown in Figure 4.3.

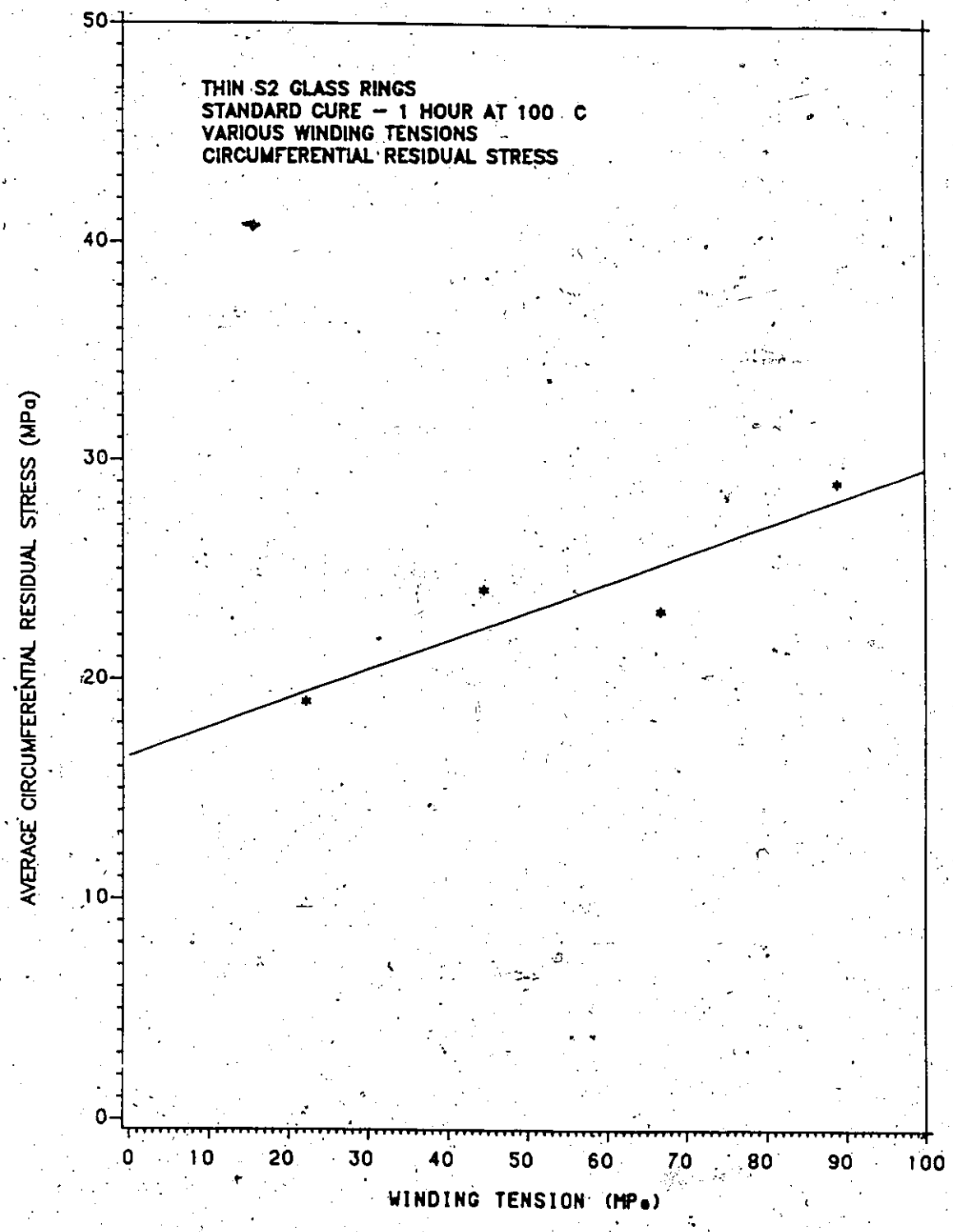

Figure 4.3: Average circumferential residual stress in thin E-glass rings.

4.3.2 Residual stress measurement in thin rings with strain gauges.

In the previous section, methods involving dimensional measurements and estimates of ring thickness were used to determine the residual stress. One aspect apparent from the results was the difficulty in determining the actual thickness of the ring i.e. excluding excess matrix on the surface. Several researchers [7,9] made use of surface mounted strain gauges to measure the strain released in the ring when it was cut. These researchers made no mention of the surface condition of their rings for strain gauge attachment. For the Flywheel Project, the outer surface produced on the ring was unacceptable for any strain gauge attachment. Due to the type of mandrel used, the inner surface of the ring was moulded and as such, acceptable for gauges. It was desirable to mount gauges on the inside and outside of the ring, opposite to each other permitting comparison of the two results as well as verifying the computer program 'OVERLAP' as listed in Appendix H.

One method of obtaining the required smooth outer surface was by manually sanding the location but this is susceptible to uneven contour problems. After careful deliberation a new method was utilized resulting in a smooth surface produced during curing of the ring. This required that, after winding the ring, exterior mold pieces be attached to the mandrel in contact with the wound composite. These attachments or pads were originally made from solid teflon

(to take advantage of its non-stick quality) and positioned with a spring clip arrangement as shown in Figure 4.4.

After removal from the oven, the newly moulded surface was examined and surface voids were detected. It was also determined from fifteen measurements of the thickness at the pad locations, as indicated in Figure 4.5, that an uneven thickness had resulted. The average thicknesses for three rings fabricated with the same procedures and materials were 1.683 ± 0.089 mm, 1.701 ± 0.064 mm and 1.716 ± 0.084 mm. Changing the type of pad was deemed necessary and new ones made of mild steel were manufactured (Figure 4.6). These new pads were evaluated on a new series of rings fabricated for determining the expansion coefficients of different fibre composite materials (Section 4.3.3.2). The pads were coated with a release agent before use, in a similar fashion to the mandrels of Section 3.3.1. The thickness measurements for the first four S2-glass rings manufactured were 9.600 ± 0.083 mm, 9.580 ± 0.005 mm, 9.600 ± 0.009 mm and 9.810 ± 0.017 mm. Compared to the previous rings, the thickness was more consistent as well as being free from any surface voids. Another point of concern was the possibility of the pads radially deforming the fibres. On examining the ring in cross-section no such evidence was apparent (Figure 4.7).

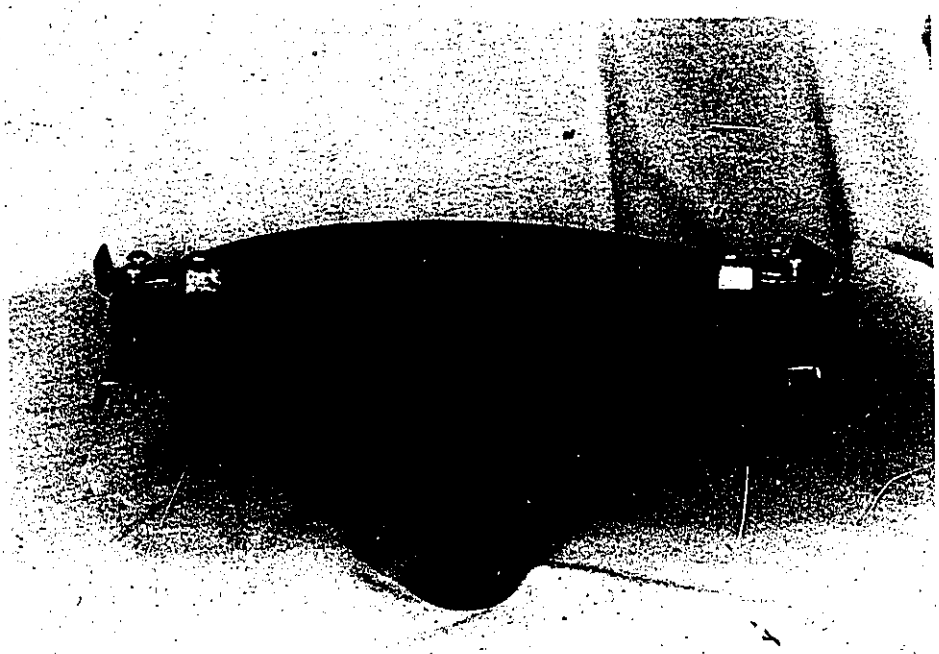

Figure 4.4: Springs used to position pads on mandrel.

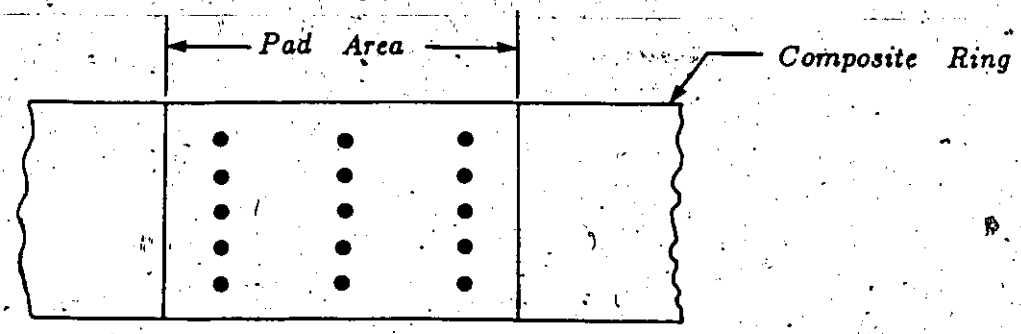

Figure 4.5: Locations of measurements on pad area.

Figure 4.6: Pads used to produce a smooth outer surface. Teflon (top) and steel (below).

Figure 4.7: Side view of the thin rings. Typical moulded surface showing no radial deformation of fibres.

4.3.3 Evaluation of factors affecting residual stress.

4.3.3.1 Introduction.

In the previous chapter, the process used in manufacturing the composite rings was described. In the course of producing these rings, residual stresses are developed due, in part to the applied winding tension, as well as the subsequent cure. The resin system chosen for manufacturing of the thin composite rings required an elevated temperature cure of approximately 1.5 hours at 100 degrees Centigrade. During the winding stage, the fibres are laid down under tension and with cure this tension becomes locked in resulting in one component of the residual stress in the ring. Residual stresses due to thermal cool down, resin cure shrinkage, and fibre migration are also produced. In the following sections, a study was undertaken to determine the magnitude of residual stresses in thin fibre composite rings contributed by each factor at each stage.

4.3.3.2 Ring thermal expansion coefficients.

In order to evaluate the residual stresses due to thermal cool down from cure to room temperature, it was necessary to determine the circumferential and radial coefficients of thermal expansion, α_θ and, α_r respectively, for the rings. In the literature [1,33], wide variations of the coefficients of the thermal expansion exist depending on the

type of fibre/resin system employed. Thus, it was necessary to determine the expansion coefficients of the particular system that was used for the flywheel program.

Five S2-glass, four E/XAS carbon and four Kevlar 49 thin fibre composite rings were fabricated. The winding tension was varied between 10 and 35N/1000Tex for the individual rings within each composite system. As mentioned in section 4.3.2, steel pads were employed in this series of rings, thus providing the required surface for application of strain gauges. Two gauges (Micro Measurements No. EA-06-500BH-120) were mounted in the fibre direction on the outer and inner surfaces of the ring opposite one another. A typical moulded surface with outer strain gauge mounted is shown in Figure 4.8. A modified version of the Micro-Measurements method (gauge on reference material mounted on steel instead of titanium silicate) for measuring thermal expansion coefficients [34] was used, thus reducing the effect of the strain gauge and cement. An additional strain gauge from the same lot number was mounted on a piece of 1018 steel plate and connected in a half bridge arrangement with the strain gauges on the ring. A Vishay P-350A Strain Indicator as well as an Automation Industries Switch and Balance unit, Model No. SB-1, were used to provide these connections (Figure 4.9).

Both the test ring and steel plate were post cured for one hour at 100 degrees Centigrade, thus insuring that the

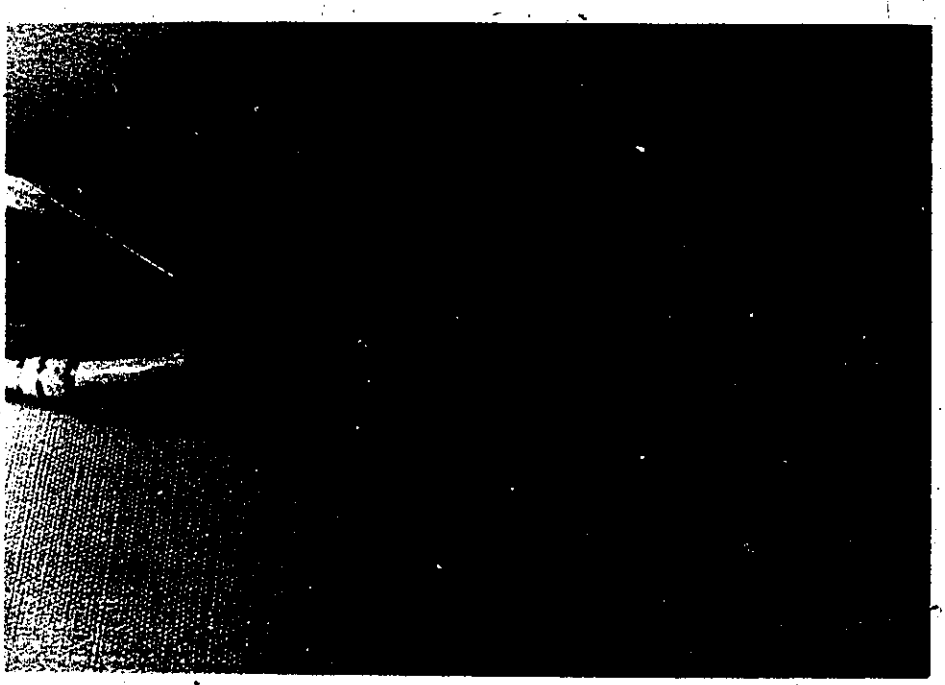

Figure 4.8: Typical moulded surface with strain gauge attached.

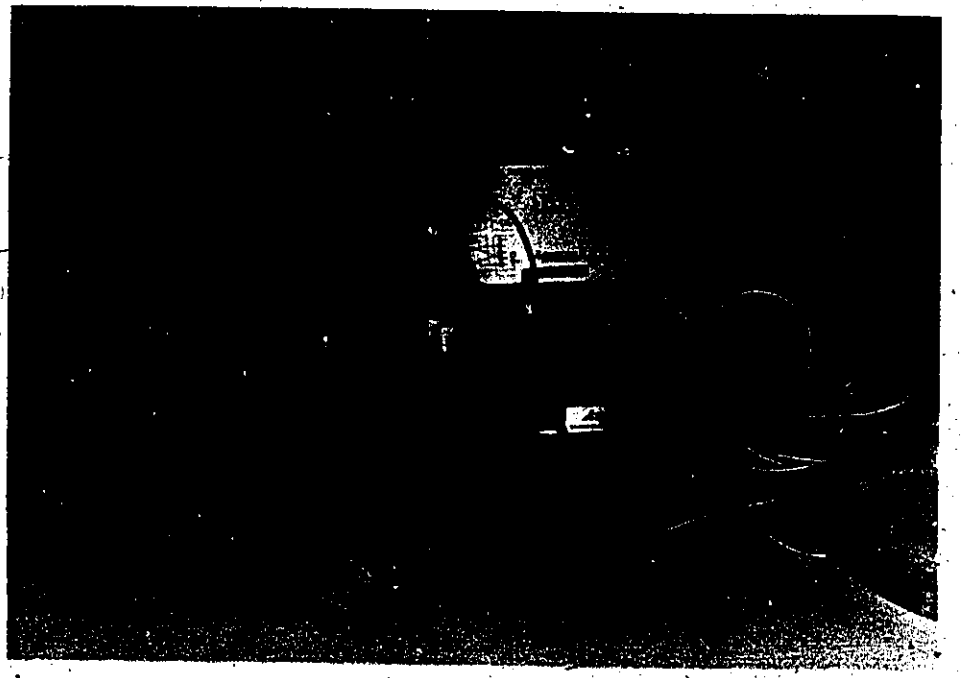

Figure 4.9: Strain indicator with switch and balance unit.

ring and gauge cement would be fully cured and above the final test temperature. A thermocouple was placed in the middle of the cross-section of a ring of the same fibre composite type to determine the amount of time for the ring to reach a predetermined temperature. The whole arrangement (two rings/steel plate) was then heated in a BLUE M Oven (Model POM570C-1) in increments of approximately 10 degrees centigrade to a maximum of 93 degrees Centigrade. After each temperature had reached equilibrium, the thermal strain readings were recorded. For each ring a graph of thermal strain versus temperature change above room temperature was prepared (Appendix D). From the slopes of the computed linear regression analysis relationships, values of inside hoop strain, ϵ_{θ_I}, and outside hoop strain, ϵ_{θ_O}, for a particular change in temperature were determined and subsequently substituted into equations 4.5 and 4.6 below, developed by J. Wong [44].

$$\epsilon_{\theta_I} = \frac{aT}{1-K^2}\left\{(\alpha_\theta - \alpha_r)(K-\nu_\theta)\frac{1-C^{-K-1}}{1-C^{-2K}}\left(\frac{1}{a}\right) - (\alpha_\theta - \alpha_r)(K+\nu_\theta)\right.$$
$$\left.\frac{1-C^{K-1}}{1-C^{2K}}\left(\frac{1}{a}\right) + \frac{(\alpha_\theta - \alpha_r)(\nu_\theta - 1)}{\mu} + \frac{\alpha_\theta(1-K^2)}{a}\right\} \qquad (4.5)$$

$$\epsilon_{\theta_O} = \frac{aT}{1-K^2}\left\{(\alpha_\theta - \alpha_r)(K-\nu_\theta)\frac{1-C^{-K-1}}{1-C^{-2K}}C^{-K}\left(\frac{1}{b}\right) - (\alpha_\theta - \alpha_r)(K+\nu_\theta)\right.$$
$$\left.\frac{1-C^{K-1}}{1-C^{2K}}C^{K}\left(\frac{1}{b}\right) + \frac{(\alpha_\theta - \alpha_r)(\nu_\theta - 1)}{a} + \frac{\alpha_\theta(1-K^2)}{a}\right\} \qquad (4.6)$$

The calculations were carried out with a computer program titled 'THEMOCOE', again developed by J. Wong [44], which simultaneously solved the two equations. This yielded the two unknown thermal expansion coefficients in the circumferential and radial directions, α_θ and α_r, respectively. The computer program 'THEMOCOE' is listed in Appendix E while the values are presented in Table 4.3

Table 4.3: Thermal Expansion Coefficients for Thin Composite Rings.

Ring Number	Thickness (cm.)	Outer Radius (cm.)	Volume Fractions			Young's Modulus		Coefficients	
			Fibre [1] (Density) (%)	Void (%)	Fibre [2] (Actual) (%)	E_θ (GPa)	E_r (GPa)	α_θ ($\times 10^{-6}$/°C)	α_r ($\times 10^{-6}$/°C)
SR-10	0.5851	13.5518	50.2	3.2	53.2	40.0	28.5	[3]	[3]
SR-15	0.5622	13.5289	51.8	3.0	54.5	43.0	28.9	3.52	40.0
SR-20	0.5644	13.5311	56.6	3.2	59.6	48.0	30.6	[3]	[3]
SR-30	0.5626	13.5293	59.5	3.1	62.4	50.0	31.5	3.28	20.3
SR-35	0.5643	13.5310	60.4	3.6	63.8	52.0	31.9	2.85	20.3
CR-10	0.5870	13.5537	46.7	5.7*	57.7	132.0	12.5	-0.83	35.7
CR-20	0.5602	13.5269	46.0	5.7*	57.1	130.0	12.5	-1.24	17.6
CR-30	0.5846	13.5513	59.9	5.7*	64.9	143.0	13.0	-1.30	43.5
CR-35	0.6112	13.5779	45.0	5.7*	55.9	129.0	12.0	[4]	[4]
KR-10	0.5577	13.5244	45.2	4.0*	65.2	78.0	5.7	-3.93	43.1
KR-20	0.5569	13.5236	48.9	4.0*	68.9	83.0	5.7	-5.44	60.4
KR-30	0.5616	13.5283	53.7	4.0*	73.7	90.0	5.8	[5]	[5]
KR-35	0.5788	13.5455	53.4	4.0*	73.4	89.0	5.8	-4.97	56.9

Notes:
1- Fibre volume fraction determined by density measurements.
2- Actual fibre volume fraction excluding voids.
3- Insufficient data - thermal strain of gauge not accounted for.
4- Insufficient data - strain gauge failure.
5- Insufficient data - inside strain gauge not mounted.
* - assumed.

4.3.3.3 Thermal residual stresses.

Using the two coefficients previously determined, the circumferential and maximum radial thermal residual stresses, $\sigma_{\theta T}$ and σ_{rT} respectively, for the inside and outside surface due to a uniform temperature change and hydrostatic external loading were calculated. These equations are presented here as equations 4.7 and 4.8 and were evaluated using computer program 'THEMOSUP' developed by J. Wong [44] a listing of which appears in Appendix F.

$$\sigma_{rT} = \frac{E_r(K^2-\nu_\theta^2)(\alpha_\theta-\alpha_r)T}{(1-\nu_r\nu_\theta)(1-K^2)}\left[\frac{1-C^{-K-1}}{1-C^{-2K}}\left(\frac{r}{a}\right)^{K-1} + \frac{1-C^{K-1}}{1-C^{2K}}\left(\frac{r}{a}\right)^{-K-1}-1\right] - P_a\left[\frac{1}{1-C^{-2K}}\left(\frac{r}{a}\right)^{K-1} + \frac{1}{1-C^{2K}}\left(\frac{r}{a}\right)^{-K-1}\right] - P_b\left[\frac{1}{1-C^{2K}}\left(\frac{r}{b}\right)^{K-1} + \frac{1}{1-C^{-2K}}\left(\frac{r}{b}\right)^{-K-1}\right] \quad (4.7)$$

$$\sigma_{\theta T} = \frac{E_r(K^2-\nu_\theta^2)(\alpha_\theta-\alpha_r)T}{(1-\nu_r\nu_\theta)(1-K^2)}\left[K\frac{1-C^{-K-1}}{1-C^{-2K}}\left(\frac{r}{a}\right)^{K-1} - K\frac{1-C^{K-1}}{1-C^{2K}}\left(\frac{r}{a}\right)^{-K-1}-1\right] - KP_a\left[\frac{1}{1-C^{-2K}}\left(\frac{r}{a}\right)^{K-1} - \frac{1}{1-C^{2K}}\left(\frac{r}{a}\right)^{-K-1}\right] - KP_b\left[\frac{1}{1-C^{2K}}\left(\frac{r}{a}\right)^{K-1} - \frac{1}{1-C^{-2K}}\left(\frac{r}{b}\right)^{-K-1}\right] \quad (4.8)$$

An assumed temperature change of -77 degrees Centigrade (100 degrees Centigrade cure to room temperature) was used. Although thirteen rings are listed in Table 4.3 on page 73,

only those with available α_θ and α_r values were used in calculating the thermal residual stresses.

4.3.3.4 Residual stress due to winding tension.

The effect of winding tension was estimated using the results of Liu and Chamis [35]. These two researchers basically developed equations which estimated the residual stress in a filament wound ring as a function of winding tension only and did not take into consideration other variables in the filament winding process. Using a computer program ('FTENSION' by J. Wong [44] listed in Appendix G) which encompasses equations 4.9 and 4.10, the radial and circumferential residual stresses of a filament wound composite ring, due to winding tension and after removal from the mandrel, were determined [44].

$$\sigma_r(r) = \frac{2KB^{2K}c^{K-1}f(b_m)}{c^{2K}-b_m^{2K}}\left[\left(\frac{c}{r}\right)^{K+1} - \left(\frac{r}{c}\right)^{K-1}\right] - b_m^{K-1}f(r)\left[\alpha\left(\frac{b_m}{r}\right)^{K+1} + \beta\left(\frac{r}{b_m}\right)^{K-1}\right] \tag{4.9}$$

$$\sigma_\theta(r) = T(r) + Kb_m^{K-1}f(r)\left[\alpha\left(\frac{b_m}{r}\right)^{K+1} - \beta\left(\frac{r}{b_m}\right)^{K-1}\right] - \frac{2K^2b_m^{2K}c^{K-1}f(b_m)}{c^{2K}-b_m^{2K}}\left[\left(\frac{c}{r}\right)^{K+1} + \left(\frac{r}{c}\right)^{K-1}\right] \tag{4.10}$$

where,

$$\alpha = K - \nu_\theta - B$$

$$\beta = K + \nu_\theta + B$$

$$B = \frac{E_\theta}{E_m(b_m^2 - a_m^2)}\left[(1-\nu_m)b_m^2 + (1+\nu_m)a_m^2\right]$$

$$f(r) = \int_r^c \frac{\rho^K T(\rho)}{\beta\rho^{2K} + \alpha b_m^{2K}} d\rho$$

a_m = inside radius of mandrel.

b_m = outside radius of mandrel.

c = outside radius of composite.

4.3.3.5 Total experimental residual stress.

Using the gauges already applied onto the rings for the thermal experiments, the rings were cut radially which resulted in two sets of experimental values being obtained - ring overlap and inside strain readings. The data was used in equations 2.8, 2.9 and 2.10, as described in Section 2.3.2, in conjunction with a computer program titled 'OVERLAP'[3], a listing of which appears in Appendix H. The total circumferential (inside and outside surfaces) as well as the maximum radial residual stresses, for the two methods were thus determined and are presented in Table 4.4.

[3] - by J. Wong [17].

Table 4.4: Total (Experimental) Residual Stresses in Thin Composite Rings.

Ring Number	Overlap (cm.)	Strain Reading From Radial Cut ($\times 10^{-6}$) Outside	Inside	Circumferential Residual Stress (MPa) From Overlap Outside	Inside	Circumferential Residual Stress (MPa) From Strain Reading Outside	Inside
SR-10	0.88	335	-369	-9.2	9.5	-14.3	14.8
SR-15	1.30	374	-386	-14.0	14.5	-16.1	16.6
SR-20	1.22	386	-403	-14.8	15.2	-18.8	19.3
SR-30	1.80	496	-523	-22.6	23.3	-25.4	26.1
SR-35	1.90	516	-535	-24.9	25.6	-27.0	27.8
CR-10	1.35	407	-420	-46.6	47.9	-53.8	55.4
CR-20	1.52	449	-459	-49.4	50.8	-58.0	59.7
CR-30	1.82	498	-526	-67.8	69.8	-73.0	75.2
CR-35	1.85	571	-587	-64.8	66.8	-73.4	75.7
KR-10	1.75	*	-443	-33.9	34.9	-33.6	34.5
KR-20	2.15	550	-563	-44.4	45.6	-45.4	46.7
KR-30	2.10	578	*	-47.4	48.7	*	*
KR-35	1.82	540	-558	-41.8	42.9	-48.2	49.7

Notes: * - Insufficient data - see Table 4.3

4.3.3.6 Residual stress due to resin shrinkage and resin flow/fibre migration.

The various residual stresses, namely the circumferential outside σ_{θ_o}, circumferential inside σ_{θ_i}, and the maximum radial stress σ_{rmax}, for the winding tension and thermal cool down terms, as well as the total experimental results are presented in Table 4.5, Table 4.6, and Table 4.7. The circumferential residual stress components are plotted in Figure 4.10, Figure 4.11, and Figure 4.12, while the radial residual stress components are plotted in Figure 4.13, Figure 4.14, and Figure 4.15.

The residual stresses due to both resin shrinkage during curing and resin flow/fibre migration and other factors have been estimated as the Total experimental residual stress less the winding tension and thermal cooldown components as shown in the figures mentioned above. It was determined that the largest constituents of the residual stress were for the unknown factors including the resin shrinkage and resin flow/fibre migration.

Table 4.5: Residual Stresses in Thin E/XAS Carbon Composite Rings.

RING NO.	CR-10			CR-20			CR-30		
RESIDUAL STRESS	σ_{θ_o} (MPa.)	σ_{θ_i} (MPa.)	σ_{rmax} (MPa.)	σ_{θ_o} (MPa.)	σ_{θ_i} (MPa.)	σ_{rmax} (MPa.)	σ_{θ_o} (MPa.)	σ_{θ_i} (MPa.)	σ_{rmax} (MPa.)
a. Winding Tension	3.94	-4.54	-0.05	7.67	-8.81	-0.09	12.39	-14.42	-0.15
b. Thermal Cooldown	-8.10	8.30	0.10	-3.80	4.00	0.09	-10.30	11.00	0.11
c. Total (Experimental)	-53.80	55.40	0.55	-58.00	59.70	0.58	-73.00	75.20	0.74
d. Difference (c-a-b)	-49.64	51.64	0.50	-61.87	64.51	0.58	-75.09	78.62	0.78

Table 4.6: Residual Stresses in Thin S2-glass Composite Rings.

RING NO.	SR-15			SR-30			SR-35		
RESIDUAL STRESS	σ_{θ_O} (MPa.)	σ_{θ_I} (MPa.)	σ_{rmax} (MPa.)	σ_{θ_O} (MPa.)	σ_{θ_I} (MPa.)	σ_{rmax} (MPa.)	σ_{θ_O} (MPa.)	σ_{θ_I} (MPa.)	σ_{rmax} (MPa.)
a. Winding Tension	2.82	-4.10	-0.04	8.48	-9.16	-0.09	10.19	-11.00	-0.11
b. Thermal Cooldown	-2.50	2.60	0.02	-1.40	1.40	0.02	-1.50	1.50	0.02
c. Total (Experimental)	-16.10	16.60	0.17	-25.40	26.10	0.27	-27.00	27.80	0.29
d. Difference (c-a-b)	-17.40	18.10	0.19	-32.48	33.86	0.34	-35.69	37.33	0.38

Table 4.7: Residual Stresses in Thin Kevlar 49 Composite Rings.

RING NO.	KR-10			KR-20			KR-35		
RESIDUAL STRESS	σ_{θ_o} (MPa.)	σ_{θ_i} (MPa.)	σ_{rmax} (MPa.)	σ_{θ_o} (MPa.)	σ_{θ_i} (MPa.)	σ_{rmax} (MPa.)	σ_{θ_o} (MPa.)	σ_{θ_i} (MPa.)	σ_{rmax} (MPa.)
a. Winding Tension	2.10	-2.28	-0.02	4.41	-4.81	-0.05	8.49	-9.37	-0.10
b. Thermal Cooldown	-5.90	6.00	0.08	-8.70	8.90	0.09	-9.10	9.40	0.11
c. Total (Experimental)	-33.60	34.50	0.32	-45.40	46.70	0.44	-48.20	49.70	0.50
d. Difference (c-a-b)	-29.84	30.78	0.26	-41.11	42.61	0.40	-47.59	49.67	0.49

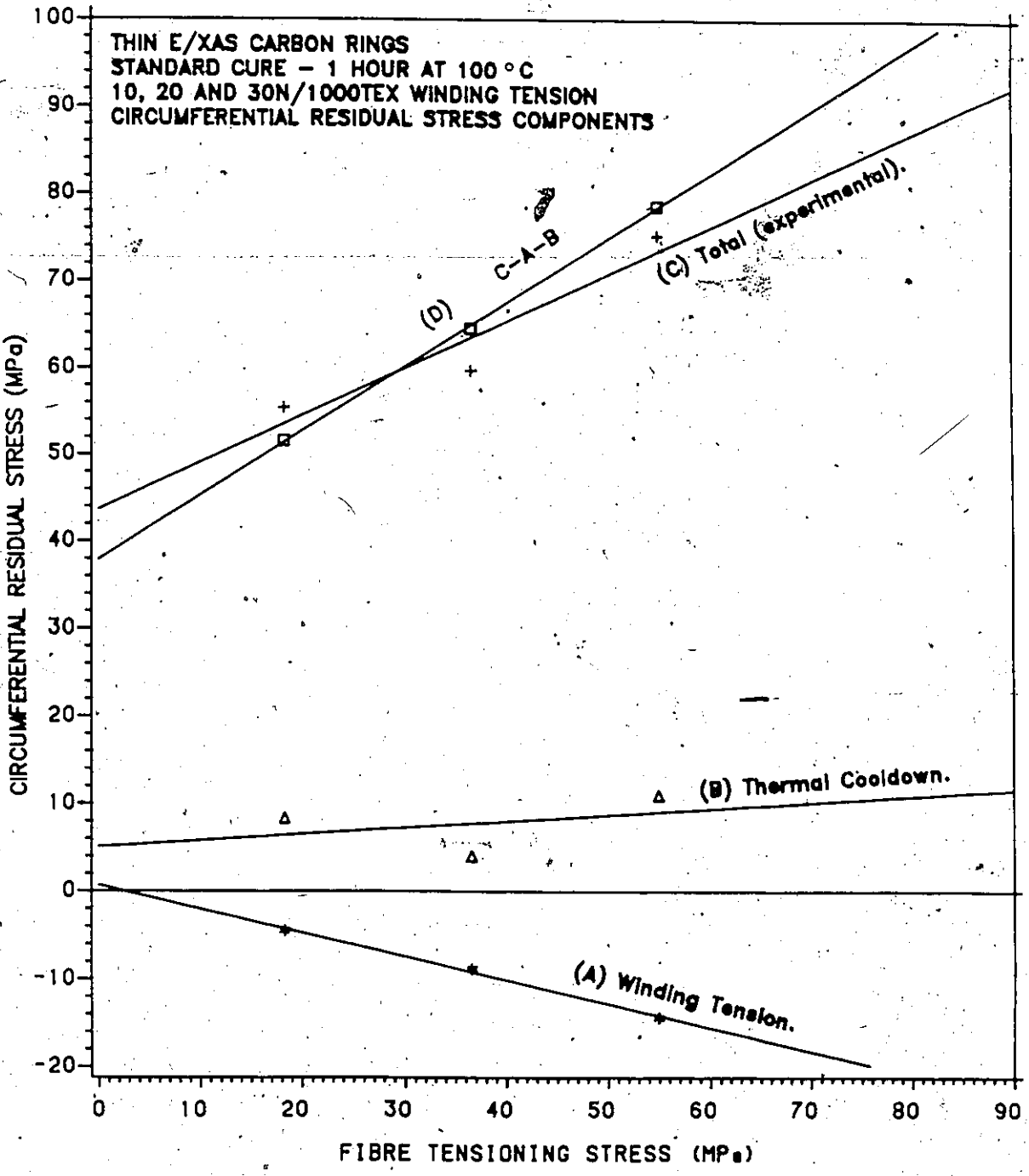

Figure 4.10: Circumferential residual stress components as a function of winding tension. (thin E/XAS carbon composite rings).

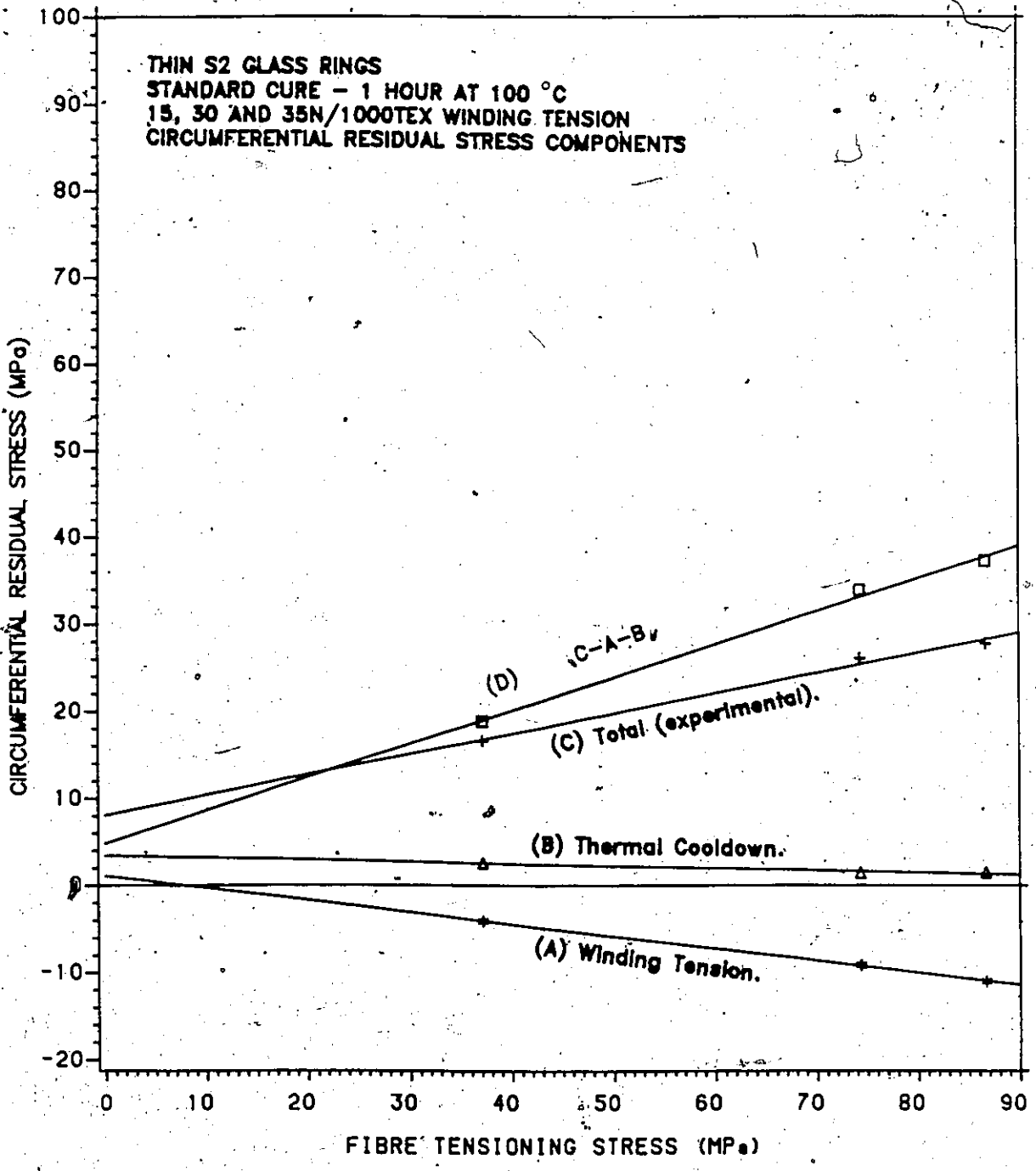

Figure 4.11: Circumferential residual stress components as a function of winding tension. (thin S2-glass composite rings).

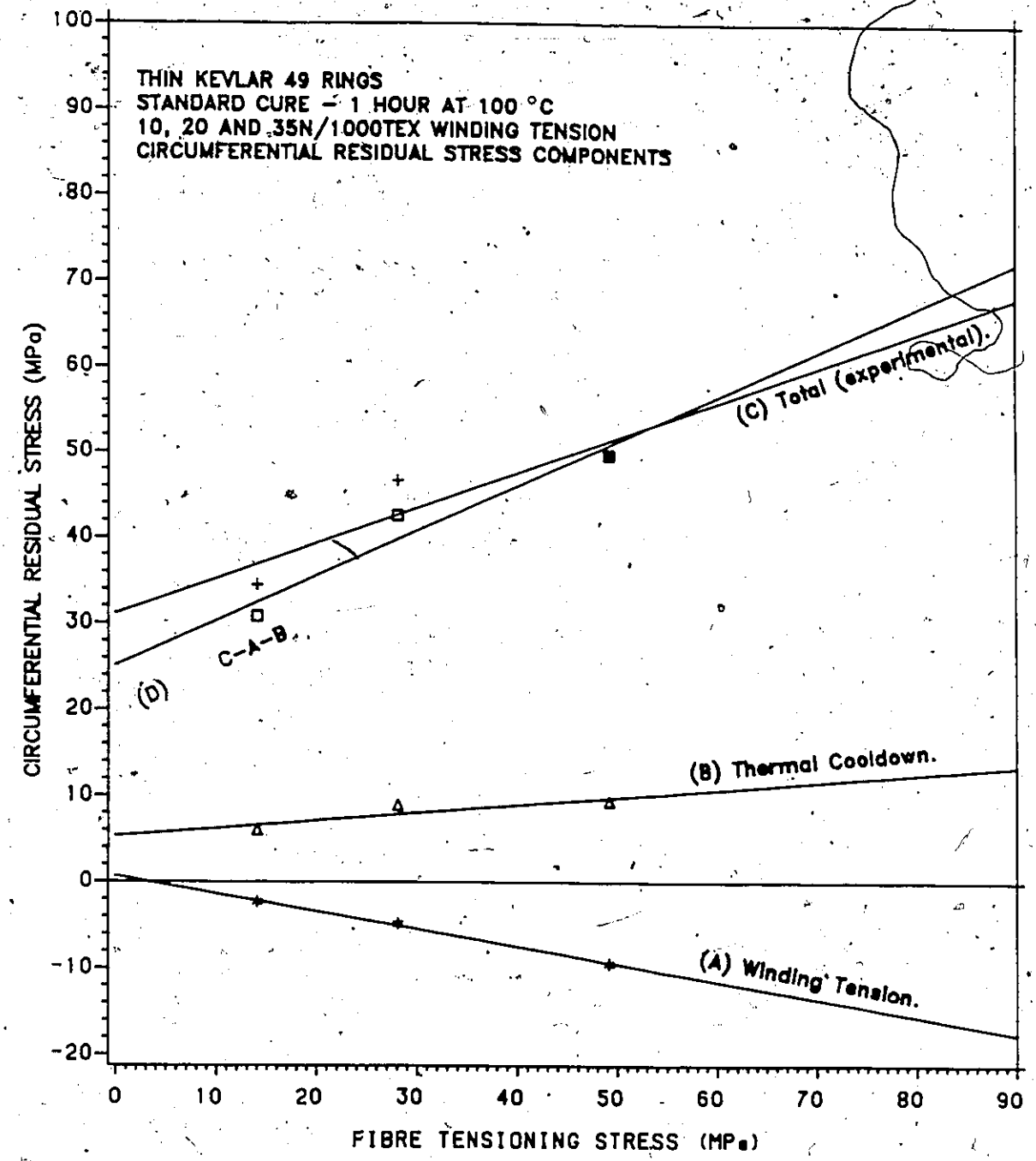

Figure 4.12: Circumferential residual stress components as a function of winding tension. (thin Kevlar 49 composite rings).

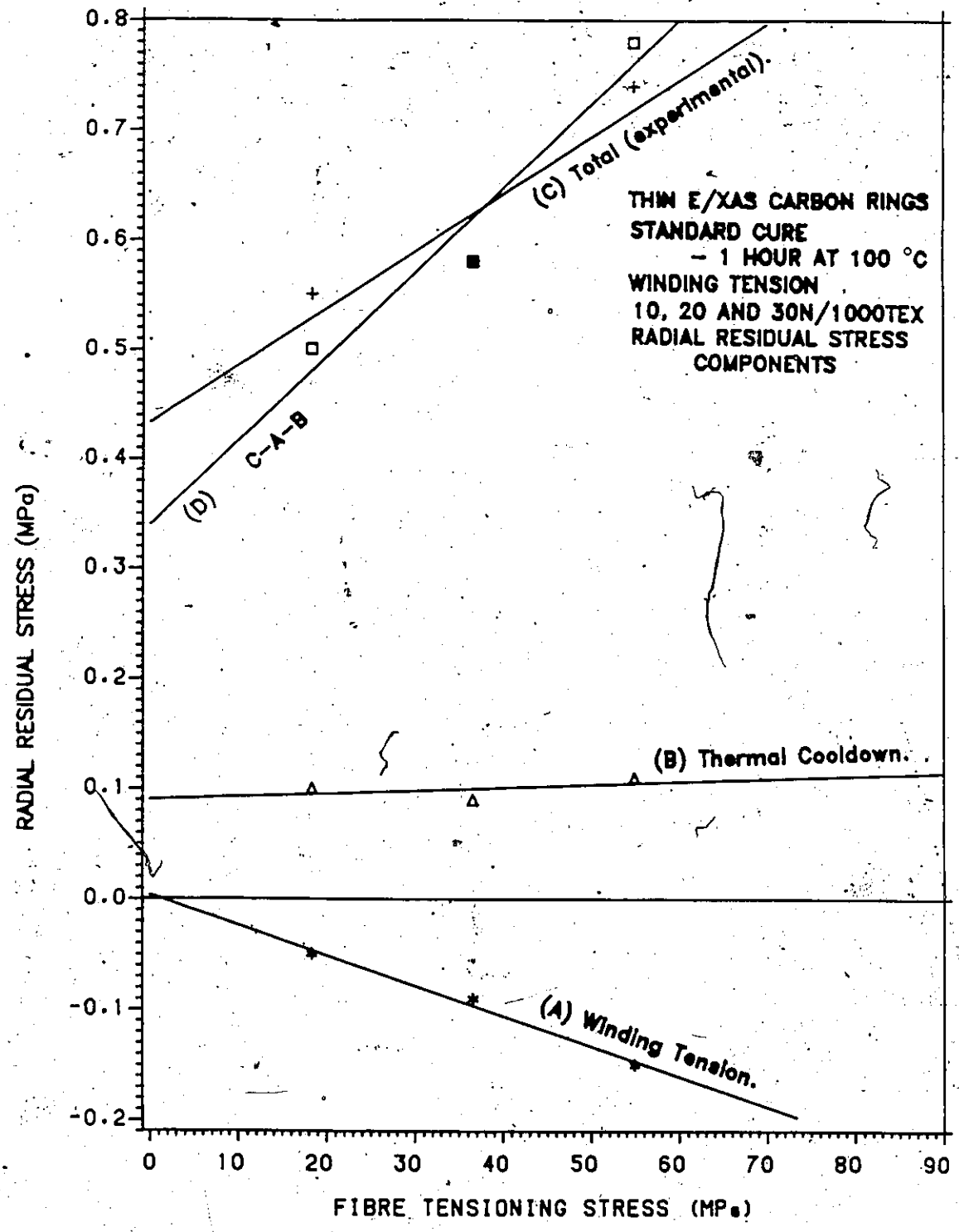

Figure 4.13: Radial residual stress components as a function of winding tension. (thin E/XAS carbon composite rings).

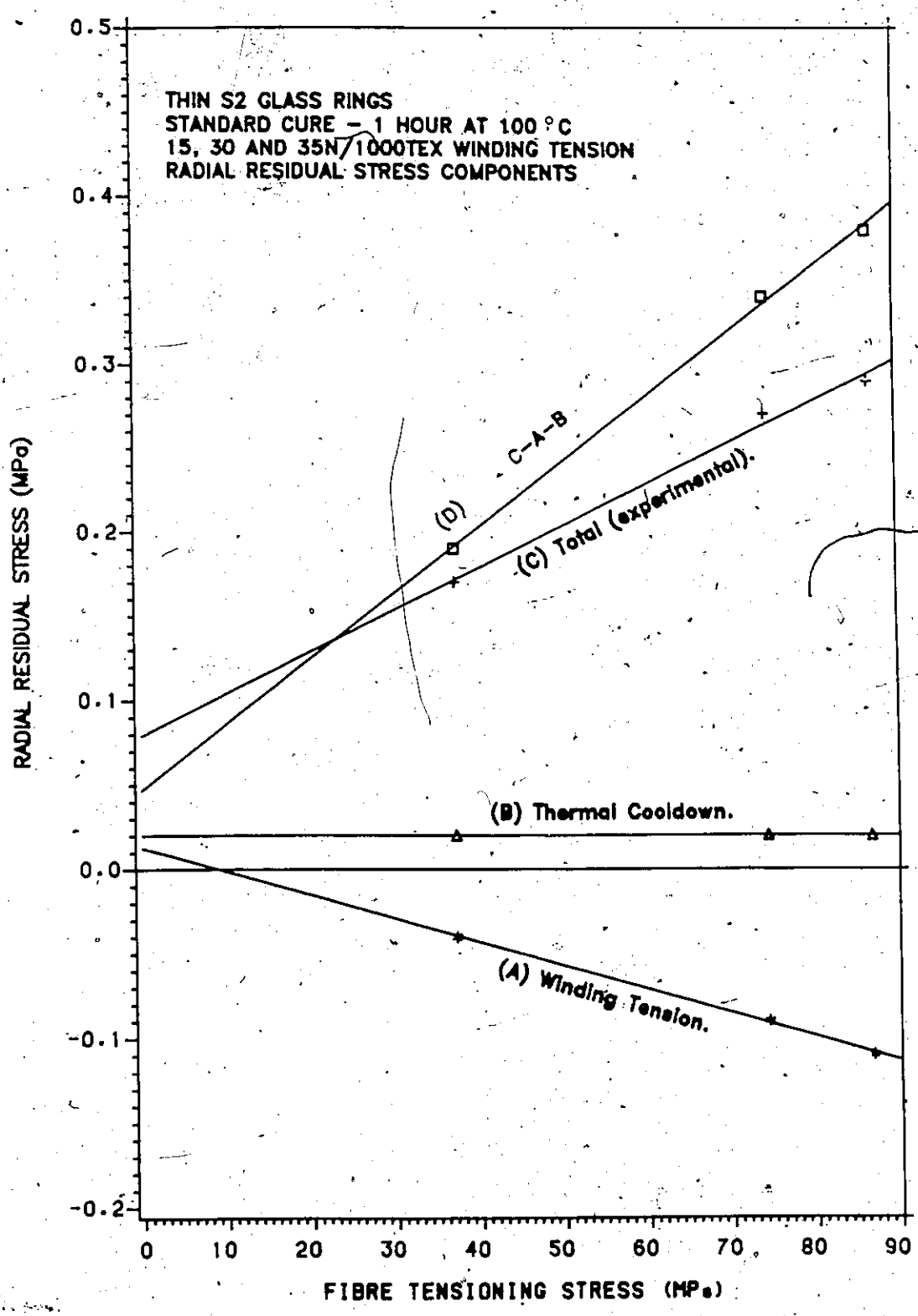

Figure 4.14: Radial residual stress components as a function of winding tension. (thin S2-glass composite rings).

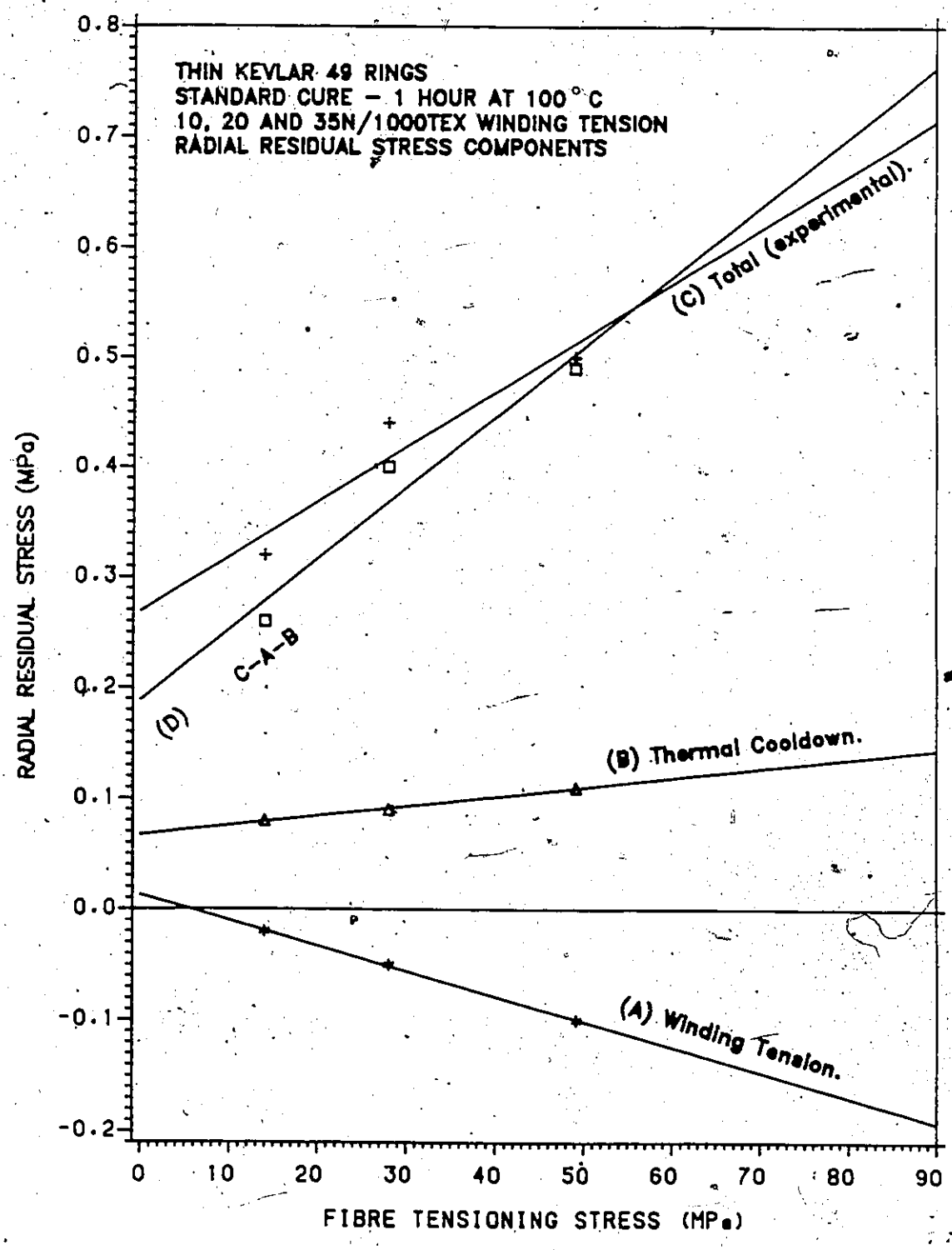

Figure 4.15: Radial residual stress components as a function of winding tension. (thin Kevlar 49 composite rings).

4.4 Residual stress measurement in thick composite rings.

4.4.1 Residual strain measurement in radially thick composite rings.

The composite rings of the previous section were on the order of 0.25 cm thick with an axial thickness of 2.54 cm. As detailed in Chapter 3, radially thick rings were wound with the same axial thickness and inner diameter but with an increased radial thickness varying from 4.2 to 8.1 cm. The results of tests carried out on these rings would give indications relating size effect to residual stress. This investigation was necessary since the final designs for the full size flywheels were between 7.5 to 9.0 cm radially thick, with an axial thickness of 7.5 to 8.9 cm. Further tests on rings with the increased axial thickness are discussed in Section 4.4.3.

Eleven S2-glass and nine E/XAS carbon rings were evaluated for residual stress. No Kevlar 49 rings were produced since this material was not considered for advanced flywheel designs[20]. For all but four of the rings (three S2-glass and one E/XAS carbon) data was obtained with strain gauges and by ring diameter change. For those four, the data was measured only in terms of a diameter change. Table 4.8 summarizes the manufacturing parameters as well as the method of obtaining the data. Details of the prediction of residual stresses from these various inputs can be found in Section 4.3.3.5.

Table 4.8: Manufacturing Parameters for Radially Thick Rings.

Ring Number	Fibre Type	Winding Tension Newtons/1000TEX	Data	Cure Schedule
S2-TK-3-35	S2-glass	Constant 35	1	Standard
S2-TK-4-VAR(i)	S2-glass	Increasing 5-55	1	Standard
S2-TK-5-VAR(d)	S2-glass	Decreasing 55-35	2	Standard
S2-TK-6-VAR(d)	S2-glass	Decreasing 55-30	2	Standard
S2-TK-7-VAR(i)	S2-glass	Increasing 30-55	2	Standard
S2-TK-8-35	S2-glass	Constant 35	2	Standard
S2-TK-10-25	S2-glass	Constant 25	2	Standard
S2-TK-16-25	S2-glass	Constant 25	2	Standard
S2-TK-17-25	S2-glass	Constant 25	2	Standard
S2-TK-24-25	S2-glass	Constant 25	1	Standard
S2-TK-26-15	S2-glass	Constant 15	2	Standard
XAS-TK-2-25	E/XAS carbon	Constant 25	2	Standard
XAS-TK-3-25	E/XAS carbon	Constant 25	2	Two Stage
XAS-TK-4-25	E/XAS carbon	Constant 25	2	Low Temp.
XAS-TK-5-25	E/XAS carbon	Constant 25	2	Low Temp.
XAS-TK-6-25	E/XAS carbon	Constant 25	2	Controlled Heat-Up
XAS-TK-10-25	E/XAS carbon	Constant 25	2	Two Stage
XAS-TK-12-25	E/XAS carbon	Constant 25	2	Two Stage + Postcure
XAS-TK-18-25	E/XAS carbon	Constant 25	2	Two Stage + Postcure
XAS-TK-25-25	E/XAS carbon	Constant 25	1	Two Stage

Notes for 'DATA' column:

1. Data obtained by 'overlap method'.
2. Data obtained by strain gauges as well as diameter change methods.

As the overlap method was previously employed on the thin rings, initial experiments on the first two radially thick S2-glass rings were carried out with this method. The amount of overlap was difficult to measure since these larger rings did not exhibit as great an overlap as did the thin ones. From this initial experience with these two rings, a more refined method was implemented. Strain gauges (Micro Measurements, EA-06-500BH-120) were attached on the inside surface of the rings, in the circumferential direction, so that the change in strain could be measured when the ring was cut. As a secondary set of measurements, the diameter change, was also taken. Readings from the ring sectioning experiments are given in Table 4.9.

The strain readings were used as input for the 'OVERLAP' computer program in a manner similar to the thin rings. This program generated the residual stress profiles for the rings in the circumferential direction and are presented for selective comparisons as Figure 4.16, Figure 4.18, Figure 4.20, Figure 4.22, and Figure 4.24, while the profiles for the radial directions are shown in Figure 4.17, Figure 4.19, Figure 4.21, Figure 4.23, and Figure 4.25.

Table 4.9: Data Used for 'OVERLAP' Program.

Ring No.	Annular Thickness (cm.)	Initial Diameter (Pre Cut) (cm.)	Final Diameter (Post Cut) (cm.)	Over Lap (cm.)	Inside Strain ($x10^{-6}$)
S2-TK-3-35	6.65	26.71	26.59	0.35	*
S2-TK-4-VAR(i)	4.15	26.71	26.59	0.36	*
S2-TK-5-VAR(d)	5.00	26.71	26.55	0.49	800
S2-TK-6-VAR(d)	6.40	26.71	26.57	0.44	800
S2-TK-7-VAR(d)	5.30	26.71	26.62	0.26	500
S2-TK-8-35	3.19	26.71	26.62	0.29	720
S2-TK-10-25	5.45	26.71	26.60	0.34	718
S2-TK-16-25	5.45	26.72	26.59	0.37	704
S2-TK-17-25	8.00	26.72	26.60	0.35	836
S2-TK-24-25	9.21	26.70	26.60	0.31	*
S2-TK-26-15	8.33	26.72	26.60	0.38	920
XAS-TK-2-25	6.20	26.73	26.61	0.37	718
XAS-TK-3-25	5.95	26.73	26.60	0.38	709
XAS-TK-4-25	6.05	26.73	26.66	0.20	422
XAS-TK-5-25	6.20	26.73	26.65	0.23	434
XAS-TK-6-25	6.70	26.74	26.62	0.37	708
XAS-TK-10-25	7.62	26.74	26.62	0.38	792
XAS-TK-12-25	7.60	26.73	26.53	0.63	1285
XAS-TK-18-25	7.74	26.73	26.55	0.60	1180
XAS-TK-25-25	8.61	26.72	26.60	0.40	*

Note: * - No gauges mounted.

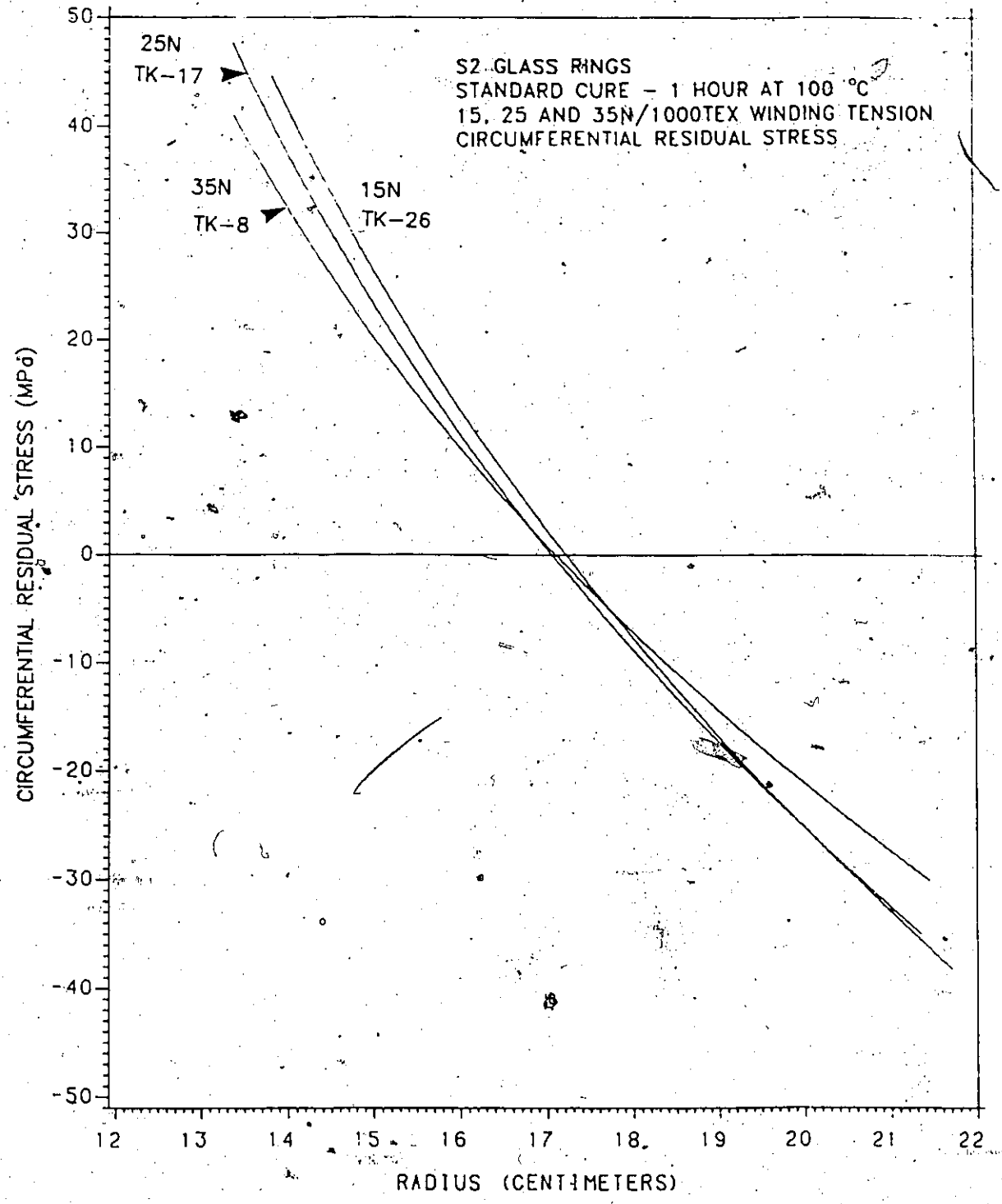

Figure 4.16: Circumferential residual stress as a function of ring thickness and constant winding tension. (radially thick S2-glass composite rings).

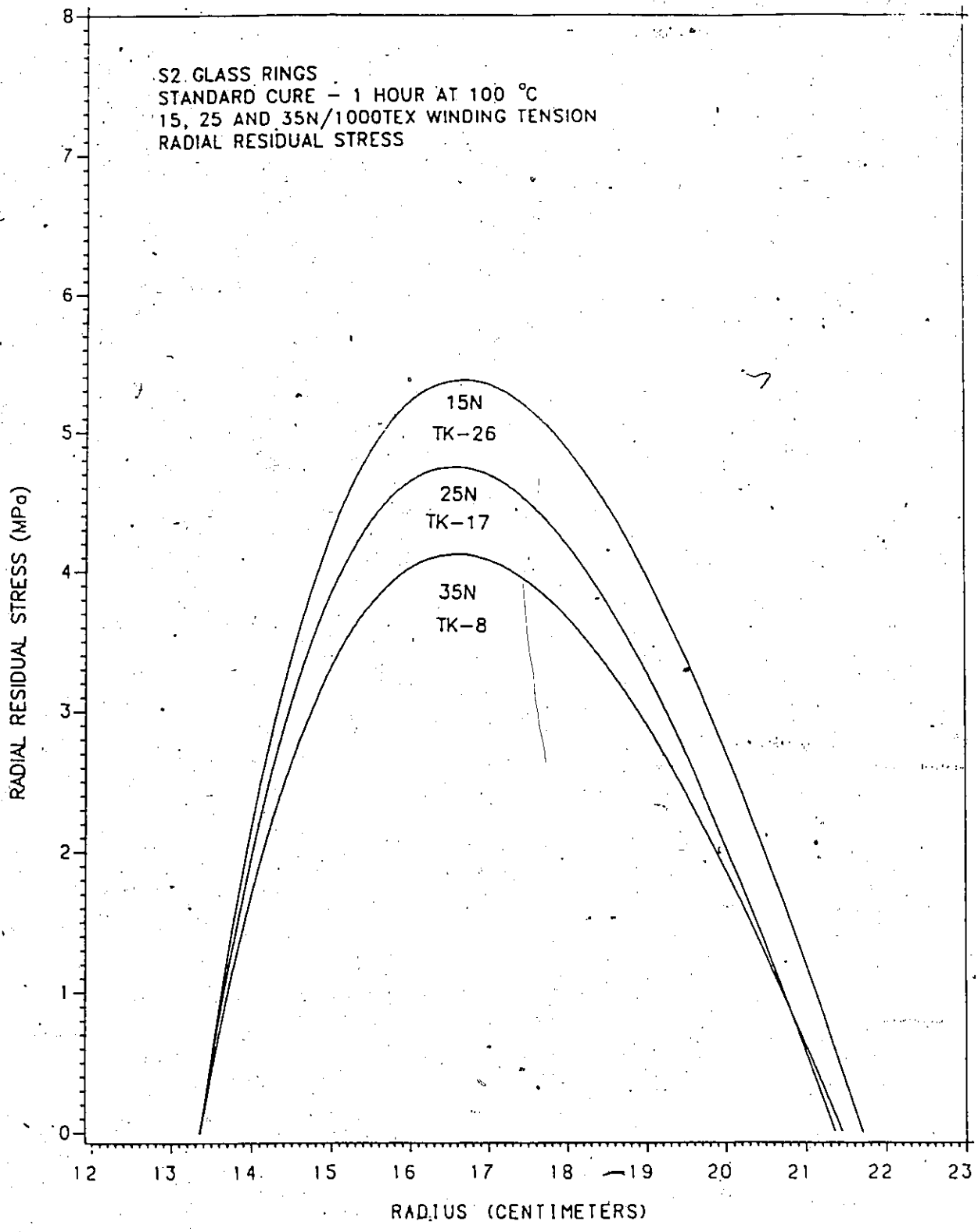

Figure 4.17: Radial residual stress as a function of ring thickness and constant winding tension. (radially thick S2-glass composite rings).

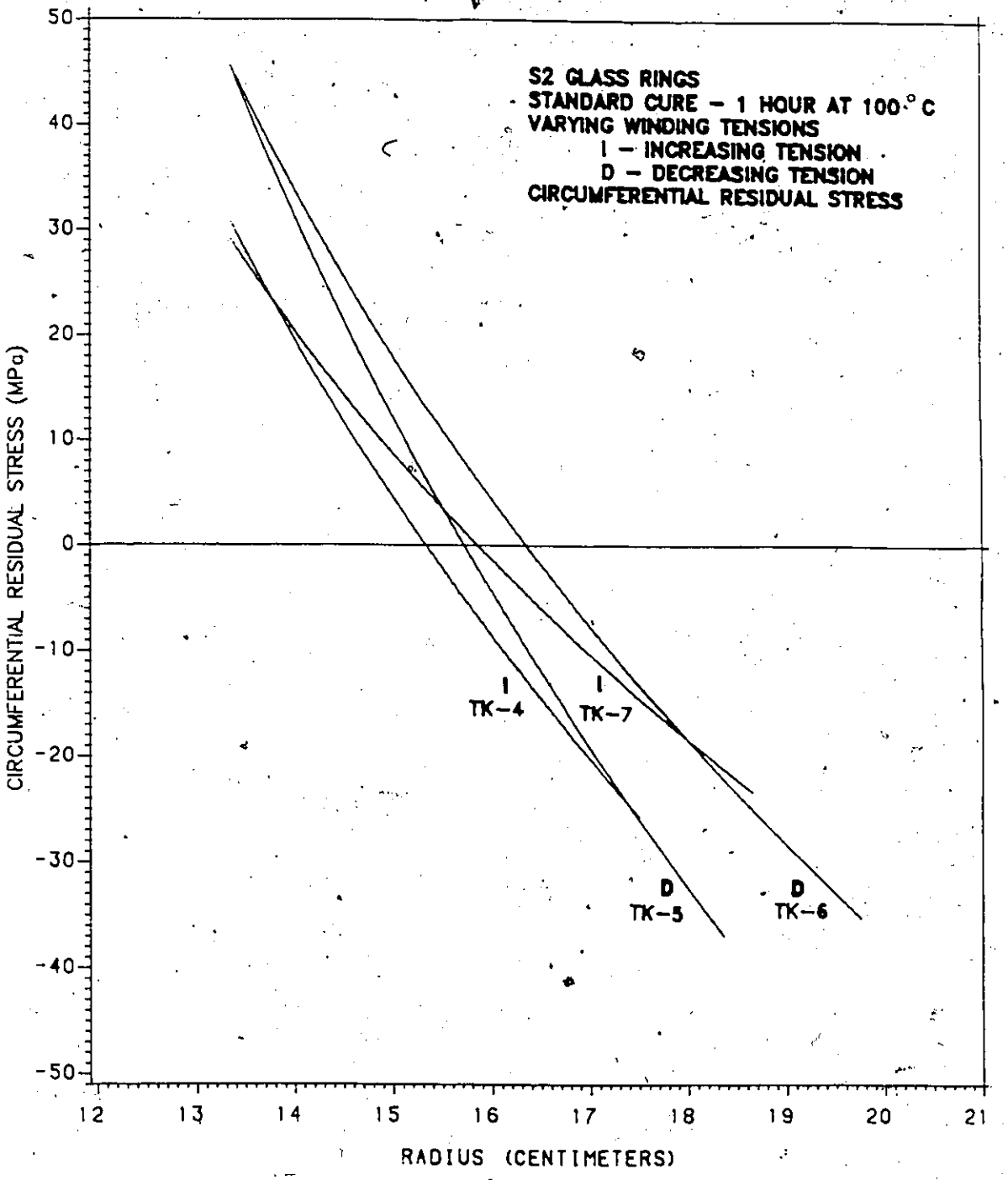

Figure 4.18: Circumferential residual stress as a function of ring thickness and variable winding tension. (radially thick S2-glass composite rings).

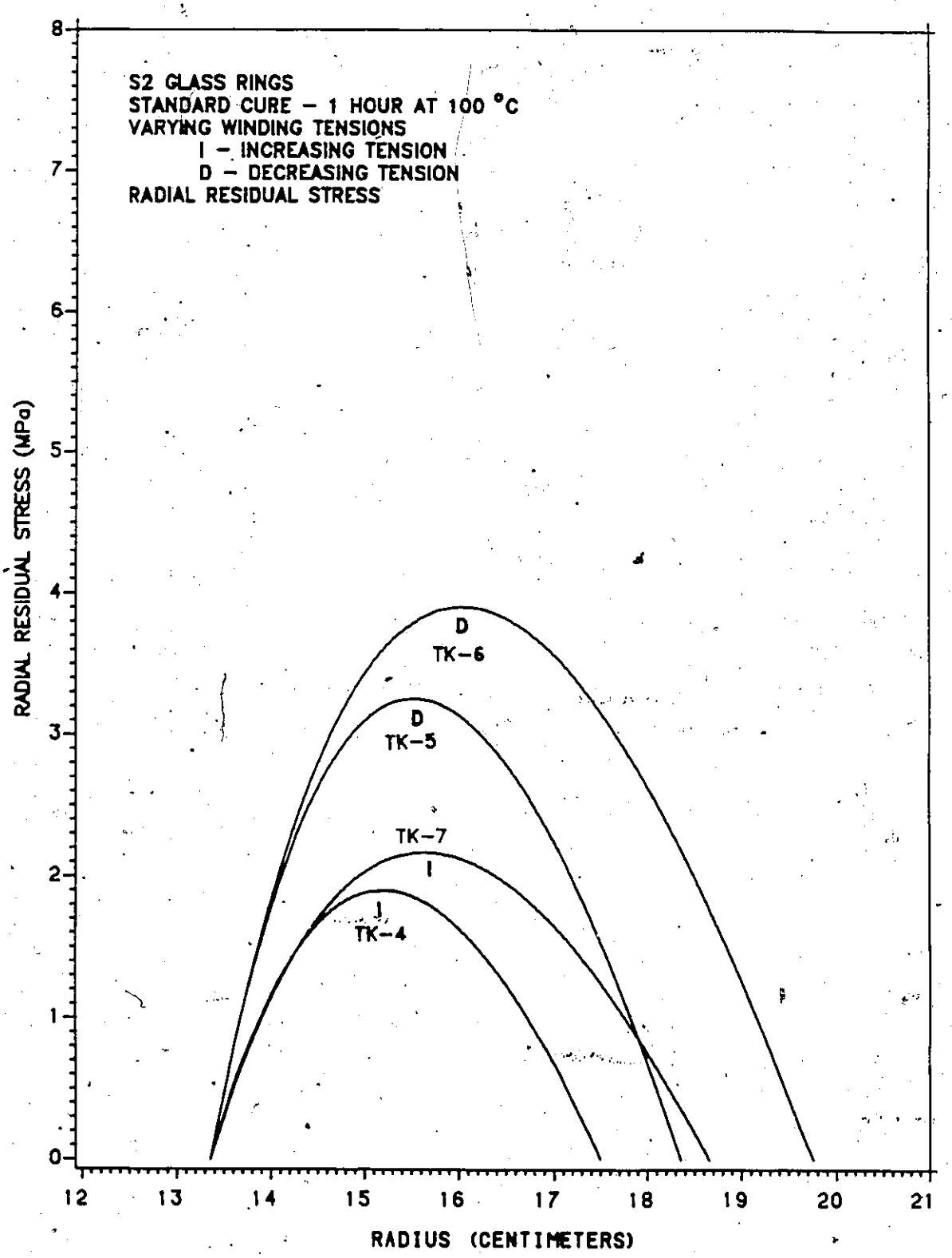

Figure 4.19: Radial residual stress as a function of ring thickness and variable winding tension. (radially thick S2-glass composite rings).

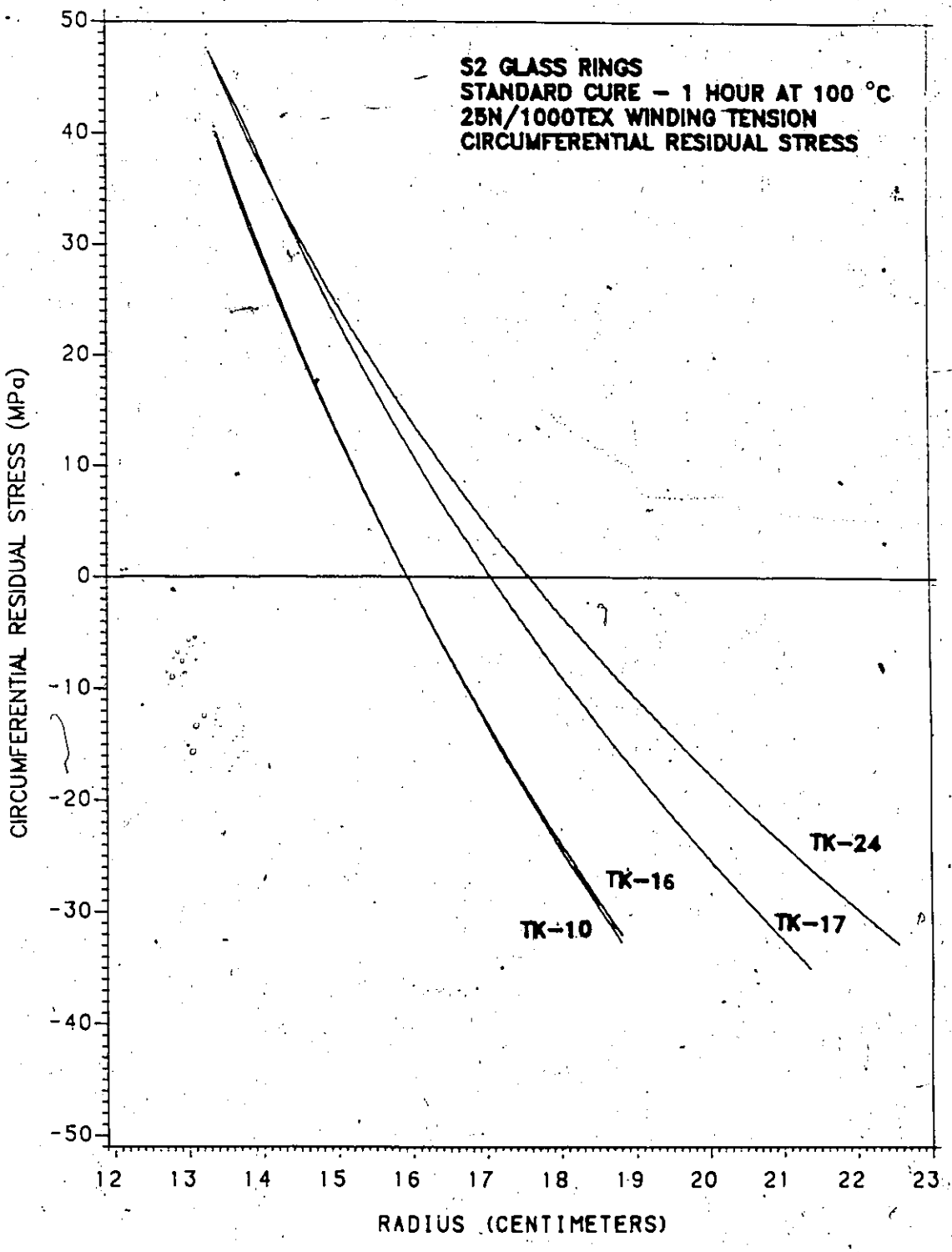

Figure 4.20: Circumferential residual stress as a function of ring thickness and constant winding tension. (radially thick S2-glass composite rings).

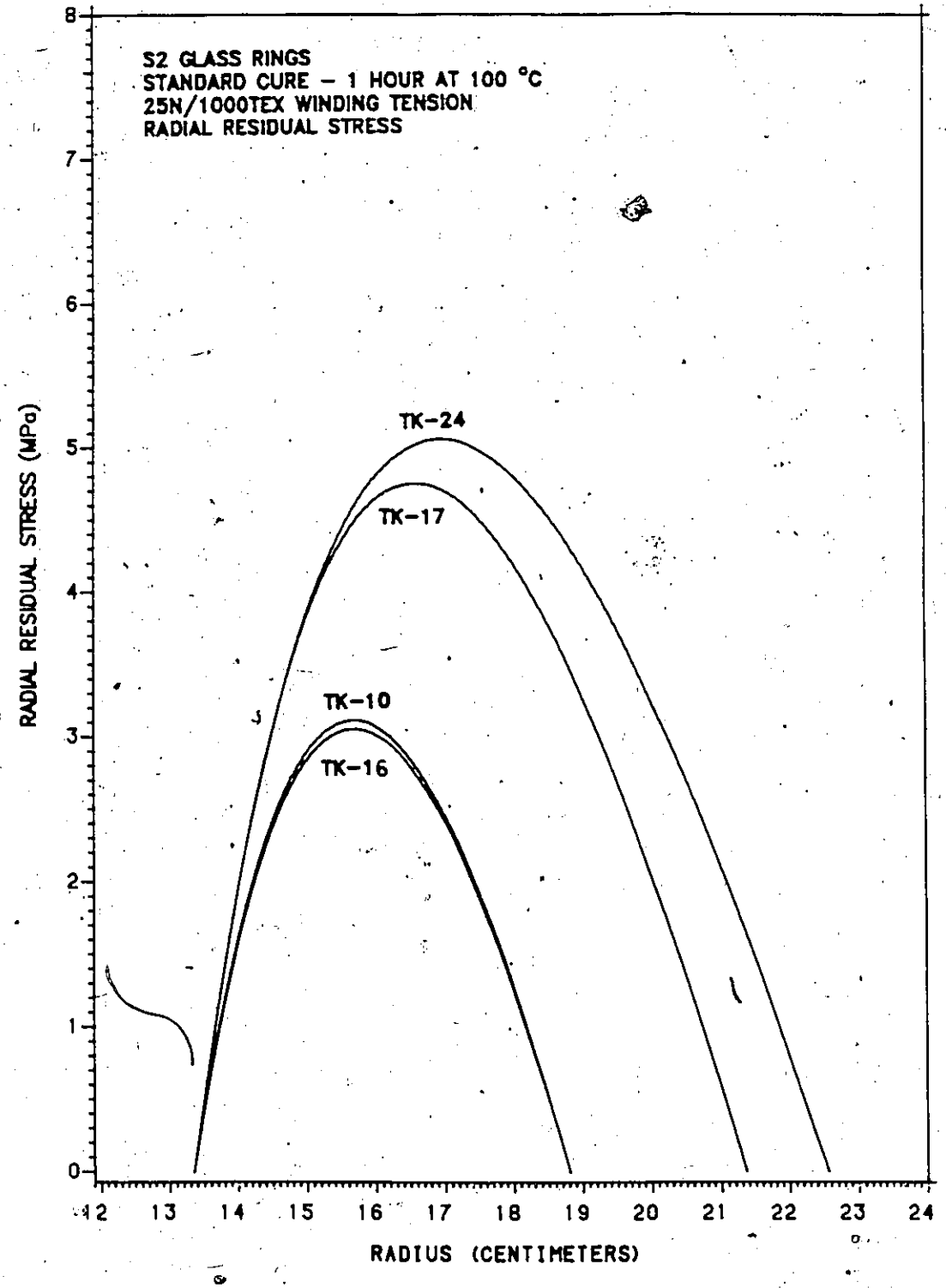

Figure 4.21: Radial residual stress as a function of ring thickness and constant winding tension. (radially thick S2-glass composite rings).

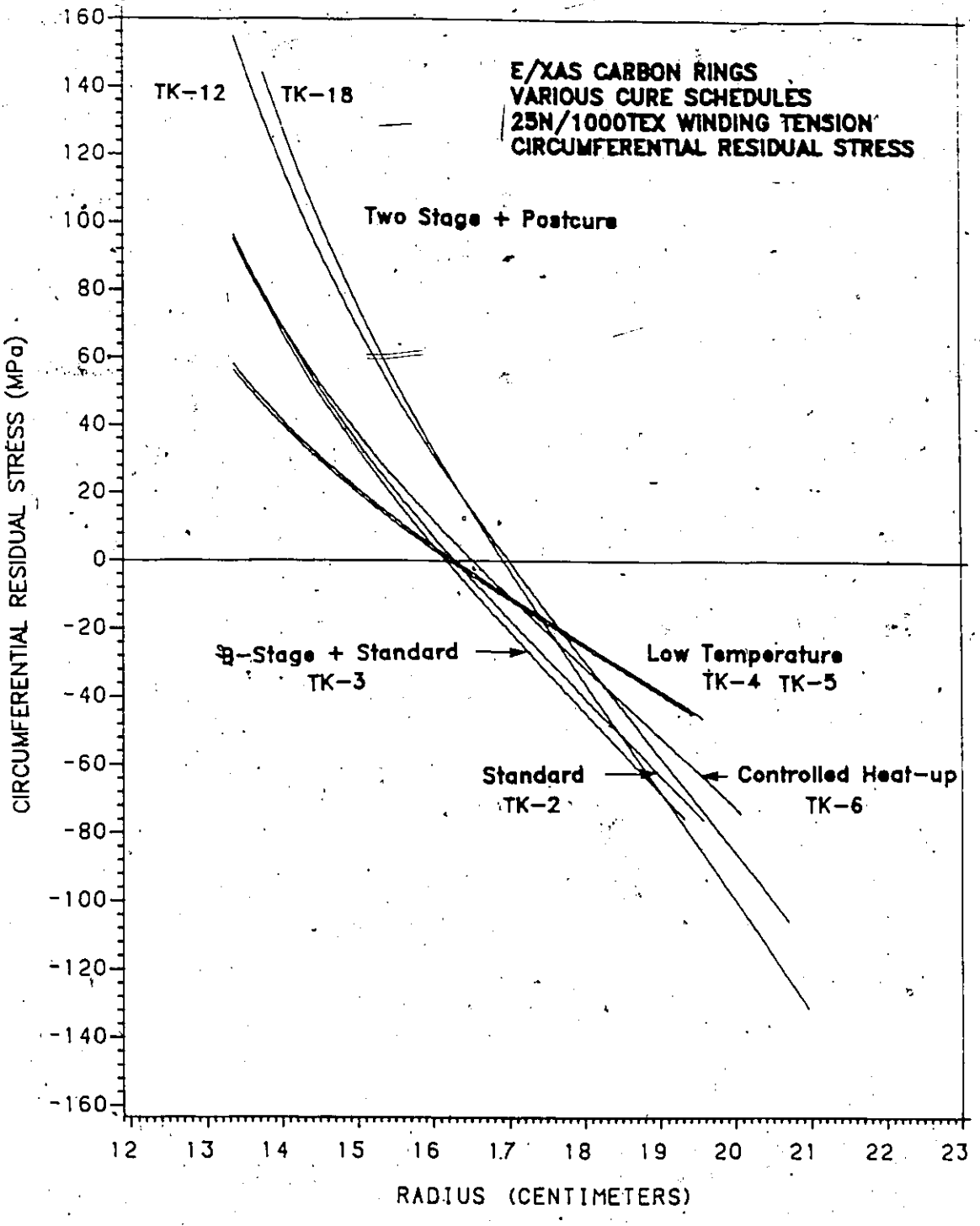

Figure 4.22: Circumferential residual stress as a function of ring thickness and cure schedule. (radially thick E/XAS carbon composite rings).

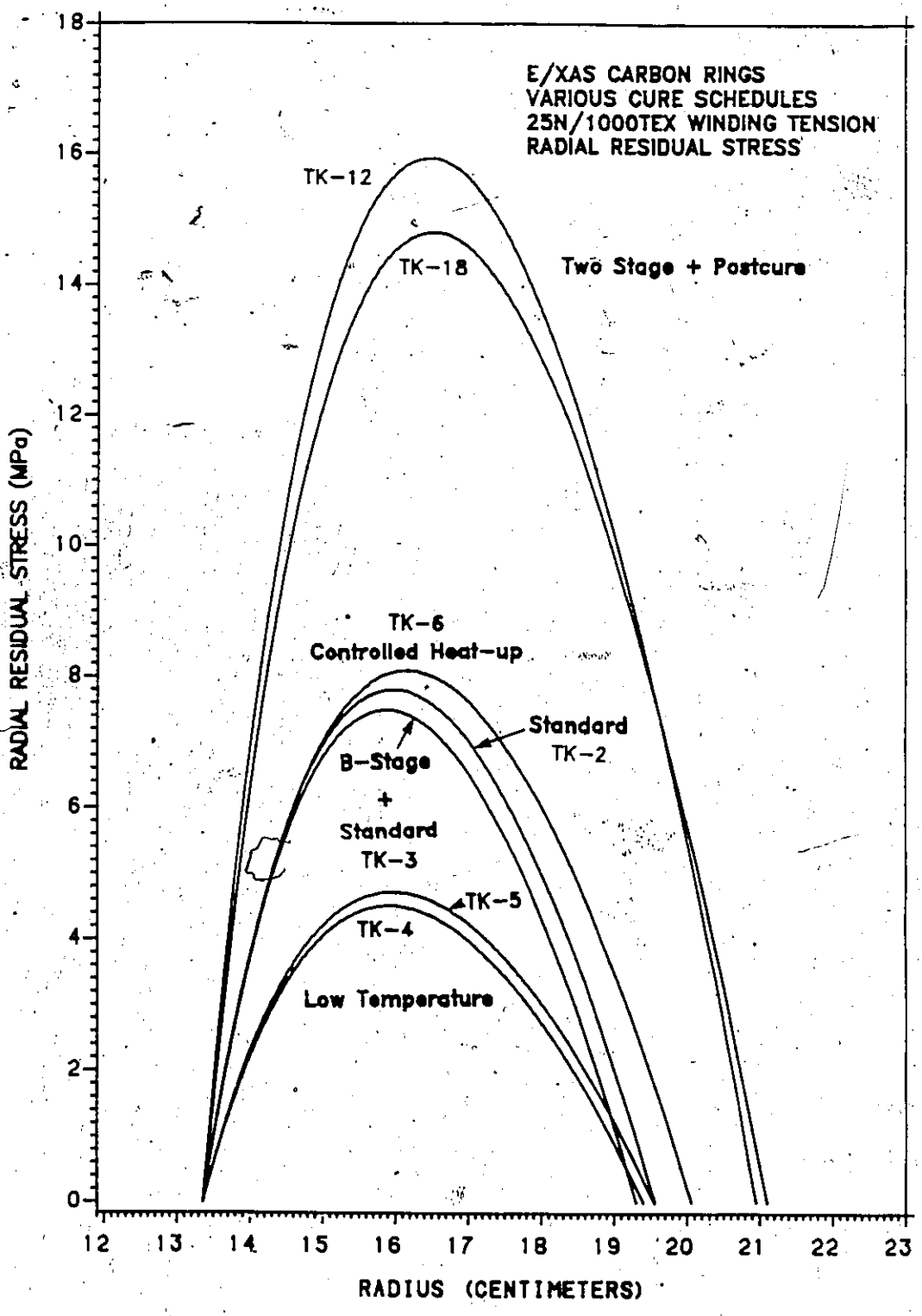

Figure 4.23: Radial residual stress as a function of ring thickness and cure schedule. (radially thick E/XAS carbon composite rings).

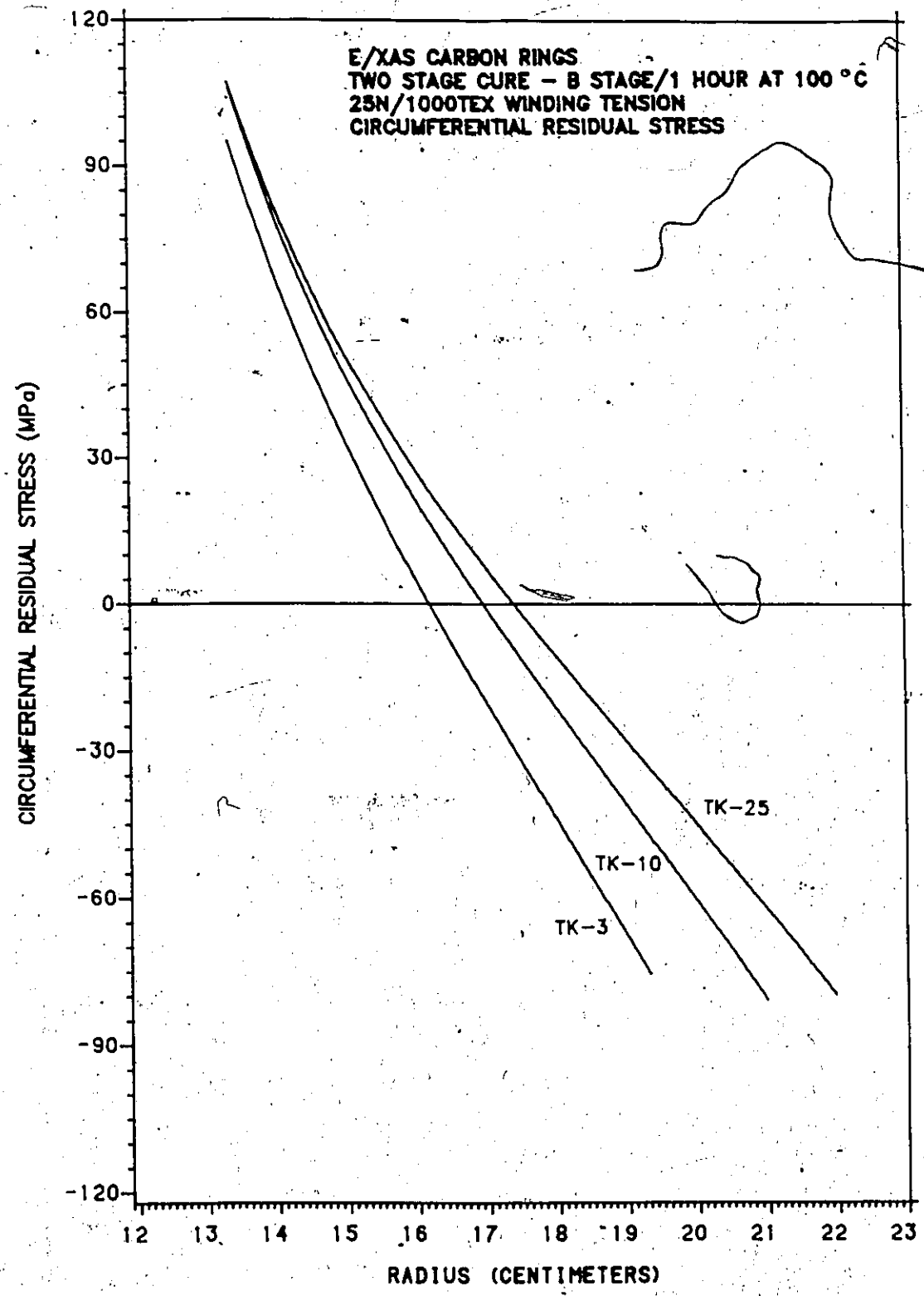

Figure 4.24: Circumferential residual stress as a function of ring thickness and constant winding tension. (radially thick E/XAS carbon composite rings).

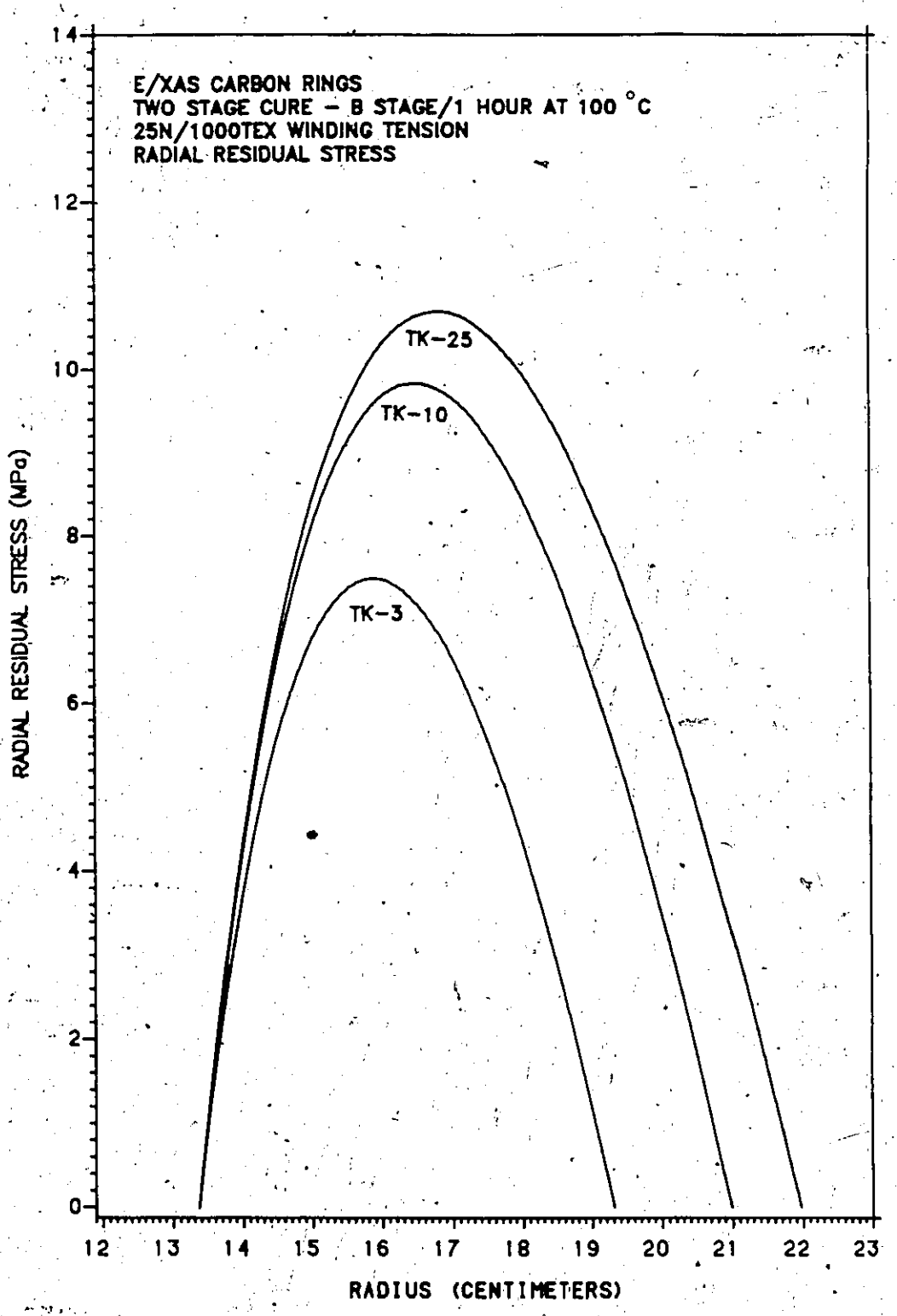

Figure 4.25: Radial residual stress as a function of ring thickness and constant winding tension. (radially thick E/XAS carbon composite rings).

4.4.2 Theoretical determination of transverse sensitivity on radially thick composite rings.

In order to determine if 0/90° rosette gauges were required for the comparison of experimental and predicted radial residual strains (Section 4.4.3), initial theoretical studies were performed. These tests were carried out on two composite rings, an S2-glass (S2-TK-8-35) and an E/XAS carbon (XAS-TK-2-25). With information from circumferential strain gauges mounted on the inner surface, radial and circumferential strain profiles were generated as shown in Figure 4.26 and Figure 4.27. Using the maximum value for the radial component and the equivalent circumferential reading, the effect of transverse sensitivity was then evaluated using equations 4.2 and 4.3. The results are tabulated in Table 4.10 with the calculations shown in Appendix I.

Table 4.10: Transverse Sensitivity Effects on S2-glass and E/XAS Carbon Composite Rings.

Ring Number	Radial Strain		Circumferential Strain	
	Computer Prediction	with Transverse Sensitivity	Computer Prediction	with Transverse Sensitivity
S2-TK-8-35	226.40	225.84	-206.21	-205.54
XAS-TK-2-25	904.09	905.06	-19.55	-15.95

Minimal effect of the transverse sensitivity led to the use of single strain gauges transversely mounted on the radially thick composite rings along with a circumferential

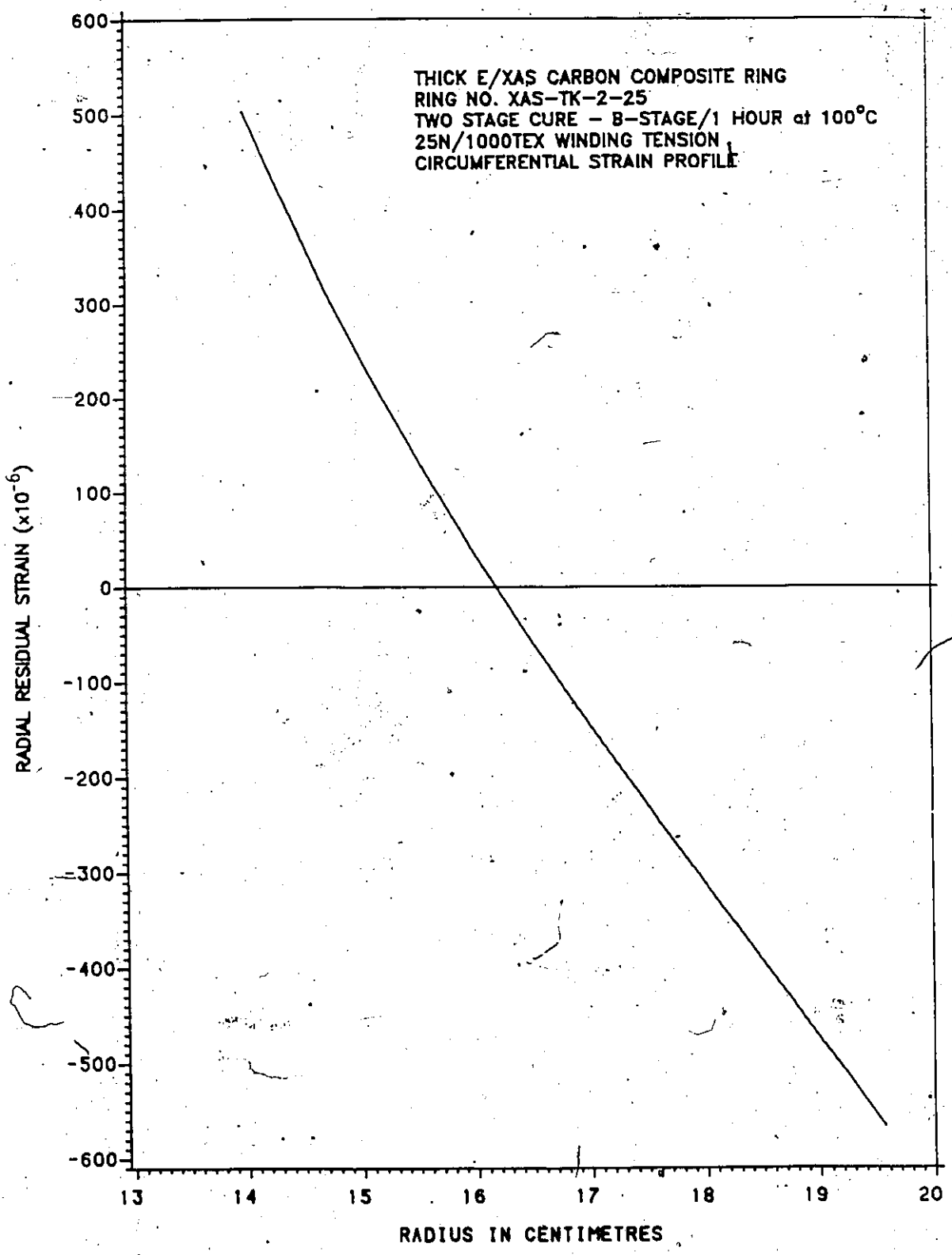

Figure 4.26: Typical circumferential strain profile generated by computer.

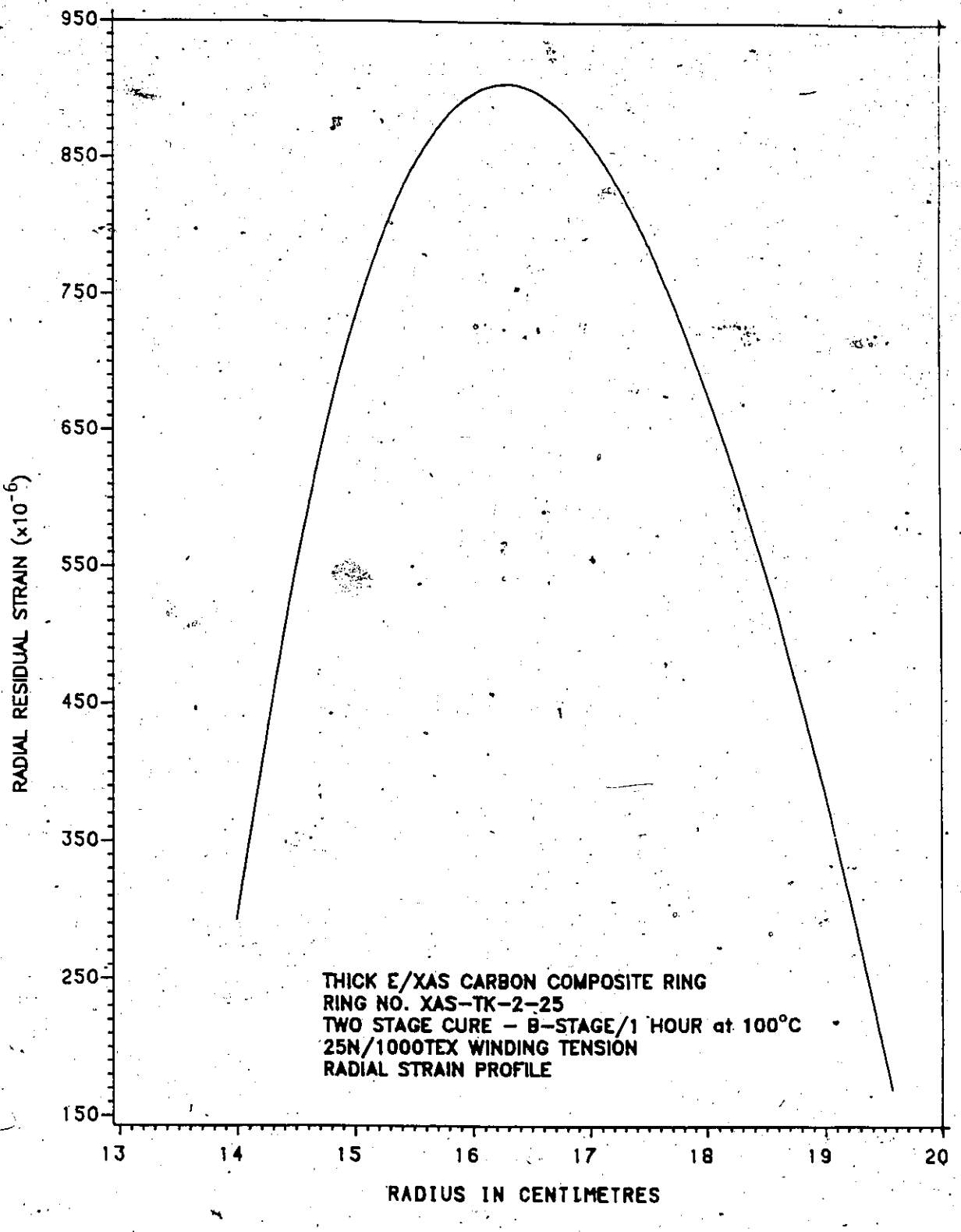

Figure 4.27: Typical radial strain profile generated by computer.

gauge on the inner surface (Figure 4.28). This was later confirmed experimentally, as part of the Flywheel Program, using 0/90° rosette gauges mounted on an S2-glass-E/XAS carbon biannular ring (Appendix I).

Figure 4.28: Typical gauge attachment on the radially thick composite rings.

4.4.3 Comparison of experimental and predicted radial residual strains.

The aforementioned computer program calculates the circumferential and radial residual stress profiles based upon experimental data generated during the radial cut technique. As an attempt to experimentally verify the radial results, strain gauges were mounted transversely on the side face of selected rings as mentioned in the previous

section and shown in Figure 4.28. These radial strain readings taken when the rings were radially cut were compared to the values produced by computer prediction. Of major interest was the radial strain profile which exhibits a parabolic profile as previously shown in Figure 4.27 on page 104. Since the radially mounted strain gauges measure the average strain over their gauge lengths, it was necessary to determine an average strain from the computer prediction. By graphically producing the strain profile (Figure 4.29) generated by the computer and superimposing the location of the strain gauge, an average reading was obtained. This was carried out by measuring the area of the profile covered by the gauge and dividing it by the gauge length of the strain gauge. Measuring the areas was performed by use of weight measurements, similar to the optical method previously mentioned (Section 4.3.1) and checked with a planimeter (SALMOIRAGH Model 236). The results from these measurements are tabulated in Table 4.11 and presented in Figure 4.30.

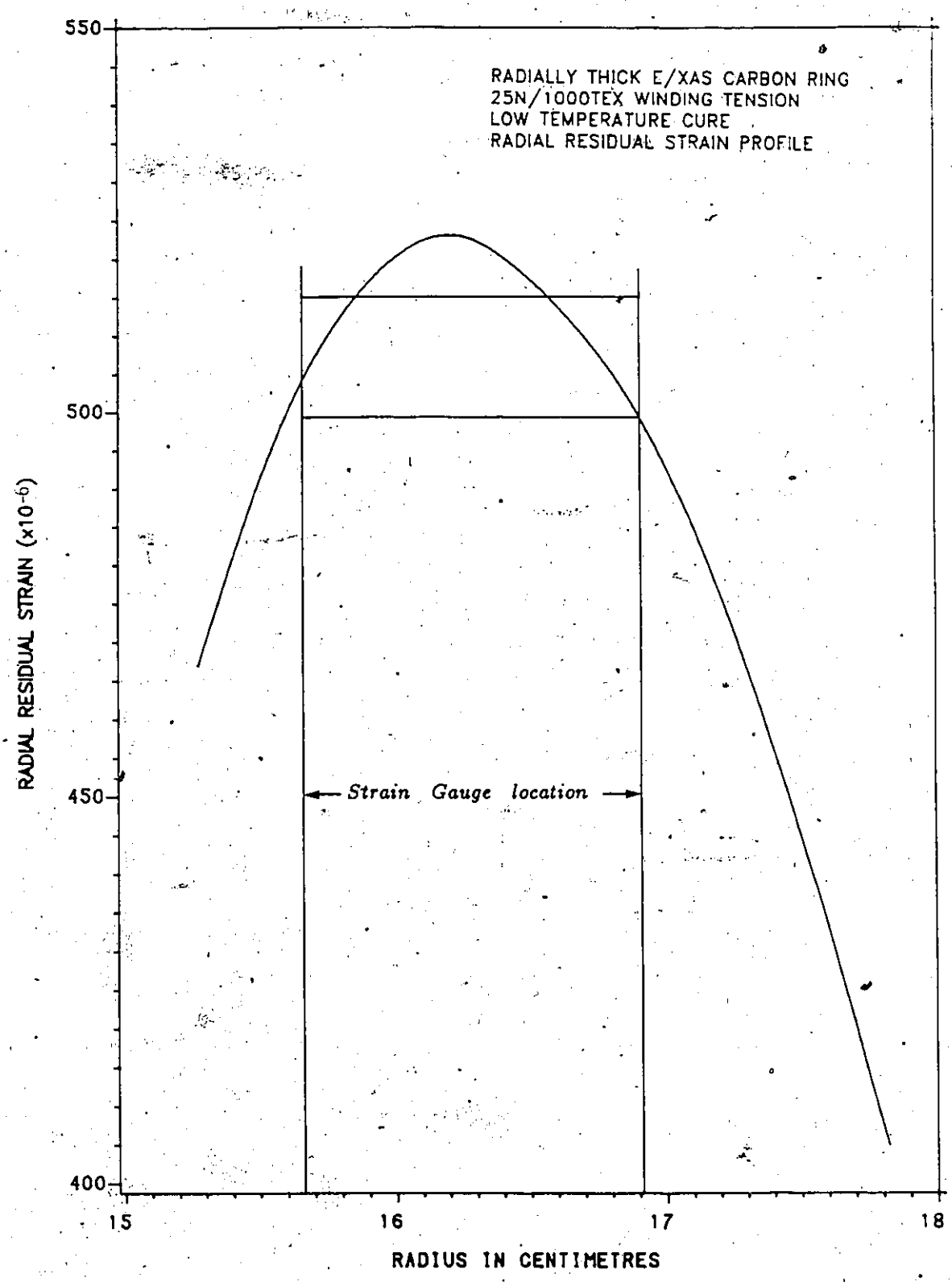

Figure 4.29: Strain profile generated by the computer. Strain gauge location superimposed onto profile.

Table 4.11: Comparison of Predicted and Experimental Residual Transverse Strains in Radially Thick Composite Rings.

Ring No.		Residual Strain ($x10^{-6}$)		Difference
Fig.4.30	Specimen	From Strain Gauge	From Area Calculation	(%)
1	XAS-TK-2-25	924	885.0	4.22
2	XAS-TK-3-25	815	854.0	4.78
3	XAS-TK-4-25	450	515.0	14.40
4	XAS-TK-5-25	505	536.2	6.20
5	XAS-TK-6-25	857	925.2	7.96
6	XAS-TK-10-25	1084	1116.9	3.03
7	XAS-TK-12-25	1807	1802.0	0.28
8	XAS-TK-18-25	1750	1651.0	5.66
9	S2-TK-10-25	206	163.3	20.75
10	S2-TK-16-25	169	134.0	20.71
11	S2-TK-17-25	276	216.8	21.47

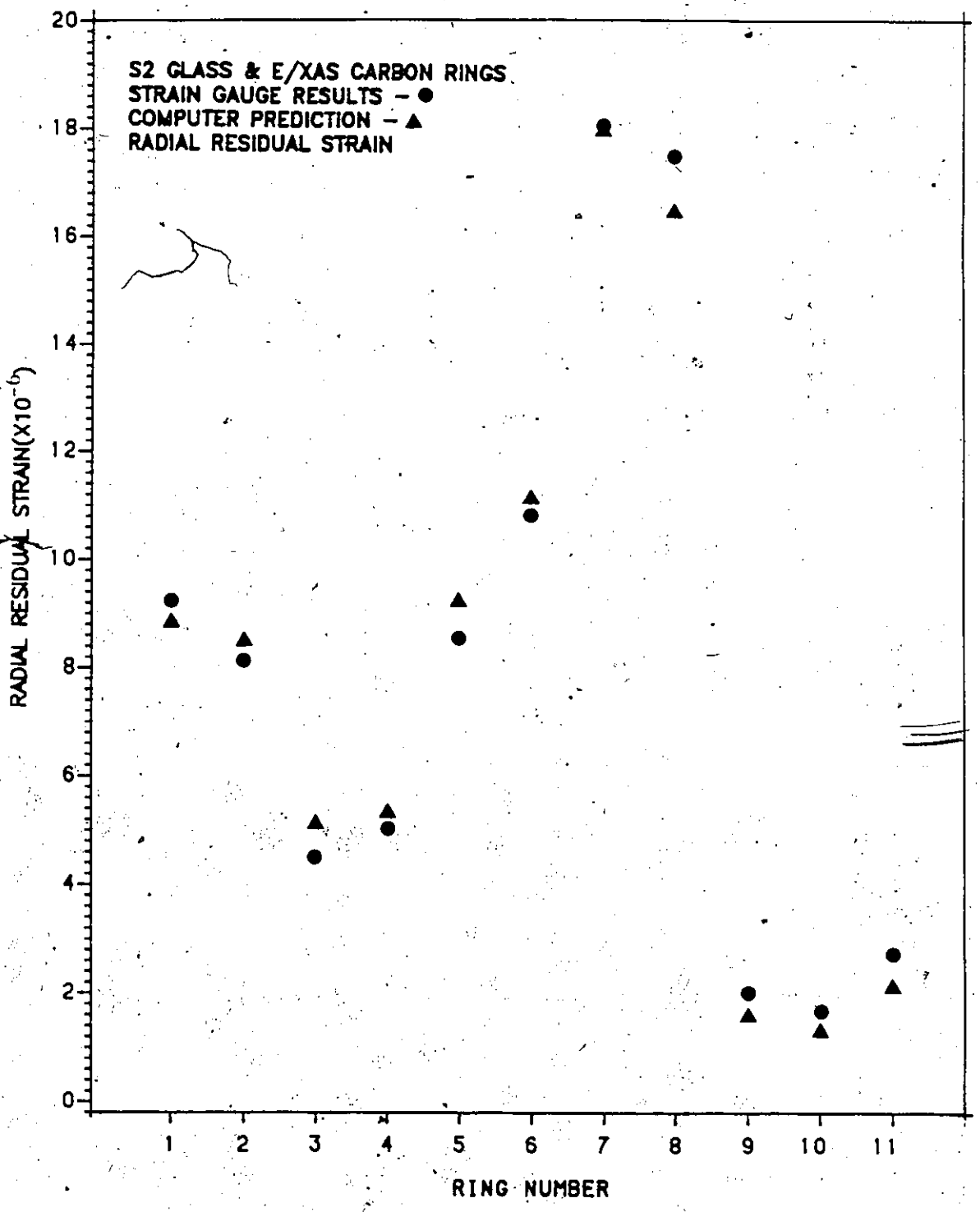

Figure 4.30: Comparison of predicted and experimental residual strains in radially thick composite rings.

4.4.4 Residual strain measurement in axially/radially thick rings.

In the previous section, many radially thick S2-glass and E/XAS carbon composite rings were evaluated for residual stress. However, full size components of the flywheels are much thicker in the axial direction and thus, it was necessary to manufacture and test full size rings. The results of such would give indications as to the magnitudes of the residual stresses existing in these larger rings. Due to the high cost and effort required, only three composite rings were made for destructive testing - one S2-glass and two E/XAS carbon. Table 4.12 gives the overall dimensions of these rings.

Table 4.12: Dimensions for Axially/Radially Thick Rings.

Ring No.	Inside Diameter (cm.)	Radial Thickness (cm.)	Axial Thickness (cm.)
S2-ATK-13-25	31.83	6.43	8.97
XAS-ATK-1-25	26.72	7.89	7.90
XAS-ATK-3-25	42.63	9.84	8.89

The S2-glass ring was not instrumented with gauges, however, the diameter change was recorded when the ring was cut. The two E/XAS carbon rings on the other hand were strain gauged with ring number XAS-ATK-1-25 being particularly heavily instrumented. This ring was the first winding of such an axially large ring and thus it was decided to mount a large number of strain gauges. Figure 4.31 shows the location of

these strain gauges on the ring with the strain readings resulting from cutting the ring listed in Table 4.13.

Table 4.13: Strain Readings for Ring XAS-ATK-1-25.

Strain Gauge	Residual Strain ($\times 10^{-6}$)
1	770
2	770
3	762
4	-658
5	876
6	490
7	520

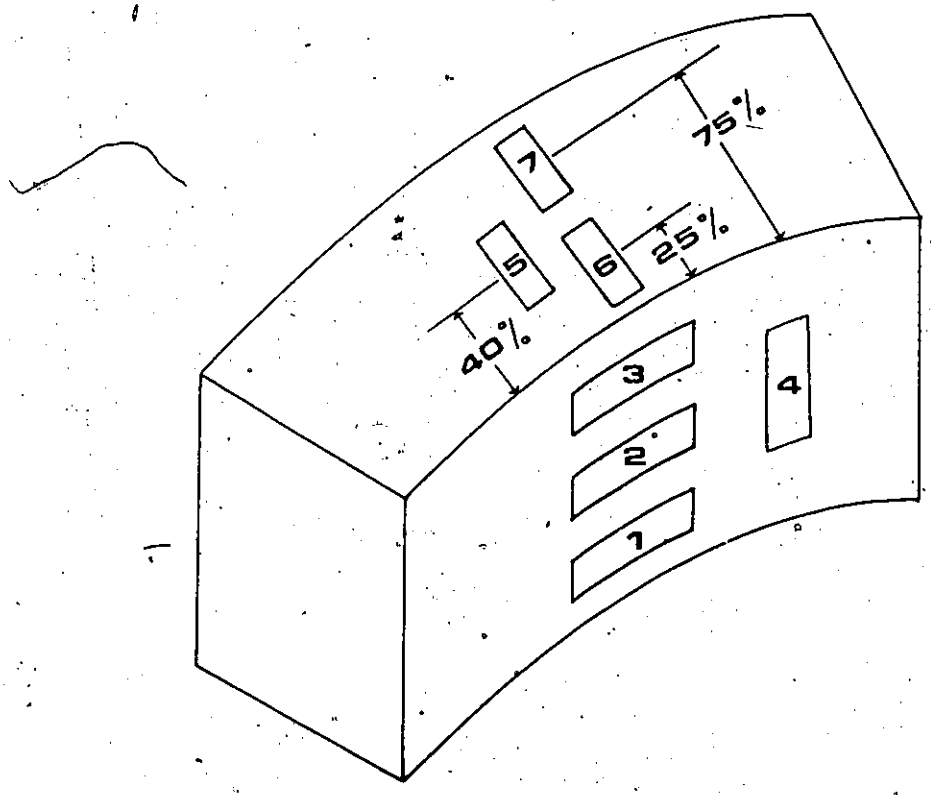

Figure 4.31: Axially radially thick ring (XAS-ATK-1-25) with gauges mounted.

As before, transverse gauges were mounted to experimentally verify the computer's prediction of the

radial strain (Gauges 5, 6 and 7). The average of the three circumferential gauges (1, 2 and 3) was used in the 'OVERLAP' program to predict the circumferential and radial residual stress profiles. Gauge No. 4 was mounted to determine the effect of such a large axial thickness as compared to the 2.54 cm axial thick rings. This gauge also proved useful in relaying information regarding the transverse sensitivity effect on the gauges. Based on the results of XAS-ATK-1-25, a new ring, with a larger inner diameter and cross-section representative of the full size rings, was fabricated (XAS-ATK-3-25). However, in this case, only three gauges were mounted, two circumferentially on the inside surface and one transversely as before (Figure 4.32).

When the ring was cut, the strain readings were recorded as shown in Table 4.14.

Table 4.14: Strain Readings for Ring XAS-ATK-3-25.

Strain Gauge	Residual Strain ($\times 10^{-6}$)
1	730
2	798
3	796
Note : Gauge 1 transversely mounted. Gauges 2 & 3 circumferentially mounted.	

As with the 2.54 cm axial thick rings the side mounted gauges provided information on the radial strain profile. The comparison of the experimental and predicted results for

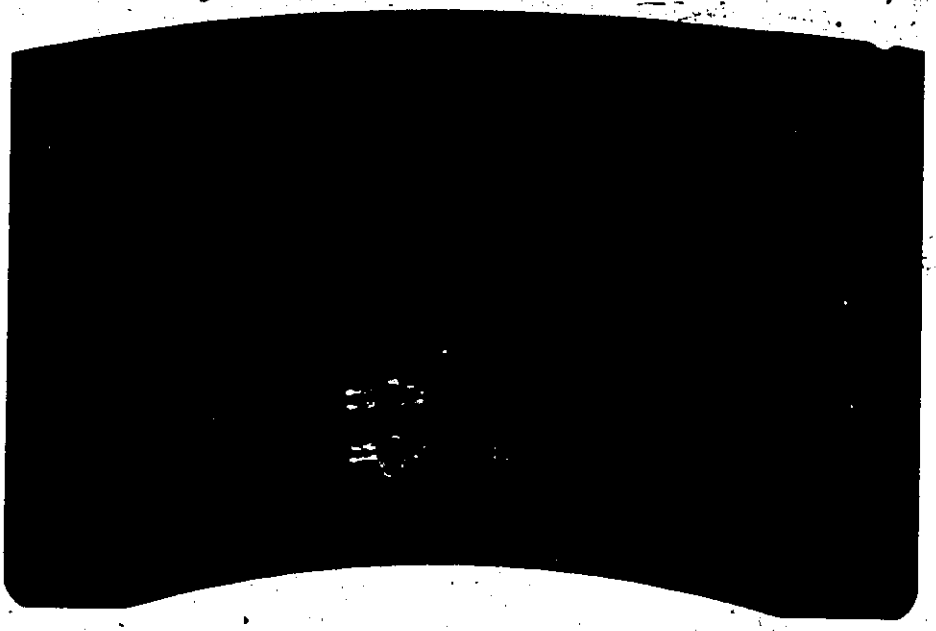

Figure 4.32: Ring XAS-ATK-3-25 with gauges mounted.

the radial strains of the radially/axially thick E/XAS carbon rings are given in Table 4.15 and Figure 4.33.

Table 4.15: Residual Strain Profile from Transverse Gauges.

Ring No.		Gauge No.	Residual Strain ($x10^{-6}$)		Difference (%)
Figure 4.33	Specimen		From Strain Gauge	From Area Calculation	
1	XAS-ATK-1-25	5	876.0	1032.5	17.8
2	XAS-ATK-1-25	6	490.0	670.0	36.7
3	XAS-ATK-1-25	7	520.0	590.0	13.5
4	XAS-ATK-3-25	1	730.0	980.0	34.2

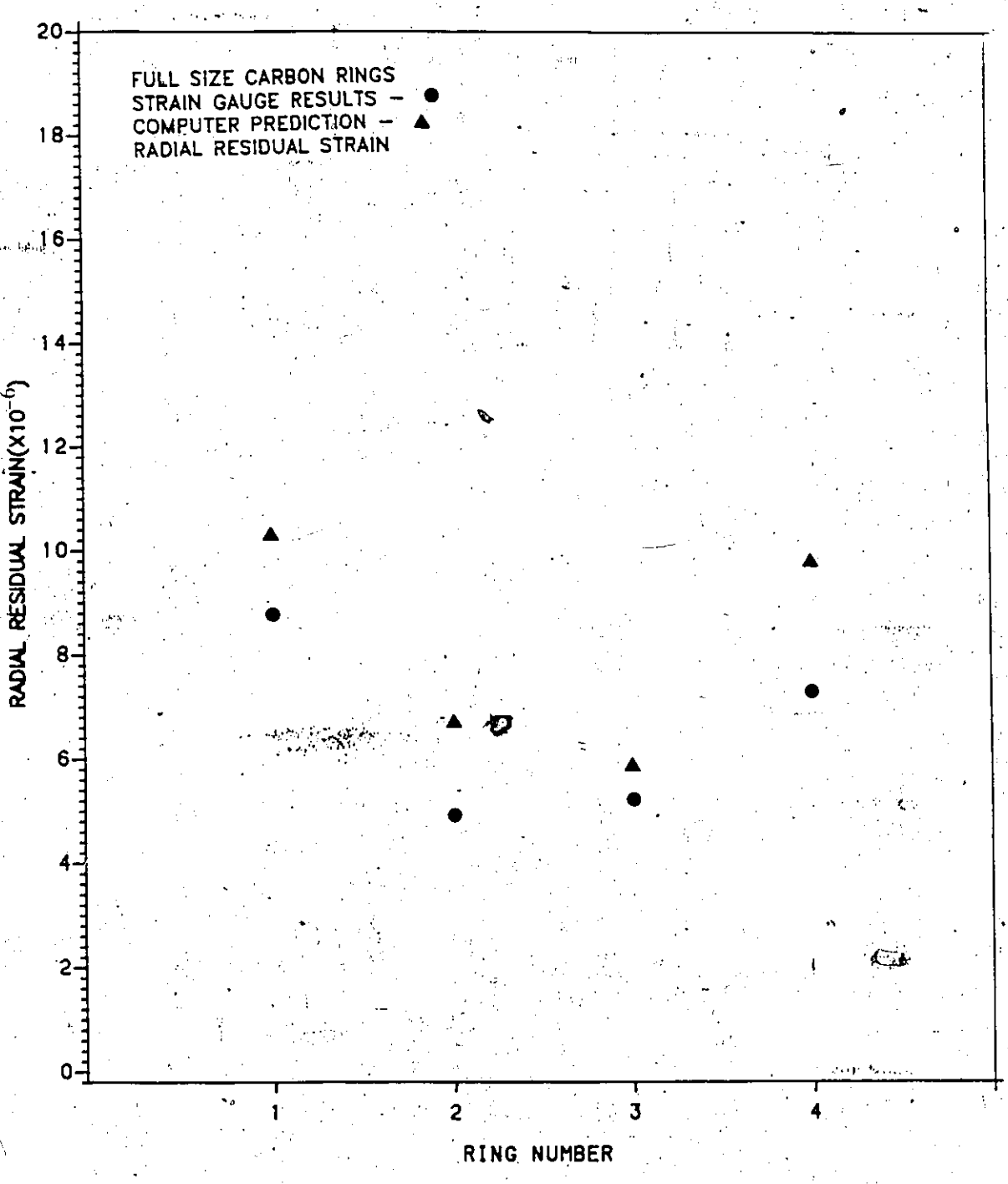

Figure 4.33: Comparison of predicted and experimental residual strains in full scale E/XAS carbon rings.

4.4.5 Radial residual stress versus radial thickness.

In order to determine the relationship between residual stress and ring radial thickness required for the design program, the results for five E/XAS carbon rings, namely one thin ring, three radially thick rings and one full scale ring were examined. These rings were all wound with the same winding tension, had approximately the same inner diameter and were all cured with the same two-stage cure schedule. For the thin carbon ring (CR-25) it was assumed that the standard cure was equivalent to the two-stage cure in the larger rings (Figure 4.19 on page 98). Table 4.16 presents this data while Figure 4.34 gives the plotted results. The amount of overlap produced when the ring was cut varied depending on the relative thickness of the rings. Figure 4.35 presents the overlap results with respect to the thickness of the ring.

Table 4.16: Radial Residual Stress in E/XAS Carbon Rings as a Function of Radial Thickness.

Ring Number	Ring Type	Annular Thickness (cm.)	Residual Stress (MPa.)	
			Strain Gauge	Diameter Change
CR-25	Th	0.572	-	0.66
XAS-TK-3-25	RT	5.949	7.50	6.97
XAS-TK-10-25	RT	7.620	9.83	9.13
XAS-ATK-1-25	FS	7.899	9.66	9.55
XAS-TK-25-25	RT	8.611	-	11.43

NOTE: Th - Thin ring.
RT - Radially thick ring.
FS - Full scale ring.

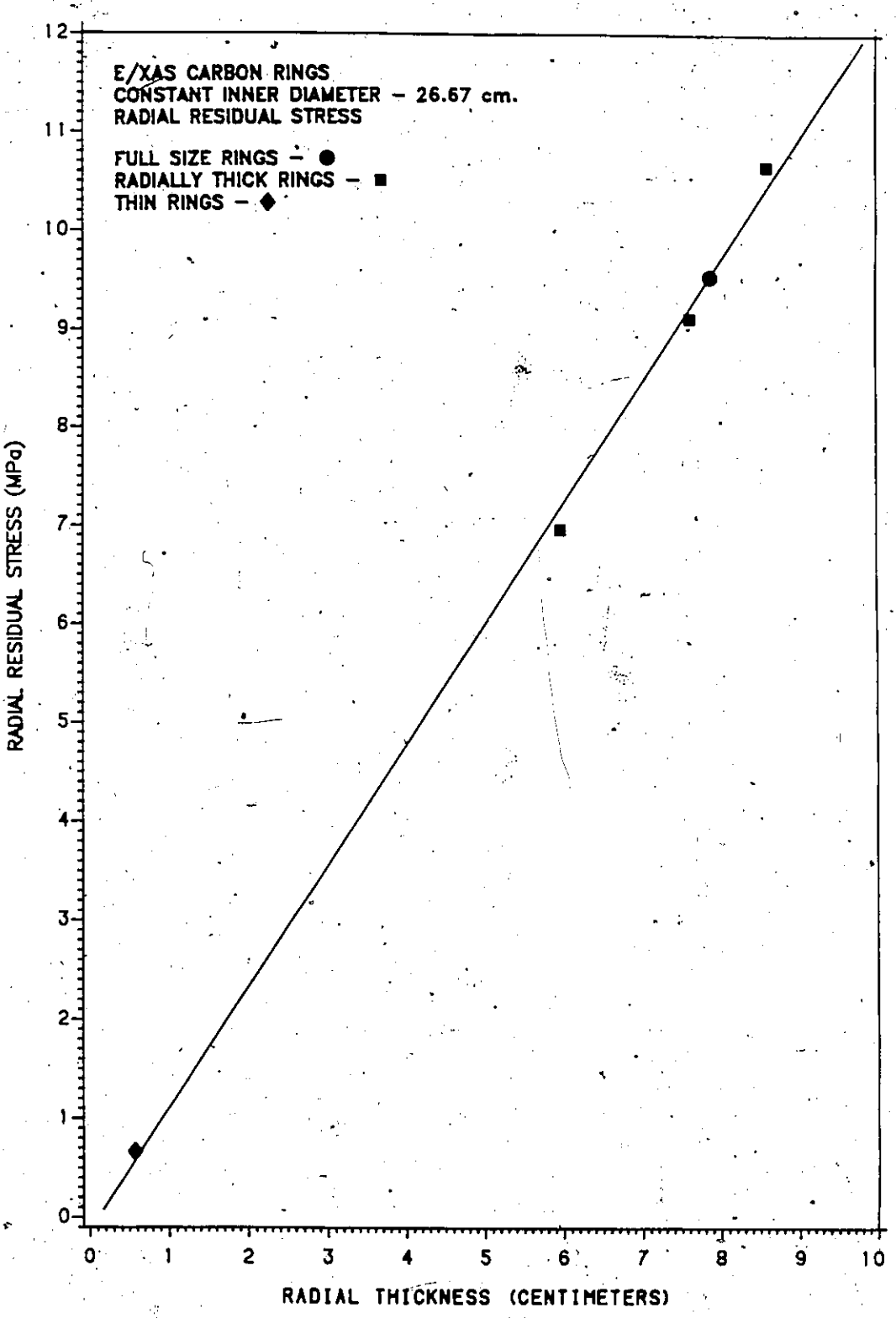

Figure 4.34: Radial residual stress as a function of ring thickness for E/XAS carbon rings.

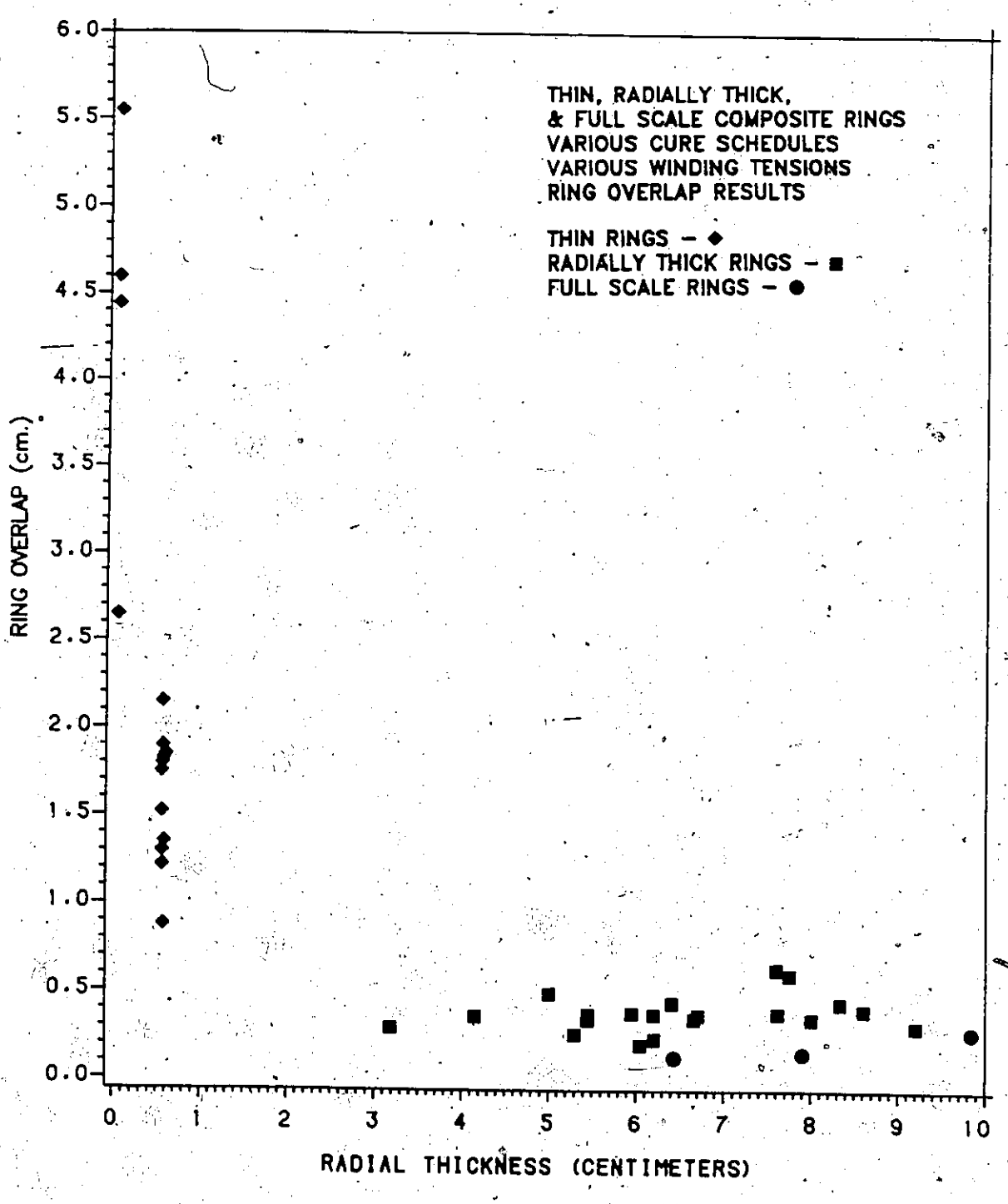

Figure 4.35: Overlap produced as a function of ring thickness.

Chapter V

DISCUSSION.

5.1 Introduction.

In high speed fibre composite flywheels, other than the stresses induced by the centrifugal loading, the residual stresses developed by the very nature of the manufacturing process are of significant importance. If residual stresses are not included in the original design analysis, they may lead to premature failure of the composite rings as well as mass shifts during spin testing of full size flywheels, as speculated by Steele [38]. Thus, it was the intention of this work to study residual stresses in fibre composite rings, in terms of the mechanisms involved and major manufacturing parameters such as winding tension and cure schedules.

5.2 Experimental techniques.

In determining the residual stresses, most of the information was gathered from radially thick or axially/radially thick composite rings. In order to manufacture rings to the proportions required, a great deal of preliminary work was necessary. The majority of the researchers in this field manufactured rings of much smaller

dimensions. The filament winding process itself had to be tailored for the fibre/resin system employed to produce specimens acceptable for testing. Problems such as fibre buckling, fibre volume fraction control and low transverse strengths of the finished products were overcome.

As mentioned, most of the data for residual stress determination was determined from the radially thick composite rings and the literature search established the experimental method. The 'radial cut with strain gauge' method appeared to be the one most preferred by other researchers in the field.

Generally, the information obtained showed that experimental repeatability was very good, even though for composites this is typically considered difficult to achieve. The repeatability was confirmed particularly in the radially thick ring tests for two S2-glass and two sets of two E/XAS carbon composite rings. Each series of rings were manufactured under varying conditions but all had the same winding tension and were tested under approximately the same conditions. The S2-glass composite rings, (S2-TK-10-25 & S2-TK-16-25), were cured with the standard cure schedule, while two E/XAS carbon composite rings, (XAS-TK-4-25 & XAS-TK-5-25) had a low temperature cure. The final two E/XAS carbon composite rings, (XAS-TK-12-25 & XAS-TK-18-25), were cured with a two stage cure and then post-cured. These different cure schedules were explained in Section 3.3.3.

When tested, the rings produced comparable results, within each set, in terms of strain readings (Table 4.9). They also exhibited similar residual stress profiles both in the circumferential as well as radial directions (Figures 4.20, 4.21, 4.22 and 4.23). For the two S2-glass composite rings the maximum relative difference, for peak values, was only 2.1%. Rings XAS-TK-4-25 and XAS-TK-5-25 produced 4.6% relative difference while XAS-TK-12-25 and XAS-TK-18-25 had a 7.7% relative difference.

Before discussing specific results, it is necessary to also comment on the various experimental methods utilized in this work. There were effectively only three types of composite rings manufactured, thin, radially thick, and full scale with two fibre types - S2-glass and Grafil 12K E/XAS carbon. Kevlar 49 fibre was only used on thin rings and during the initial stages of this work. Basically two methods were employed in gathering the experimental data - 'radial cut with overlap measurement' and 'radial cut with circumferential strain gauge'. For the first set of thin composite rings (VS-2 to VS-8 in Table 4.2) only the 'radial cut with overlap measurement' method was used and specifically Prosen's method [4]. The residual stress results were only average circumferential values but the experiments did give an idea as to magnitudes expected with the fibre/resin system used in the Flywheel Program. This initial analysis showed that a relationship existed between

the winding tension and the residual stress in that a four fold increase in the winding tension (22 to 88 MPa.) produced a 53% increase in the residual stress (18.96 to 29.07 MPa.). With the experience gained from the thin rings, a new series of rings were evaluated,(as described in Section 4.3.3.2), for determining the thermal expansion coefficients for three composite types. In this case 'radial cut' methods were utilized for these rings, but the stresses were evaluated using equations 2.8 to 2.10 of Section 2.3.2. The results for the circumferential and radial residual stresses for both methods were presented in Table 4.4 and showed that data from the overlap measurements were comparable to those produced from the strain gauges. A graphical representation of the comparison of the experimental methods for determining the radial residual stress is shown in Figure 5.1 with the 45 degree line indicating 100% agreement.

When the thin rings were radially cut the ends would overlap as was shown in Figure 2.1. This was physically impossible in the radially thick rings, moreover the overlap produced by the thin rings ranged from 2.7 cm. to a high of 5.6 cm. The radially thick rings on the other hand showed overlap values below 0.7 cm. including the full scale composite rings, as shown in Figure 4.35 on page 117. This small overlap was initially observed in the first radially thick composite ring to be tested (S2-TK-3-35). The initial

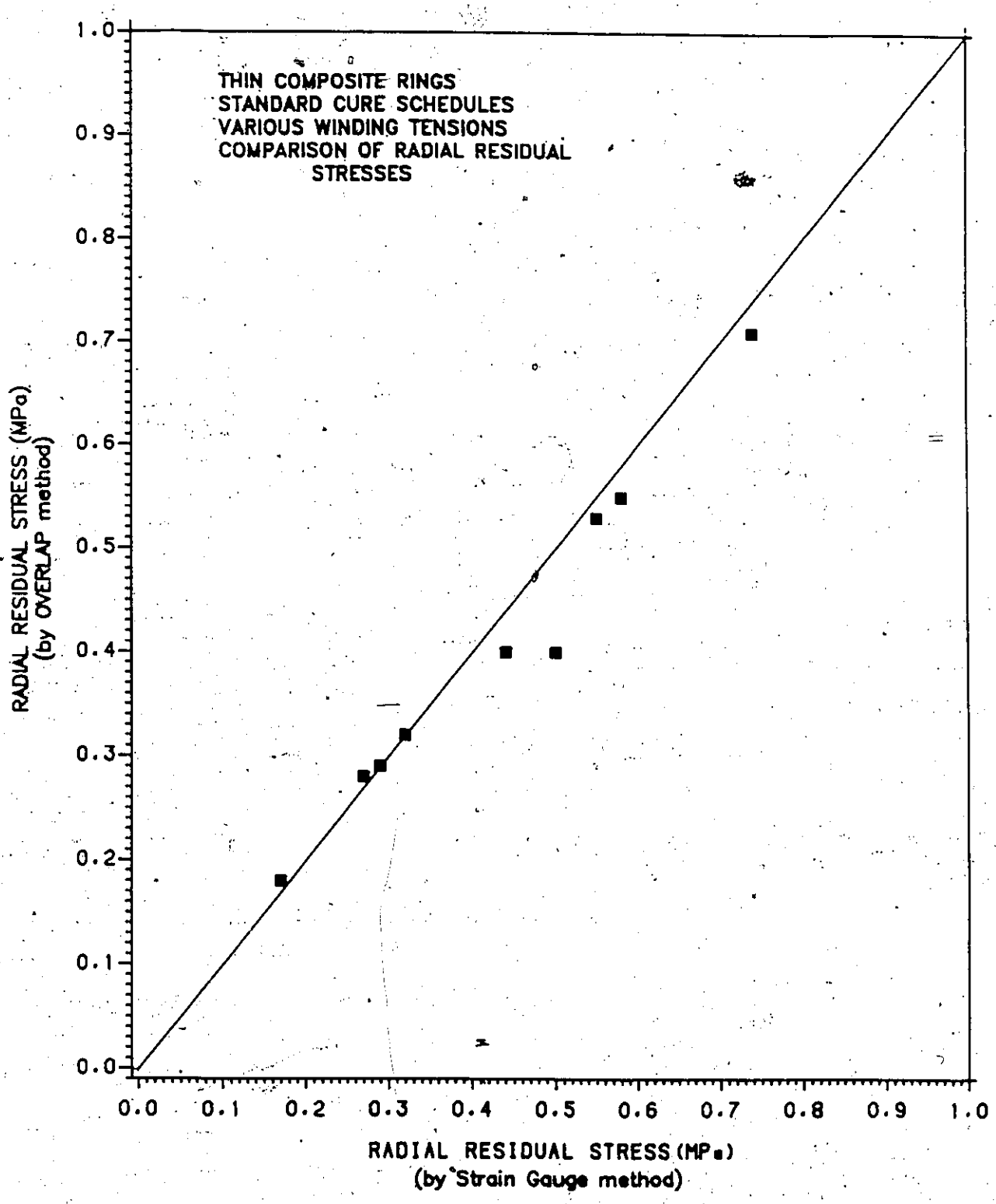

Figure 5.1: Comparison of methods to determine radial residual stress. (thin ring results).

diameter was measured and when radially cut, the final diameter was taken. By so doing a change in diameter was established and then converted into an overlap. The residual stresses could be determined after substitution into the appropriate equations as previously mentioned.

Due to the difficulty in accurately measuring small overlaps and because of the success achieved with the second set of thin rings, strain gauges were mounted on the inner surface of these radially thick rings. The diameter measurements, for the overlap calculations, were also taken and the residual stresses calculated as before. Table 5.1 tabulates the readings taken for the radially thick composite rings while Figure 5.2 presents the comparison in a graphical fashion. Again the 45 degree line on the figure indicates 100% agreement.

For the thick rings, the average error for the two methods was 6.23% while for the thin rings it was 5.73%. In the latter case the largest error (20%) occured with the Kevlar 49 rings (KR-10, KR-20 & KR-35). This may be due to the difficulty in measuring the amount of overlap since a large degree of fraying occured from the cutting process. However, as mentioned earlier, Kevlar 49 was removed from further analysis.

As an example of the accuracy of the diameter change method, an 0.001 inch (0.0025 cm) error in the diameter reading produced a 2% error in the radial residual stress

Table 5.1: Radial Residual Stress Comparison for Thick Composite Rings.

Ring Number	Residual Stress (MPa.)		Difference (%)
	Diameter Method	Strain Gauge Method	
S2-TK-5-VAR(i)	3.43	3.25	-5.6
S2-TK-6-VAR(d)	4.44	3.90	-13.7
S2-TK-7-VAR(i)	2.03	2.17	6.4
S2-TK-8-35	3.97	4.12	3.6
S2-TK-10-25	2.75	3.11	11.6
S2-TK-16-25	3.01	3.05	1.4
S2-TK-17-25	4.78	4.75	-0.7
XAS-TK-2-25	7.18	7.80	8.1
XAS-TK-3-25	6.98	7.49	6.9
XAS-TK-4-25	3.71	4.51	17.8
XAS-TK-5-25	4.43	4.72	6.1
XAS-TK-6-25	7.82	8.10	3.4
XAS-TK-10-25	9.13	9.83	7.1
XAS-TK-12-25	15.01	15.93	5.8
XAS-TK-18-25	14.50	14.79	2.0
XAS-ATK-1-25	9.55	9.71	1.7
XAS-ATK-3-25	8.27	8.63	4.1

results. This was taken as being typical for the experimental overlap data for the radially thick rings and within acceptable levels. From the foregoing it can be inferred that the 'overlap/diameter change' method is as accurate as that of the 'radial cut strain gauge' method.

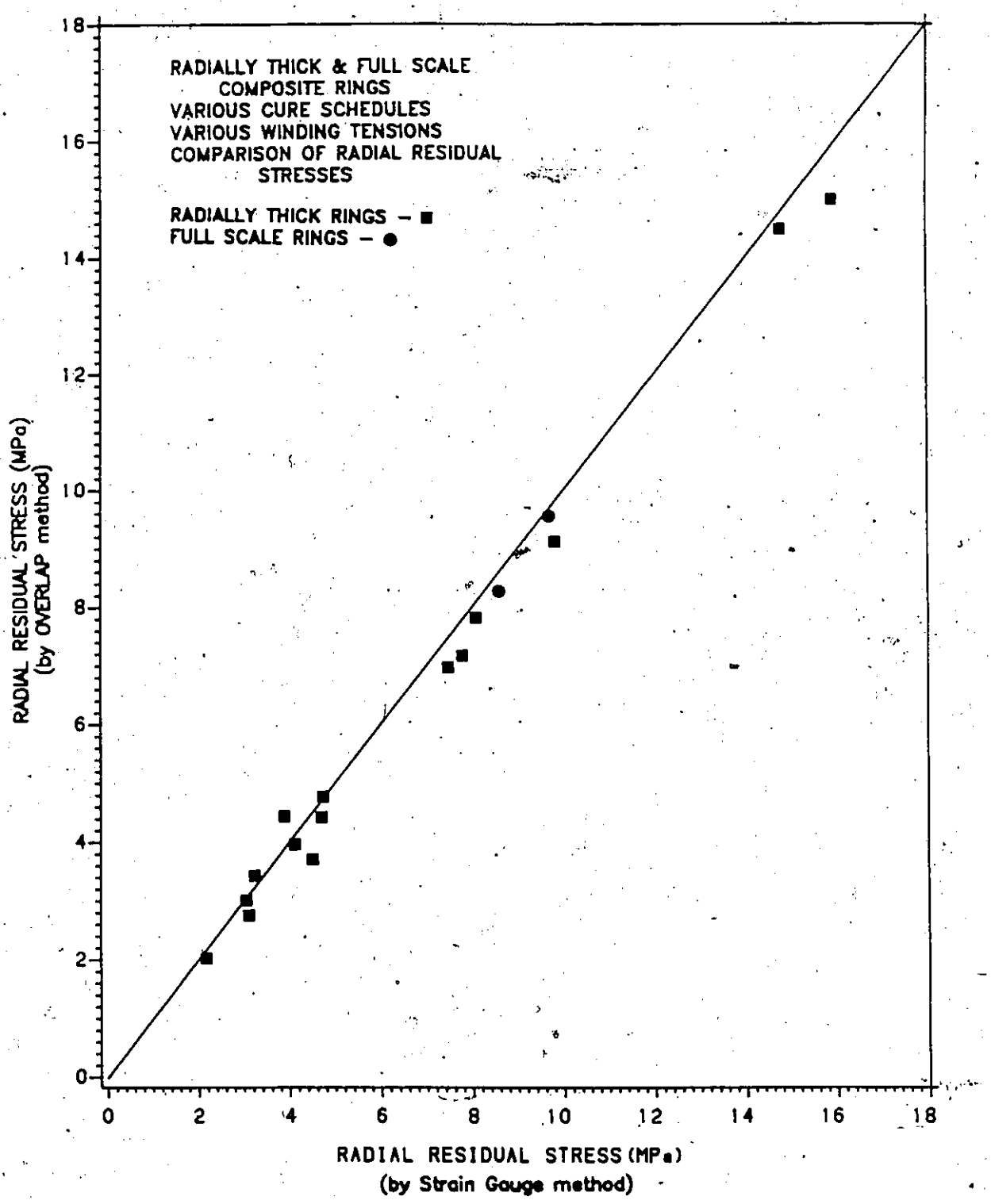

Figure 5.2: Comparison of methods to determine radial residual stress. (thick ring results).

5.3 Experimental verification.

As far as experimentally verifying the results, two techniques were investigated, depending on the type of rings manufactured.

For thin composite rings, (less than 1 cm. radially thick), outside gauges were applied. This was possible due to steel pads applied during curing of the manufactured rings which produced a smooth surface as described in Section 4.3.2. On the other hand, the radially thick composite rings, (larger than 1 cm. radially thick), the outer surface was not similarly prepared and instead transverse gauges were mounted on selected rings. In both cases the experimental data was compared to that obtained from the 'OVERLAP' computer program.

With the thin rings, the circumferential strain released at the inner surface was the input data. The computer program predicted the outer circumferential strain and this was compared to that measured with the outer strain gauge. Table 5.2 tabulates this computer and experimental data with the relative error observed.

As can be readily seen, no error was larger than 3% and in fact the average was calculated at $0.95 \pm 0.97\%$. These results were considered to be well within acceptable limits and initially verified the 'OVERLAP' computer program. With the above data checked with experimental inputs, the 'radial cut with strain gauge' method was deemed satisfactory and

Table 5.2: Comparison of Predicted and Experimental Strains.

Ring Number	Strain Reading From Radial Cut ($x10^{-6}$) Inside	Outside	Strain Reading Computer Prediction ($x10^{-6}$) Outside	Difference (%)
SR-15	-386	374	375	0.3
SR-30	-523	496	508	2.4
SR-35	-535	516	520	0.7
CR-10	-420	407	408	0.7
CR-20	-459	449	446	0.6
CR-30	-526	498	511	2.6
KR-10	-443	*	*	*
KR-20	-563	550	547	0.5
KR-35	-558	540	542	0.3

NOTE:- * - Gauge failure.

was chosen for measuring the residual stress in the thin composite rings.

As mentioned, the radially thick composite rings were not instrumented with strain gauges on the outer surface. Instead gauges were mounted in the usual manner on the inner surface and another on the side face, transverse to the fibres. This transverse gauge provided direct indication of the radial residual strain existing in the composite ring and could be compared to that generated by the 'OVERLAP' computer program. Section 4.4.3 explained the way in which the data was compared while Table 4.11 presented the data with the relative difference. The values for the E/XAS carbon composite rings showed much closer correlation to the computer results than did the S2-glass values. The average error was 5.8% and 20.9% for the E/XAS carbon and S2-glass respectively. Although appearing high, the error in the

S2-glass composite rings are based on significantly smaller transverse gauge strains (200 vs 1800 $\mu\epsilon$). The largest error for the E/XAS carbon composite rings was 14.4% for ring XAS-TK-4-25. This ring was cured with a low temperature cure and not the final cure schedule settled on. There may also have been some other factor such as malfunction of the gauge, since a similar ring, XAS-TK-5-25, was also cured with the low temperature cure and it's relative error was only 6.2%. These results were shown in a graphical fashion in Figure 4.30. For the axially/radially thick composite rings only two E/XAS carbon composite rings were instrumented with strain gauges (XAS-ATK-1-25 & XAS-ATK-3-25). Again the comparison of the radial residual strain was made and an average error of 25.6% was determined. The computer predicted a higher value, in each case, compared to that of the strain gauge. The transverse strain gauge readings were compared to those of the radially thick composite rings and were seen to be of similar magnitudes (Tables 4.11 and 4.15). This may indicate that with the axially/radially thick composite rings, transverse gauges are not as suitable as with the radially thick composites. However, the circumferentially mounted gauges are as accurate as those of the radially thick composite rings as was evidenced from Figure 5.2. This in effect verified that the transverse gauges are more suitable for the radially thick rings while the circumferentially mounted

gauges are valid for radially as well as axially/radially thick composite rings.

The results from the radially transversely mounted strain gauges were of concern due to the effect of transverse sensitivity. In Section 4.4.2 this matter was investigated using computer generated values. First indications were that the transverse sensitivity of the gauges produced minimal effect on the radial strain gauge readings. The experimental confirmation was obtained from 0/90° rosette gauges mounted on a biannular composite ring (Appendix I). The calculations showed that the errors as a percentage of the actual strain along the gauge axis were -2.61% and -0.16%. These values confirmed that single and not rosette gauges could be employed in determining the radial residual strain in the radially thick composite rings.

5.4 Effect of variables on the residual stress.

One of the intentions of this work was to attempt to understand the nature of the residual stresses existing in the composite rings. From the literature, [14], it was determined that the total residual stress was made up of several components. To this end, experiments were carried out on a series of thin rings, (Section 4.3.3), separating the stresses into a winding tension component, a thermal component and a resin shrinkage/fibre migration component. The first factor considered was the thermal component of the

residual stress and in order to obtain this information, thermal expansion coefficients were required. The results of these tests were shown in Table 4.3. The average circumferential thermal expansion coefficient for S2-glass composite rings was determined as $3.2 \times 10^{-6}/°C$ and $26.9 \times 10^{-6}/°C$ for the transverse value. For E/XAS carbon composite rings, $-1.1 \times 10^{-6}/°C$ and $32.3 \times 10^{-6}/°C$ were obtained for the circumferential and transverse coefficients, respectively. The Kevlar 49 composite ring results were coefficients of $-4.7 \times 10^{-6}/°C$ circumferentially and $53.5 \times 10^{-6}/°C$ transversely. Examining the literature [39,33] typical values for carbon composites are $-1.8 \times 10^{-6}/°C$ and $33.9 \times 10^{-6}/°C$ circumferentially and transversely, respectively. Circumferential S2-glass values of $3.5 \times 10^{-6}/°C$ and $28 \times 10^{-6}/°C$ transversely were reported. With Kevlar 49 a circumferential coefficient of $-4 \times 10^{-6}/°C$ with a transverse value of $72 \times 10^{-6}/°C$ were found. These coefficients had to be determined since in the literature the particular fibre/resin system employed was not reported, moreover the spread in the values of the coefficients in the literature necessitated α_θ and α_r to be calculated.

With these coefficients measured, they were inserted into a computer program[4] and the thermal residual stresses calculated. As presented in Table 4.4 the circumferential and radial residual stresses showed different trends for the different materials. The S2-glass composite rings produced

[4] 'THERMOSUP' by J. Wong [17].

a decreasing thermal stress profile with increasing winding tension while both the E/XAS carbon and Kevlar 49 composite rings showed increasing trends (Figures 4.10 to 4.15). Moreover, both the E/XAS carbon and Kevlar 49 thermal residual stress values generally exhibited the same magnitudes while the S2-glass values were approximately 75% lower. The magnitudes of the thermal residual stresses also indicated that these stresses were only a small fraction of the total residual stresses existing in the rings (Tables 4.5, 4.6 and 4.7). For the circumferential values this represented 5-19% of the total stresses while radially the value was 8-22% of the total. The largest differences (18.5-22.3%) occured with the Kevlar 49 composites and as mentioned earlier these rings were removed from final analysis.

The second factor evaluated was the residual stresses due to the applied winding tension (Section 4.3.3.4). The trend shown with the thin rings was that with an increase in the winding tension the residual stresses increased but in a negative fashion (Figures 4.10 to 4.15). Thus, in a sense this was beneficial as this would lower the overall residual stress in the composite rings. The circumferential values were also noted to be two order of magnitudes larger than the transverse values. However, the transverse strength of the composite is also substantially lower than the circumferential. Typical values as a percentage of the

circumferential strength were determined as 2% for the S2-glass and E/XAS carbon with 0.5% for the Kevlar 49 composites (Table 1.1). It was also noted that the overall residual stress still increased with an increase in winding tension. This is due to the fact that the winding tension component is not large enough to significantly affect the total residual stress.

With two factors evaluated, the other unknown components including the resin cure and resin shrinkage/fibre migration was approximated by finding the difference between the total stress and the two previously determined components (Tables 4.5 to 4.7). It was believed that the final components do represent these unknown factors and as such appear to form a substantial part of the total residual stresses. The results are shown in Figures 4.10 to 4.15 and continue the trend of increasing residual stress with increasing winding tension. The only other researcher who reported similar work was R.C. Reuter Jr. [14] at Sandia Laboratories, but no comparison with his results were possible since no residual stress data was reported. However, he did present data indicating that the fibre migration phase produced the most dramatic change in the residual stress profile.

The full scale composite rings for the flywheels have a radial thickness of approximately 9 cm. Thus, the small rings previously discussed were predominantly for the measuring techniques and evaluating the components of

residual stress. With the radially thick composite rings several variables were investigated, that being effect of winding tension, of ring thickness and of cure cycle.

An increase in winding tension produced a decrease in the residual stresses in the radially thick composite rings. This was shown in Figures 4.16 and 4.17 for two S2-glass rings of approximately the same dimensions. A 40% increase in the applied winding tension resulted in a 13% decrease in the residual stresses. Further investigation was carried out by varying the winding tension on a series of four S2-glass composite rings. Instead of keeping a constant tension, increasing as well as decreasing schedules were implemented. The results are shown in Figures 4.18 and 4.19 and again, as expected, the results showed that the increasing tension schedule decreased the residual stress while the converse was true for a decreasing schedule. It was speculated that in these radially thick composite rings the effect of the resin shrinkage and fibre migration was more pronounced due to the larger mass of the composite. Also the transverse coefficient of thermal expansion would have a much greater effect on these larger composite rings than it would on the thin composite rings. The final tension schedule chosen was dependant on such factors as fibre buckling, transverse tensile strength and void shape.

The resin system used in manufacturing the fibre composite rings required an elevated temperature for a

proper cure. By reviewing the literature [14,40], it was noted that other researchers were concerned with the curing stage of the manufacturing process. Dick [40] suggested that a room-temperature cure resin system or a controlled stepped cure program are two methods which can be used to control the cure-related thermal stresses. The former was out of the question with the latter given serious consideration. This concern came about due to tensile tests of specimens from filament wound rings. The S2-glass rings were cured with the standard cure and strength tests showed quite acceptable results. However, the E/XAS carbon composite specimens on the other hand showed results below levels necessary to satisfy the design requirements.

As discussed in Section 3.3.3 several different cures were evaluated on the E/XAS carbon composites. They were the standard, B-stage plus standard (two-stage), low temperature, controlled heat-up and two-stage plus post-cure. Residual stress experiments were carried out to evaluate these different cures and the results were presented in Figures 4.22 and 4.23. The highest residual stress was produced from the two-stage plus post-cure cure cycle with the lowest being the low temperature cure cycle. Mid-way between were the three others, standard, controlled heat-up and B-stage plus standard cures. The post-cured composite rings were approximately four times greater in terms of the radial residual stress than the Low Temperature

ones. As noted earlier, the other composite rings were midway between the low temperature and the two-stage plus post-cure. It is interesting to note that the final cure temperature for this group was approximately 100xC. This provided evidence that the thermal cooldown was the dominant factor in the final residual stress result. The final cure schedule chosen (two-stage) was based on the void distribution, the residual stress and the transverse tensile properties of the composite [20]. Micro-photographs of specimens from a radially thick S2-glass ring showed that the void shape was quasi-circular and fairly evenly distributed[5]. However, E/XAS carbon composite ring specimens (XAS-TK-1-69) showed voids to be elongated in the winding direction (normal to the radial direction) and concentrated between tows. This observed shape seemed to be detrimental to the radial tensile strength of the composite. In terms of the transverse tensile strengths of the various cure schedules, tensile tests were carried out[6]. These tests were conducted for three E/XAS carbon composite rings all manufactured under identical winding parameters but cured with different cure schedules. The results are given in Table 5.3 and show that the cure schedule has a significant effect on transverse tensile strength with the two-stage cure possessing the highest transverse strength.

[5] by Akira Miyase [18].

[6] by Akira Miyase [18].

Table 5.3: E/XAS Carbon Composite Radially Thick Ring Transverse Tensile Test Results.

Ring Number	Ultimate Tensile Strength (MPa.)	Cure Schedule
XAS-TK-2-25	29.8 ± 1.4	Standard
XAS-TK-3-25	43.7 ± 1.4	Two-Stage
XAS-TK-4-25	37.3 ± 1.4	Low Temperature

The results of the foregoing confirmed that the selected cure schedule was to be the two-stage (B-stage plus standard cure) cure cycle since this produced acceptable residual stress levels and transverse tensile strength values.

Along with the two effects covered, winding tension and cure, the relative size of the full scale composite rings was of concern. The thin rings were all manufactured to the same dimensions and as such no trend as regards to thickness was established. In the radially thick rings, however, a trend of increasing residual stress with increasing radial thickness was observed. In Figures 4.20 and 4.21 this result is shown for four S2-glass composite rings.

For Figure 4.21, the results showed that a relative increase in thickness of 14% produced an increase in the maximum radial residual stress of 53% (Rings S2-TK-10-25 and S2-TK-17-25). In a similar fashion a 20% increase in thickness produced a 62% increase in the maximum radial residual stress (Rings S2-TK-10-25 and S2-TK-24-25).

As stated earlier, the E/XAS carbon composite rings were cured under different conditions than the S2-glass

composites. It was assumed that this factor would affect the final result regarding the residual stress and the thickness. If, however, Figure 4.25 is examined it was found initially that the same holds true for the E/XAS carbon composite rings. On closer examination it appears that the residual stress is not as sensitive to the thickness variations as is the S2-glass. A 9% increase in the radial thickness produced a 31% increase in the radial residual stress (Rings XAS-TK-3-25 and XAS-TK-10-25) while a 14% increase in the radial dimension produced a 43% increase in the maximum radial residual stress (Rings XAS-TK-3-25 and XAS-TK-25-25). This same 14% increase in the S2-glass composite rings produced a 53% increase in the maximum radial residual stress. However, E/XAS carbon composite maximum radial residual stress results were double those of the S2-glass.

The effect of thickness on the residual stress was also investigated in the full scale composite rings. As mentioned in Section 4.4.4, the high cost and effort required precluded any large number of specimens to be manufactured. By comparing a radially thick with an axially/radially thick composite ring (XAS-TK-10-25 and XAS-ATK-1-25) it was observed that the radial residual stress was of approximately the same magnitude. The dimensions and residual stresses of the composite rings are given in Table 5.4.

Table 5.4: Dimensions and Radial Residual Stress Comparisons for E/XAS Carbon Composite Rings.

Ring Number	Inner Diameter (cm.)	Radial Thickness (cm.)	Axial Thickness (cm.)	Radial Residual Stress (MPa.)
XAS-TK-10-25	26.73	7.62	2.54	9.8
XAS-ATK-1-25	26.72	7.89	7.90	9.7
XAS-ATK-3-25	42.63	9.84	8.89	8.6

As can be seen from Table 5.4 on page 137 the inner diameters of the first two rings were essentially the same but each had slightly different radial thicknesses. Furthermore, the axial dimension of the axially/radially thick composite ring was approximately three times that of the radially thick ring but had a very similar maximum radial residual stress. This information showed that the residual stress was insensitive to an increase in the axial thickness.

As far as the radial thickness is concerned one further E/XAS carbon composite ring was manufactured and destructively tested (XAS-ATK-3-25). Compared to the previous full scale composite ring, XAS-ATK-1-25, all dimensions were increased as shown in Table 5.4. The resulting radial residual stress was determined to be 8.6 MPa., a value 12% smaller than XAS-ATK-1-25. No real comparison can be made between these two rings since a number of variables were changed, however it is believed that the inner diameter may be a controlling factor in the residual stress change. This full scale composite ring was

representative of the prototype rings in the completed flywheel and as such indicated the amount of residual stress to be expected with similar rings manufactured under the same conditions.

The only full scale S2-glass composite ring manufactured for destructive testing was S2-ATK-13-25 with dimensions as given in Table 4.12 on page 110. The most striking point noticed was that the radial residual stress was significantly lower as compared to that of the E/XAS carbon composite rings. In fact the S2-glass maximum radial residual stress of 2.2 MPa. was only 22% of the E/XAS carbon composite value, but again comparisons are hard to make since two different cures were performed. The fact remains, however, that the destructive testing of these rings provided the necessary residual stress information and were used in the design of the full scale flywheels of the Flywheel Program. The residual stress information also ensured a closer correlation with the predicted values and the spin test evaluations.

Not only is the radial residual stress insensitive to an increase in axial thickness, but further investigation revealed that it was also linear with respect to the radial thickness. This fact was presented in Figure 4.34 and included the full range of rings tested, from the smallest to the largest again basically confirming the earlier results of Figure 4.25 where an increase in radial thickness produced an increase in the residual stress.

Chapter VI

CONCLUSIONS AND RECOMMENDATIONS.

The significant features of this work can be summarized by the following points:

1. Due to the manufacturing techniques developed, consistency and repeatability of the results were achieved in the composite rings.
2. The 'radial cut with overlap measurement' method was shown to be as accurate as the 'radial cut with strain gauges' method.
3. Both the 'radial cut with overlap measurement' method and the 'radial cut with strain gauges' method, used to determine the residual stresses, were found to confirm the computer predictions.
4. The important manufacturing variable of winding tension, for the thick rings, was evaluated experimentally and showed that an increase in the winding tension produced a decrease in the residual stress.
5. For the E/XAS carbon composite rings the residual stress increased with increased final cure temperature and that the most appropiate cure was that of B-staging then curing at 100 degrees centigrade.

6. The unknown variables including the resin shrinkage/fibre migration component appeared to be a significant portion of the total residual stresses in thin rings.
7. The computer predictions of residual strains generated by the computer program 'OVERLAP' showed good agreement with transversely mounted strain gauges on the radially thick rings.
8. For rings of similar inner diameters and manufacturing parameters, the radial residual stress increases linearly with radial thickness.
9. The radial residual stress is insensitive to an increase in the axial thickness of the composite rings.

The following recommendations should be noted,

1. Further investigation into the unknown and resin shrinkage/fibre migration components of the residual stress should be carried out with aims of experimentally determining the magnitude.
2. More thorough evaluation of the effect of size, in terms of the radial and axial dimensions, on the residual stresses in thick composite rings should be undertaken.
3. Further investigation should be carried out for axially/radially thick composite rings to account for the poorer agreement (as compared with the thin rings)

between the experimental results and the theoretical predictions.

BIBLIOGRAPHY

1. Flanagan, R.C., Munro, M., Miyase, A. and Wong, J.; Evaluation of and Program Recommendations for Anisotropic Material Flywheels (Road Vehicle Applications), Interim Report, Department of Mechanical Engineering, University of Ottawa, February 1981, 112pp.
2. Wong, J., Flanagan, R.C., Munro, M., and Miyase, A.; Analysis and Design of 1.0 KW-Hr Anisotropic Material Flywheels, Technical Report No. UOME-FP-8102-1, Department of Mechanical Engineering, University of Ottawa, October 1981, 63pp.
3. Wong, J., Flanagan, R.C., Munro, M.B., Miyase, A.; High Energy Fibre Composite Rotor Design & Analysis, Report No. UOME-FP-8303-1, Dept. of Mechanical Engineering, University of Ottawa, January 1983, 176pp.
4. Prosen, S., Karpe, S., Kinna, M., Mueller, C., Perry, H., Barnet, F.; Compression, Fatigue and Stress Studies on NOL Ring Specimens, ASTM STP 327, American Society for Testing and Materials, 1963, p.105.
5. Nimmer, R., Torossian, K., and Wilkening, W.; Laminated Composite Disc Flywheel Development, Fourth Interim Report, January 10, 1980 to September 30, 1980.UCRL-15383

6. Al-Qureshi, H.A.; Spring-Back in Hoop-wound Fibre Glass Rings, Proceedings, Ninth Canadian Congress of Applied Mechanics, May 30 - June 3, 1983, University of Saskatchewan, Saskatoon, Saskatchewan, Canada.

7. Fourney, W.L.; Residual Strain in Filament Wound Rings, Journal of Composite Materials, Vol. 2, 1968, p.408.

8. Dewey, B.R.; Knight, Jr. C.E.; Residual Strain Distribution in Layered Rings, Journal of Composite Materials, Vol. 3, July 1969, p.583.

9. Knight, Jr., C.E.; Orthotropic Photoelastic Analysis of Residual Stresses in Filament-wound Rings, Experimental Mechanics, February 1972, pp.107

10. Olson, W.A. and Bert, C.W.; Analysis of Residual Stresses in Bars and Tubes of Cylindrically Orthotropic Materials, Experimental Mechanics, September 1966, pp.451-457.

11. Knight, Jr. C.E., Huddleston, R.L: and Kelly, J.J.; Composite Flywheel Development Completion Report, May 1-Sept 30, 1976, Report No. Y-2080, Union Carbide Nuclear Division, Oak Ridge,Tenn.

12. Dove, R.and, Adams, P.; Experimental Stress Analysis and Motion Measurement, Charles E. Merrill Publishing Co., 1964.

13. Cocker, E. G. and Filon, L. N.; A Treatise on Photoelasticy, Cambridge University Press, 1931.

14. Reuter, R.C.,Jr.; Prediction and Control of Macroscopic Fabrication Stresses in Hoop-wound Fiberglass Rings, Analysis and Test Methods for High Modulus Fibre Composites, ASTM STP 521, American Society for Testing and Materials, 1973, pp.264-276.

15. Shiratori, E., Ikegami, K., Hattori, T., Shimizu, K.; Application of the Fiber Reinforced Composite to Rotating Discs, Bulletin, JSME, Vol. 18, No. 122, August 1975, pp.784.

16. Shiratori, E., Ikegami, K., Hattori, T.; Strength of the Circumferentially Fibre Reinforced Composite Rotor, 23rd National SAMPE Symposium and Exhibition, Anaheim, California, 2-4 May 1978.

17. WONG. Jim, M.; Department of Mechanical Engineering, University of Ottawa, Ottawa, Ontario, Canada, 1981.

18. Miyase, Akira; Department of Mechanical Engineering, University of Ottawa, Ottawa, Ontario, Canada, 1983.

19. Lindstrom, Douglas; Department of Mechanical Engineering, University of Ottawa, Ottawa, Ontario, Canada, 1983.

20. Flanagan, R.C., Munro, M., Miyase, A., Wong, J. and Aleong, C.; Full-Size Rotor Component/Material Selection and Ring Manufacture, Report No. UOME-FP-8607-1, Dept. of Mechanical Engineering, University of Ottawa, March 1986, 100pp.

21. Flanagan, R.C., Munro, M., Miyase, A., Lindstrom, D., Bouchard, D., Aleong, C. and Wong, J.; Advanced Materials and Manufacturing Studies for Fibre Composite Flywheels, Report No. UOME-FP-8304-1, Dept. of Mechanical Engineering, University of Ottawa, January 1983, 99pp.

22. Bouchard, D.and Munro, M.; Transverse Tensile Properties of Unidirectional Fibre Composites, Final Report, April 1982, Dept. of Mechanical Engineering, University of Ottawa, 90pp.

23. Brinkmann Instruments (Canada) Ltd., Toronto, Ontario, Canada.

24. Lindstrom, D.and Munro, M.; Development of a Method of Design and Manufacture of Composite Material Containers for Ultra-High Pressure Applications, Annual Report 1983-1984, Dept. of Mechanical Engineering, University of Ottawa, 75pp.

25. Flanagan, R.C., Munro, M.B., Miyase, A., Wong, J., and Aleong, C.; Fabrication and Test Phase High Energy Density Fibre Composite Rotor, Report No. UOME-FP-8302-1, Dept. of Mechanical Engineering, University of Ottawa, May 01-September 30, 1983, 148pp.

26. Errors Due to Misalignment of Strain Gages, M-M Tech. Note TN-511, 1983, Micro-Measurements Division, Measurement Group, Inc., Raleigh, North Carolima.

27. Tuttle, M.E. and Brinson, H.F.; Reisitance-foil Strain-gage Technology as Applied to Composite Materials, Experimental Mechanics, March 1984, pp.54-65.

28. Whitney, J.M., Daniel, I.M., and Pipes, R.B.; Experimental Mechanics of Fibre Reinforced Composite Materials, The Society for Experimental Stress Analysis, Monograph No. 4, 1982.

29. Baldwin-Lima-Hamilton Corporation, Philadelphia, Pennsylvania.

30. Errors Due to Transverse Sensitivity in Strain Gages, M-M Tech. Note TN-509, 1982, Micro-Measurements Division, Measurement Group, Inc., Raleigh, North Carolina.

31. Strain Measurement on Composite Materials, Epsilonics, Volume IV, Issue 1, April 1984. Measurements Group, Inc., Raleigh, North Carolina 27611.

32. Strain Measurement on Composite Materials, Epsilonics, Volume IV, Issue 2, June 1984. Measurements Group, Inc., Raleigh, North Carolina 27611.

33. Rogers, K., Phillips, L., Kingston-Lee, D., Yates, B., Overy, M., Sargent, J., and McCalla, B.; The Thermal Expansion of carbon Fibre-Reinforced Plastics, Journal of Materials Science, Volume 12, 1977.

34. ANSI/ASTM E 251-67, Standard Test Method for Performance Characteristics of Bonded Resistance Strain

Gages; American Society for Testing and Materials, 1980 Annual Book of ASTM Standards, Part 41.

35. Liu, C.Y. and Chamis, C.C.; Residual Stresses in Filament-wound Laminates and Optimum Programmed Winding Tension, Proceedings of the 20th Annual Meeting of Society of the Plastic Industry, Section 5-D, 1965.

36. ASTM D2584-68, Standard Test Methods for Ignition Loss of Cured Reinforced Resins; American Society for Testing and Materials, Volume 08.02 Plastics (II): D1601-D3099,1984.

37. ASTM D2734-70, Standard Test Methods for Void Content of Reinforced Plastics; American Society for Testing and Materials, Volume 08.02 Plastics (II): D1601-D3099,1984.

38. Steele, R.S.; Composite Flywheel Balance Experience, Proceedings of the 16th Intersociety Energy Conversion Engineering Conference, Atlanta, Georgia, August 9-14, 1981.

39. Flanagan, R.C., Munro, M.B., Miyase, A., and Wong, J.; Rotor Design Assessement and R&D Program Definition, Report No. UOME-8301-1, University of Ottawa, Department of Mechanical Engineering, January 1983, 112pp.

40. Dick, W. E.; Design and Manufacturing Considerations for Composite Flywheels, Proceedings of the Flywheel Technology Symposium, Berkeley, California, November 10-12, 1975.

41. Knight, Jr., C.E. and Dewey, B.R.; Experimental and Theoretical Determination of Residual Stresses in Filament-wound Rings, Report No. Y-1701, Union Carbide Corporation, Nuclear Division, Y-12 Plant, Oak Ridge, Tenn., January 6, 1970.

42. Flanagan, R.C., Munro, M.B., Miyase, A., and Wong, J.; Fabrication and Test Phase High Energy Density Fibre Composite Rotor, Report No. UOME-8401-1, University of Ottawa, Department of Mechanical Engineering, June 1984, 93pp.

43. Flanagan, R.C., Munro, M.B., Miyase, A., Wong, J. and Aleong, C.; Basic Materials Studies for Fibre Composite Flywheels, Report No. UOME-FP-8302-1, University of Ottawa, Department of Mechanical Engineering, January 1983, 59pp.

44. Flanagan, R.C., Munro, M.B., Miyase, A., and Wong, J.; High Energy Density Fibre Composite Rotor Design and Analysis, Report No. UOME-FP-8303-1, University of Ottawa, Department of Mechanical Engineering, January 1983, 176pp.

Appendix A

FILAMENT WINDING PROGRAM FOR THICK RING WINDING

This program 'FLYWHEEL' was developed by Doug Lindstrom in 1983 [19] and controls the filament winder for manufacture of the filament wound radial and axially/radially thick rings.

```
10  REM  RING WINDING ROUTINE
20  REM  PRESS ANY KEY TO PAUSE MOTORS
30  REM  PRESS R TO RESTART MOTORS
40  HOME
50  PRINT "RING WINDING PROGRAM"
60  PRINT ""
70  PRINT "PRESS ANY KEY TO PAUSE MOTORS"
80  PRINT ""
90  PRINT "PLEASE INPUT FOLLOWING DATA"
95  PRINT ""
96  PRINT ""
97  PRINT ""
105  PRINT "INPUT RF": INPUT RF: REM
     TRAVERSE PULSE RATE
108  PRINT "INPUT EE": INPUT EE: REM
     TRAVERSE TRAVEL
111  PRINT "INPUT DP": INPUT DP: REM
     NO. OF DOUBLE PASSES
120  DR = 2000: REM  DECELERATION RATE
125  BS = 250: REM  BASE SPEED
127  TT = .1: REM  TIME INCREMENT
141  MR = 1540: REM  MANDREL PULSE RATE
142  GOSUB 8000
150  PR#1: IN# 1
151  PRINT "W,30"
152  PRINT "D,0,"BS","DR",Y"
169  PRINT "S,1,"MR",F,0"
170  FOR J = 1 TO DP
220  PRINT "S,3,"RF",F,"EE"
230  GOSUB 5000
```

```
235  PRINT "F,3"
280  PRINT "S,4,"RF",F,"EE"
290  GOSUB 5200
295  PRINT "F,4"
300  NEXT J
305  GOSUB 9000
306  PRINT "F,0"
310  PR# 0: IN# 0
320  PRINT "END"
5000  REM  CHECK SWITCH MOTOR ROUTINE 1
5010  PRINT "M,3"
5014  INPUT A,B
5020  PR# 0: PRINT "FORWARD";"";J;"      ";B
5022  GOSUB 7000
5024  PR# 1
5025  IF A = 1 THEN GOTO 5010
5057  RETURN
5200  REM  CHECK SWITCH MOTOR ROUTINE 2
5205  X =  FRE (0)
5210  PRINT "M,4"
5214  INPUT A,B
5220  PR# 0: PRINT "REVERSE";"";J;"      ";B
5222  GOSUB  7000
5224  PR# 1
5225  IF A = 1 THEN GOTO 5210
5257  RETURN
7000  I = I + 1
7005  X = PEEK ( - 16384)
7010  IF X > 127 THEN GOTO 7100
7020  IF X < 10 THEN GOTO 7000
7030  GOTO 7210
7100  PR# 0
7110  PRINT "HALT MODE"
7120  PRINT ""
7130  PRINT ""
7140  PRINT "PRESS  R  TO RESTART"
7150  PR# 1
7160  GOSUB 9000
7165  PR# 0
7170  INPUT A$
7180  IF A$ = "R" THEN GOTO 7200
7190  GOTO 7170
7200  GOSUB 9300
7210  I = 0
7220  RETURN
8000  GOTO 8005
8005  DIM RT(75): DIM MM(75)
8010  REM  SET UP DECREMENT TABLES
8020  NM = INT (18000 / DR)
8030  FOR SP = 1 TO NM
8040  MM(SP) = MR - TT * DR * SP
8050  IF MM(SP) > BS GOTO 8150
8060  MM(SP) = BS
8150  NEXT SP
```

```
8170  RETURN
9000  REM  DECELERATION MODE
9010  FOR QR = 1 TO NM
9020  IF MM(QR) < = BS GOTO 9030
9025  GOTO 9055
9030  QF = QR
9050  QR = NM
9055  NEXT QR
9060  FOR QR = 1 TO QF
9070  PRINT ",1,"MM(QR)""
9080  NEXT QR
9090  PRINT "P,0"
9095  RETURN
9300  REM  ACCELERATION MODE
9305  PR# 1
9310  FOR QR = 1 TO NM
9320  IF MM(QR) > BS GOTO 9330
9322  QP = NM - QR
9325  QR = NM
9330  NEXT QR
9340  PRINT "R,0"
9345  QP = QP + 4
9350  FRO JP = QP TO 1 STEP  - 1
9360  PRINT "A,1,"MM(JP)""
9380  NEXT JP
9385  PRINT "A,1,"MR""
9390  RETURN
```

Appendix B

DATA PROGRAM FOR FILAMENT WINDER PROGRAM

This program 'FLYWHEEL DATA', developed by Doug Lindstrom in 1983 [19], provides the inputs for the Filament Winder Program of Appendix A.

```
10  HOME
1000  REM
1010  PRINT "INPUT FEED RATE (INCH/MIN.)"
1020  INPUT FR
1030  GOSUB 2000:RF = R
1040  PRINT "INPUT TOTAL TRAVEL (INCHES)"
1050  INPUT TR
1060  GOSUB 2200:EE = EP:ME = ML
1070  PRINT "INPUT NO. OF DOUBLE PASSES"
1080  INPUT DP
1090  HOME
1100  PRINT "FEED RATE =";FR;" INCH/MIN."
1110  PRINT "TRAVEL =";TR;" INCH."
1120  PRINT "NO. OF DOUBLE PASSES =";DP
1130  PRINT ""
1140  PRINT ""
1150  PRINT "TYPE 1 IF CORRECT"
1160  PRINT "TYPE 2 IF ERROR"
1170  GET G$
1180  IF G$ = "1" THEN GOTO 1200
1190  IF G$ = "2" THEN GOTO 1000
1200  GOTO 3000
2000  REM FEED RATE ROUTINE
2010  FF = 64
2020  R = FF * FR
2030  RETURN
2200  REM  TRAVEL ROUTINE
2210  TF = 3840
2230  NP = TF * TR
2240  ML = INT (NP / 65535)
2250  EP = NP - ML * 65535
2260  RETURN
3000  HOME
3010  PRINT "ENTER THIS DATA IN NEXT PROGRAM"
3021  PRINT ""
```

```
3022  PRINT ""
3023  PRINT ""
3024  PRINT ""
3030  PRINT "RF=      ";RF
3040  PRINT "EE=      ";EE
3050  PRINT "DP=      ";DP
3055  PRINT "ME=      ";ME
3060  PRINT ""
3070  PRINT ""
3080  PRINT "PRESS  RESET"
3090  PRINT ""
4000  PRINT "TYPE RUN FLYWHEEL"
4005  PRINT ""
4010  PRINT "THEN PRESS RETURN"
```

Appendix C

DETERMINATION OF FIBRE VOLUME FRACTION IN FILAMENT WOUND FIBRE COMPOSITE RINGS.

As discussed in the text, three different fibre types were examined, S2-glass, E/XAS carbon and Kevlar 49. Depending on the fibre type, a variety of techniques were employed for determining the fibre volume fraction as well as the void fraction of the composites. In all cases several values were required - the density of the composite both measured and calculated, the fibre and matrix density and the weight fractions of the fibre and matrix. These were then used with the necessary equations to determine the real fibre volume fraction as well as the associated voids. Table C.1 lists the variables as used.

Again depending on the fibre type, a variety of techniques were employed for determining the weight percent of the resin. For the E-glass and S2-glass composites, the weight percents were found using ASTM D2584, Ignition Loss of Cured Reinforced Resins [36], while acid digestion of the epoxy resin was the method used for both the E/XAS carbon and Kevlar 49 composites. Sulphuric acid and hydrogen peroxide or 70% nitric acid solution were the digestion

Table C.1: Variables Used in Volume Fraction Equations.

Volume Fraction (%)	Weight Fraction (%)	Density
V_f V_m V_v	W_f W_m	ρ_f ρ_m
subscripts: A - Apparent (ignoring voids). R - Real. D - from matrix dissolution method.		
Density: ρ_M - Measured density. ρ_c - calculated from matrix dissolution method.		
S2-glass = 2.49 g/cc E/XAS carbon = 1.82 g/cc Ancamine 1482/Epon 825 = 1.2 g/cc		

agents for the carbon composites. With the weight fractions known a volume fraction can be determined from equation (D1).

$$V_{fD} = \frac{W_f/\rho_f}{W_f/\rho_f + W_m/\rho_m} \qquad (D1)$$

The above equation is not the true fibre volume fraction in that it does not take into consideration the void content of the composite. Void contents, evaluated according to ASTM D2734 - Void Content of Reinforced plastics [30], were calculated according to equation (D2).

$$V_v = 1 - \frac{\rho_M}{\rho_c} \qquad (D2)$$

where,

$$\rho_c = (\rho_f - \rho_m)V_{fD} + \rho_m \qquad (D3)$$

Actual fibre volume fractions were determined using equation (D4),

$$V_{fR} = \frac{\rho_M - [\rho_m(1 - V_v)]}{\rho_f - \rho_m} \qquad (D4)$$

Appendix D

FIGURES FOR THERMAL EXPANSION COEFFICIENT DETERMINATION

The following figures were produced with data gathered from the thermal experiments performed on thin S2-glass, E/XAS carbon and Kevlar 49 composite rings. As discussed in Section 4.3.3.2 these figures were instrumental in the determination of the thermal expansion coefficients for the different materials used in this study.

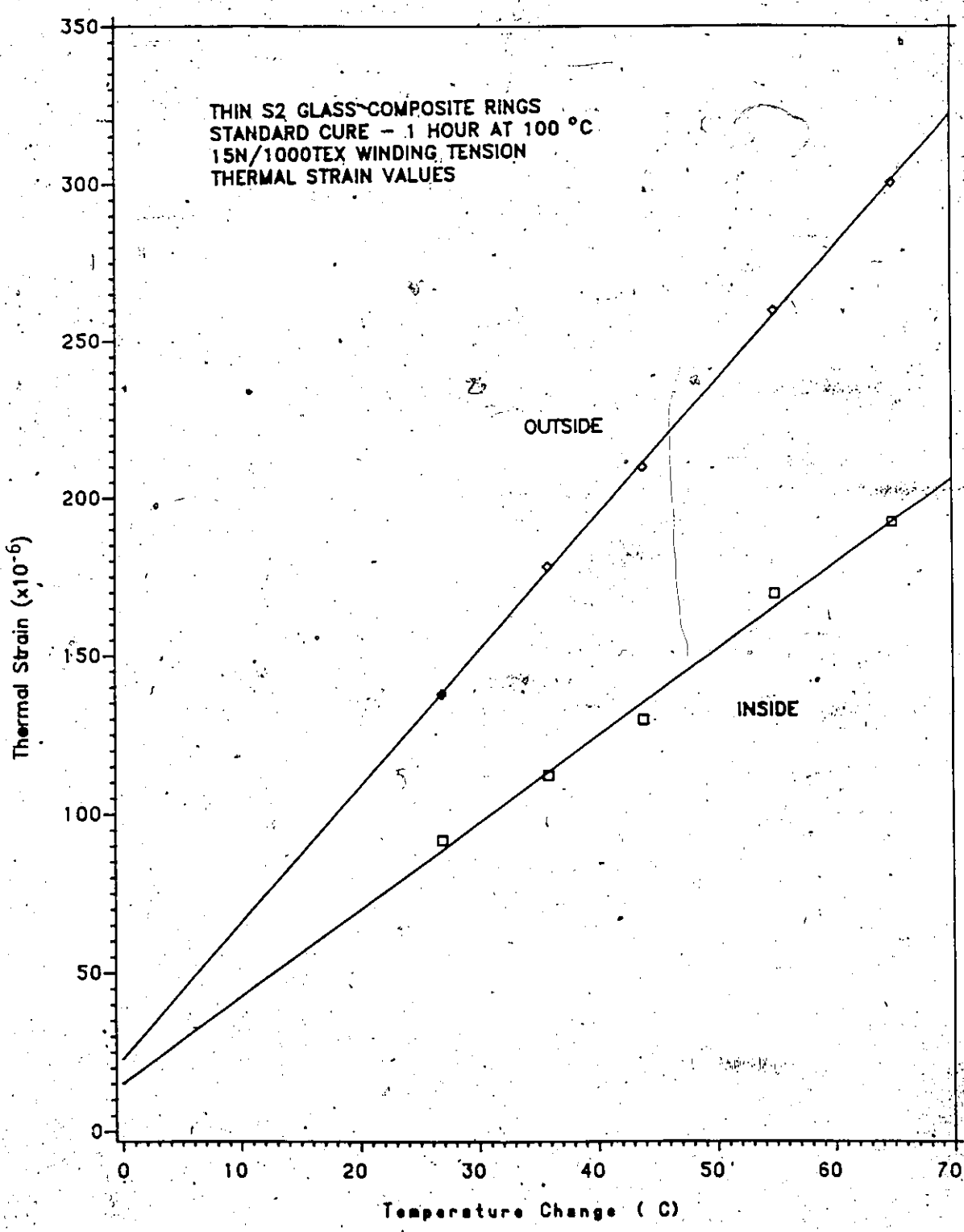

Figure D.1: Thermal strain as a function of temperature change (thin S2-glass composite ring with 15N/1000Tex winding tension).

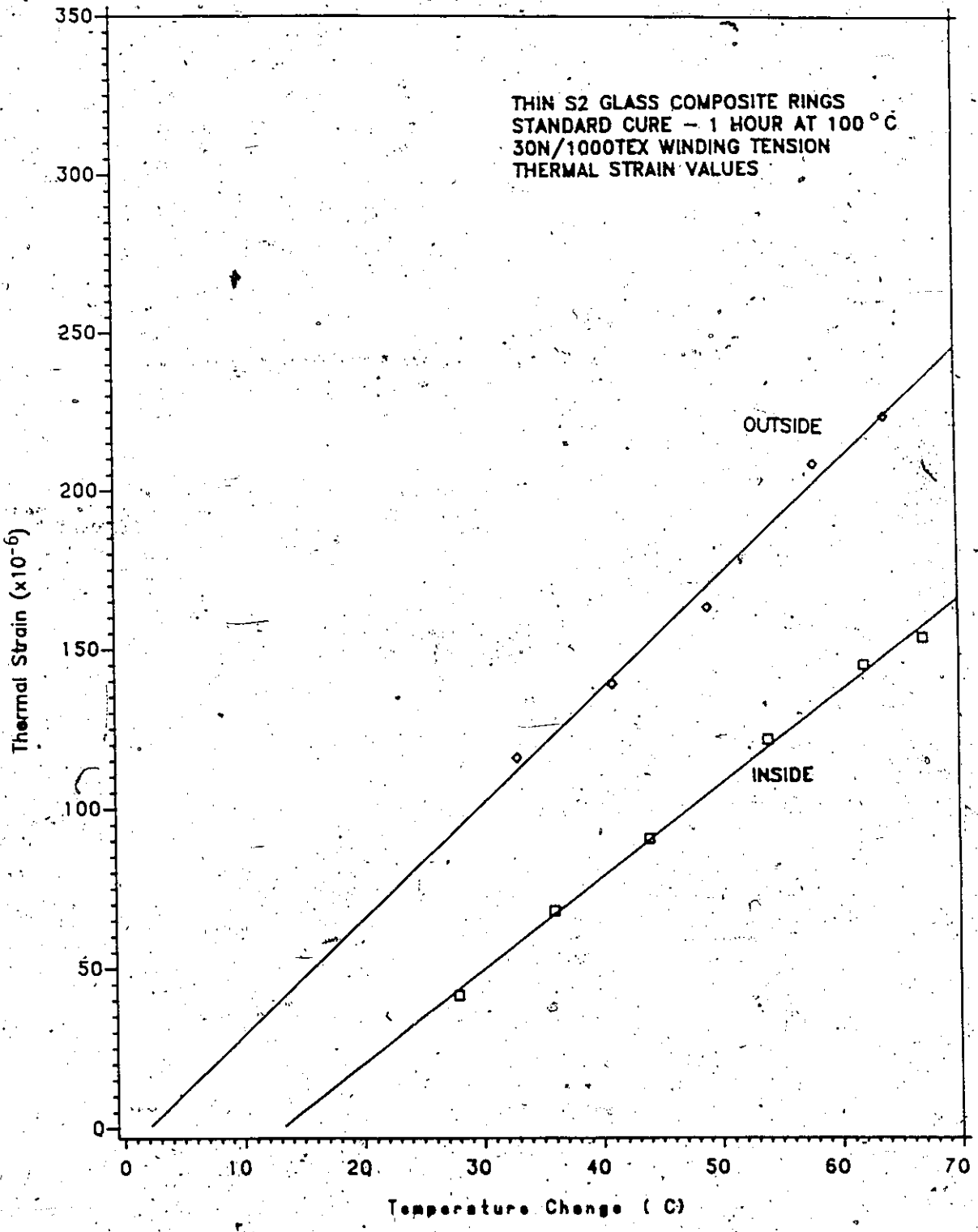

Figure D.2: Thermal strain as a function of temperature change. (thin S2-glass composite ring with 30N/1000Tex winding tension).

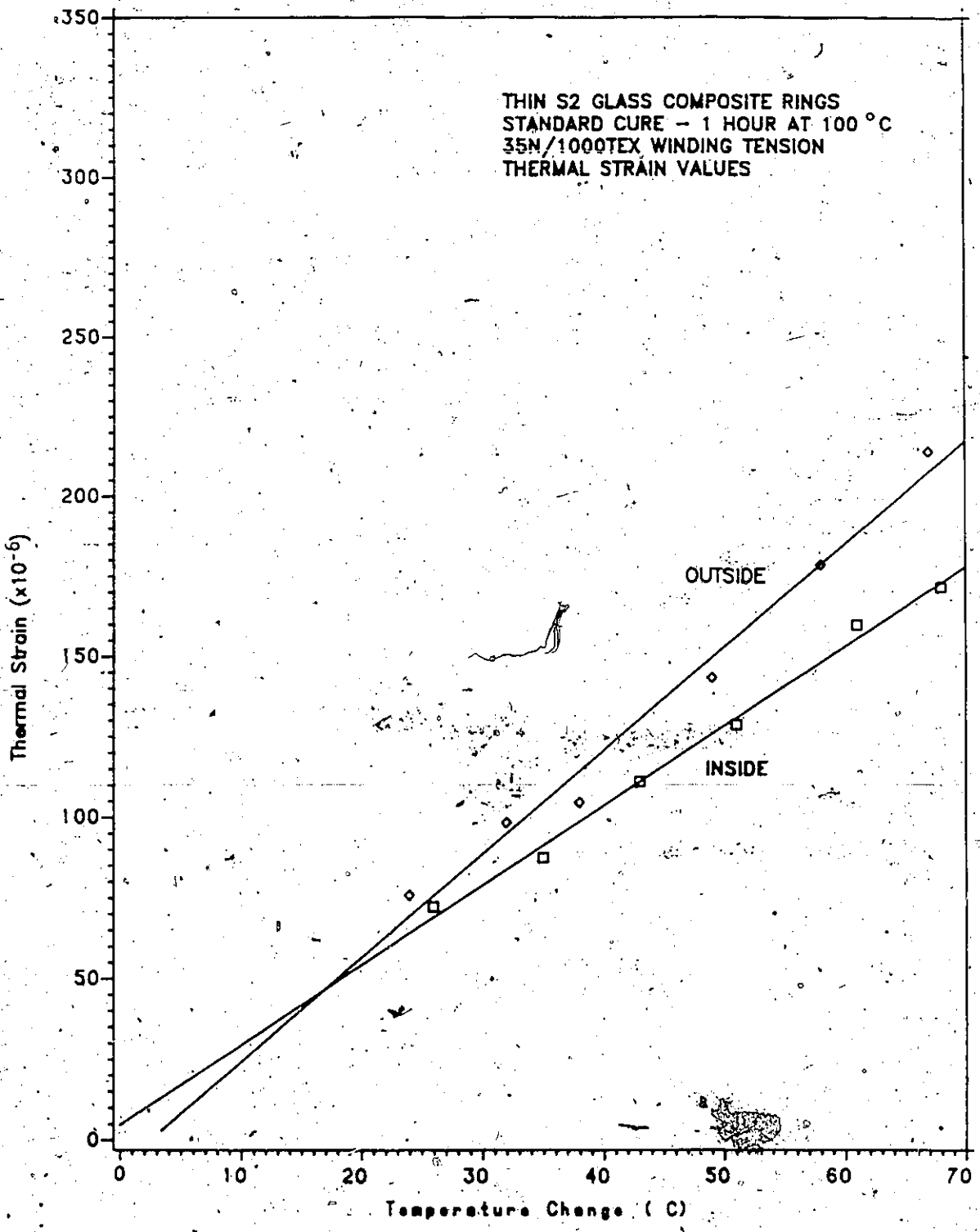

Figure D.3: Thermal strain as a function of temperature change. (thin S2-glass composite ring with 35N/1000Tex winding tension).

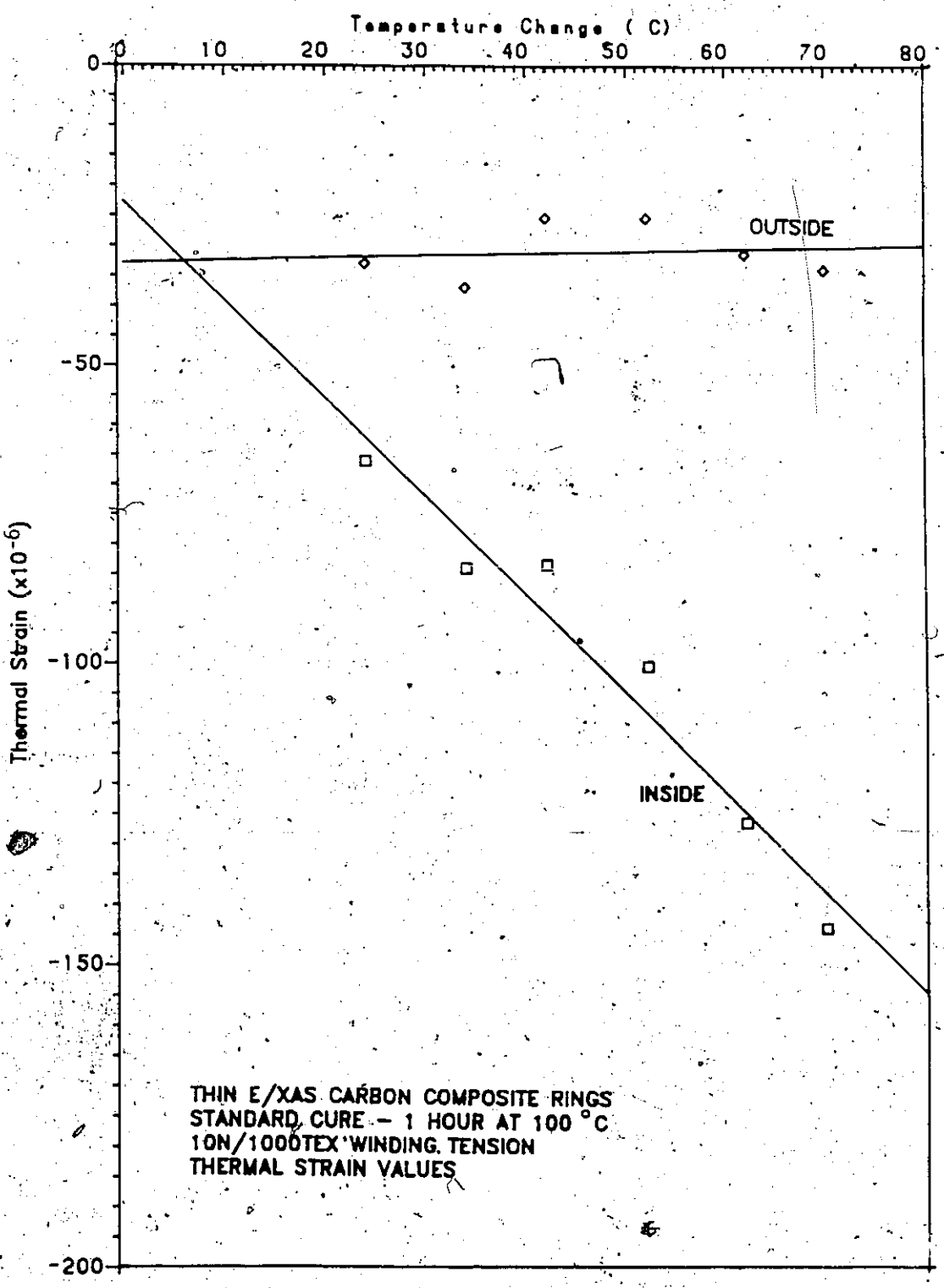

Figure D.4: Thermal strain as a function of temperature change. (thin E/XAS carbon composite ring with 10N/1000Tex winding tension).

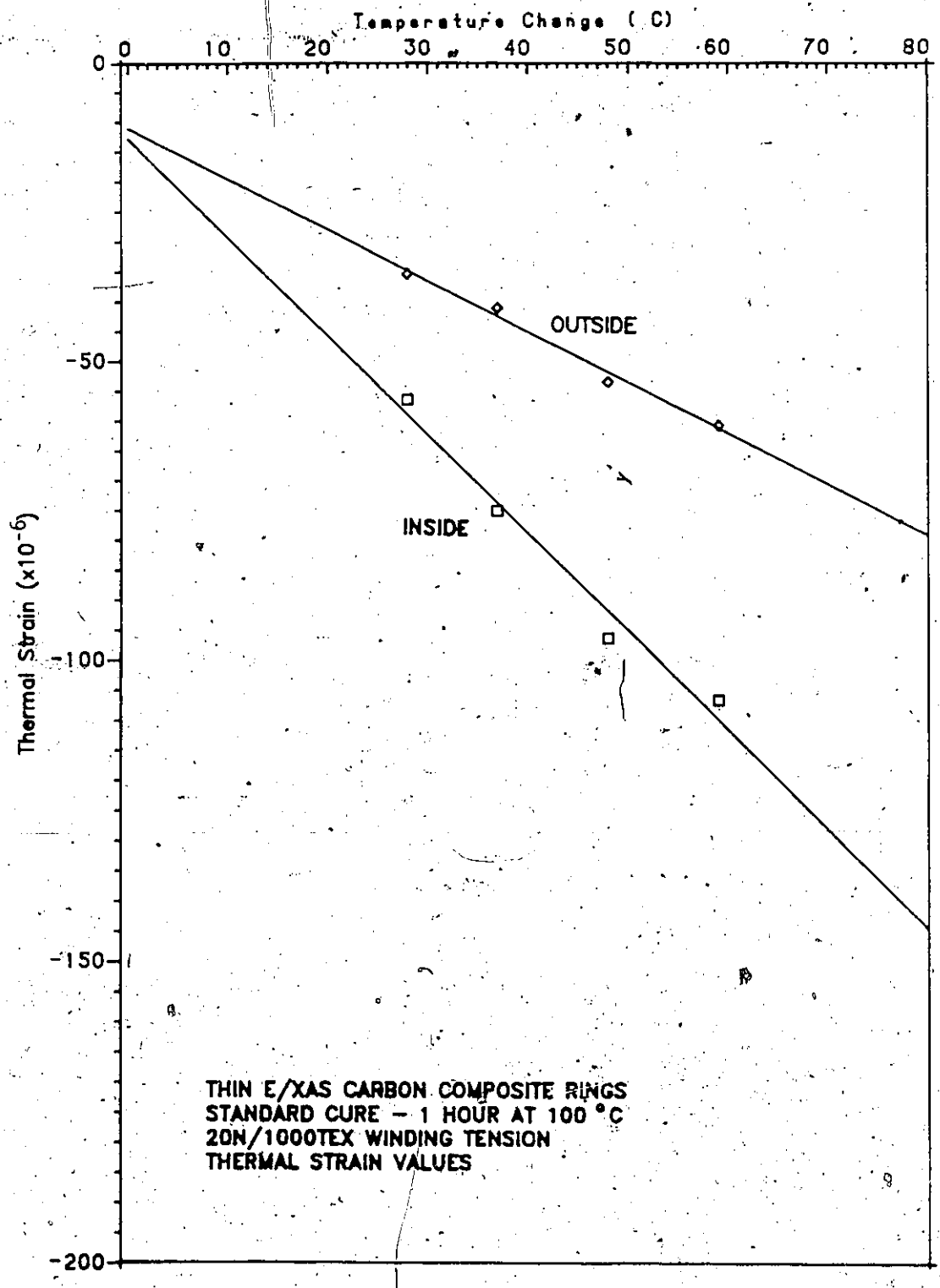

Figure D.5: Thermal strain as a function of temperature change. (thin E/XAS carbon composite ring with 20N/1000Tex winding tension).

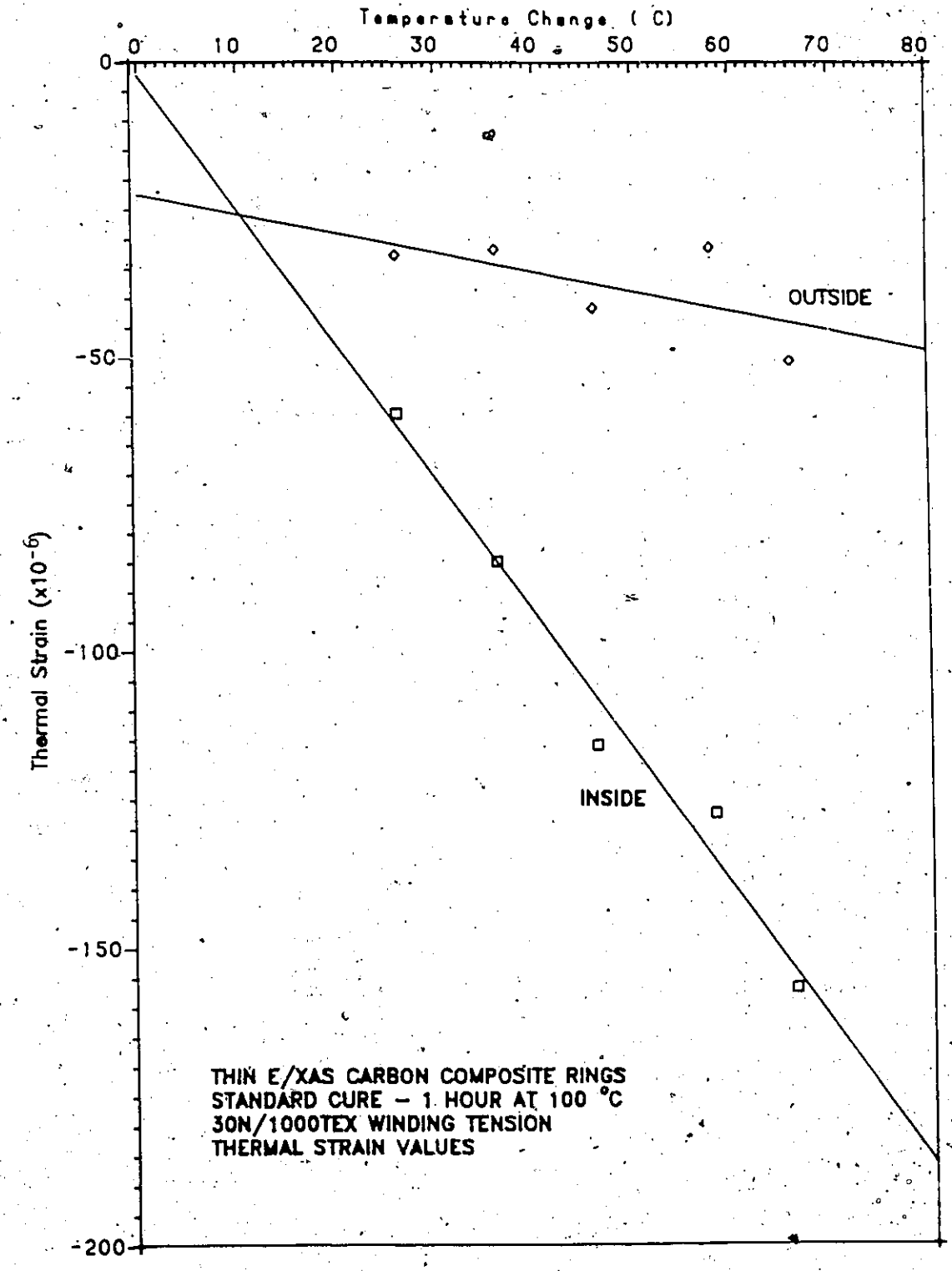

Figure D.6: Thermal strain as a function of temperature change. (thin E/XAS carbon composite ring with 30N/1000Tex winding tension).

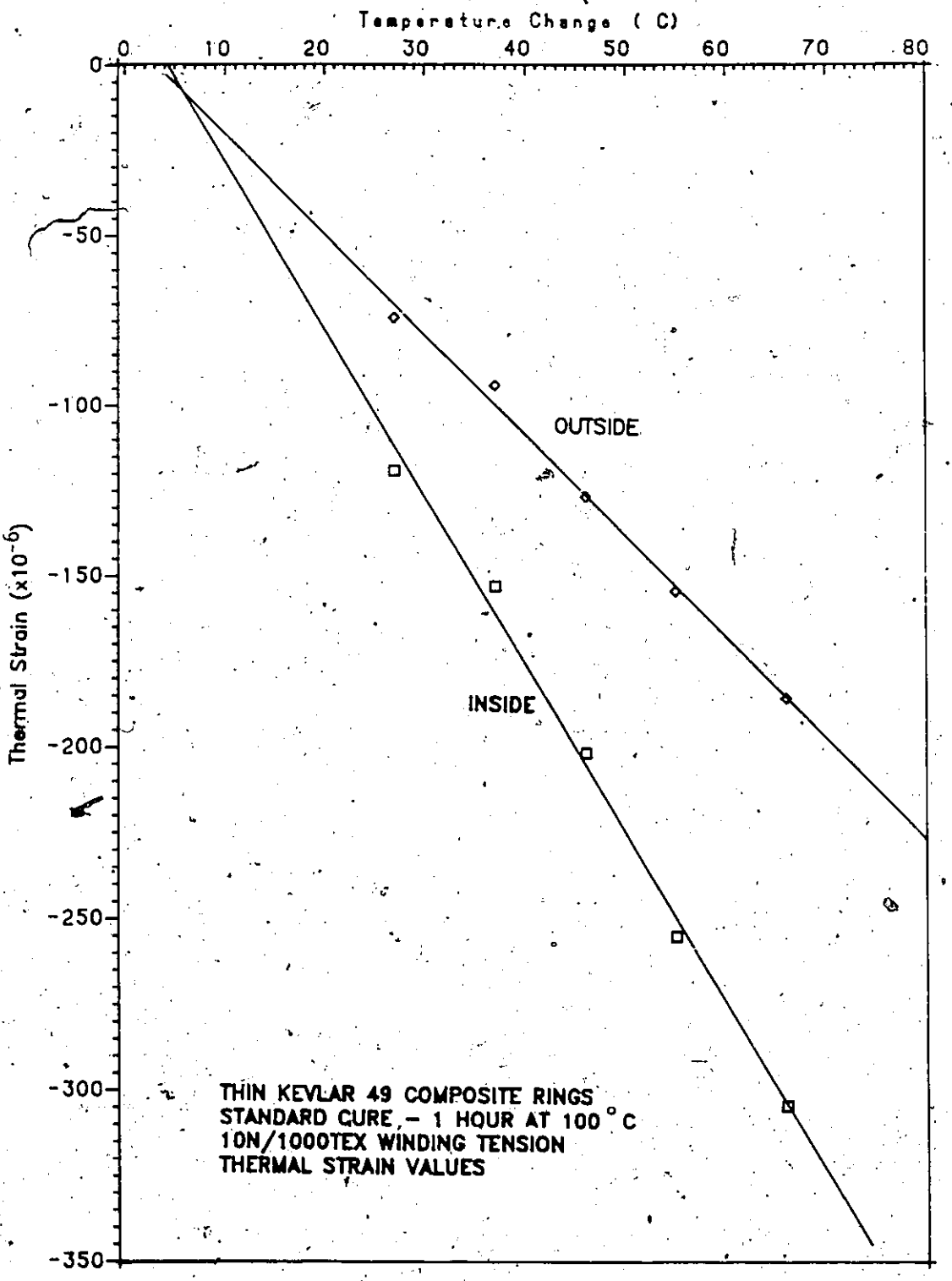

Figure D.7: Thermal strain as a function of temperature change. (thin Kevlar 49 composite ring with 10N/1000Tex winding tension).

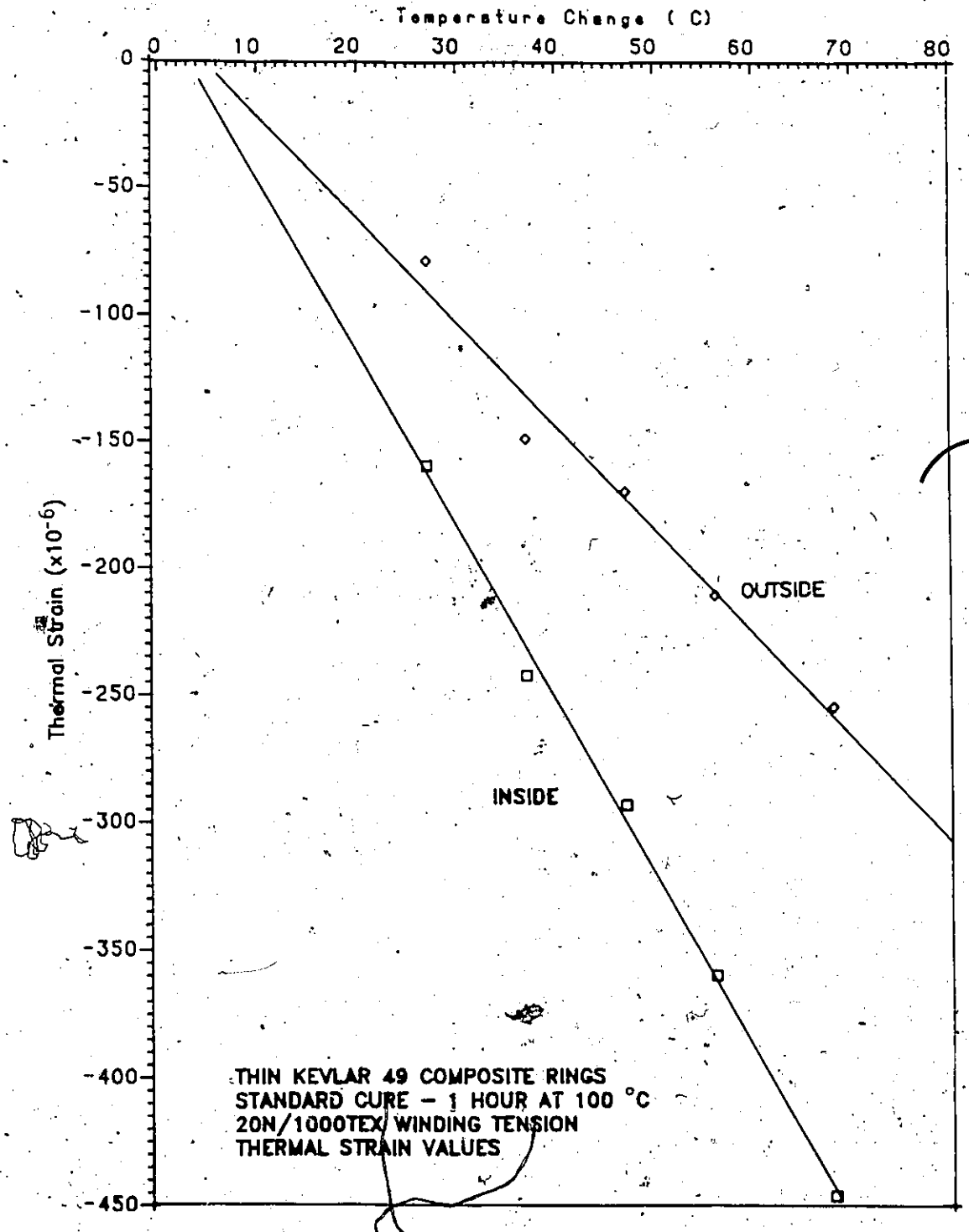

Figure D.8: Thermal strain as a function of temperature change. (thin Kevlar 49 composite ring with 20N/1000Tex winding tension).

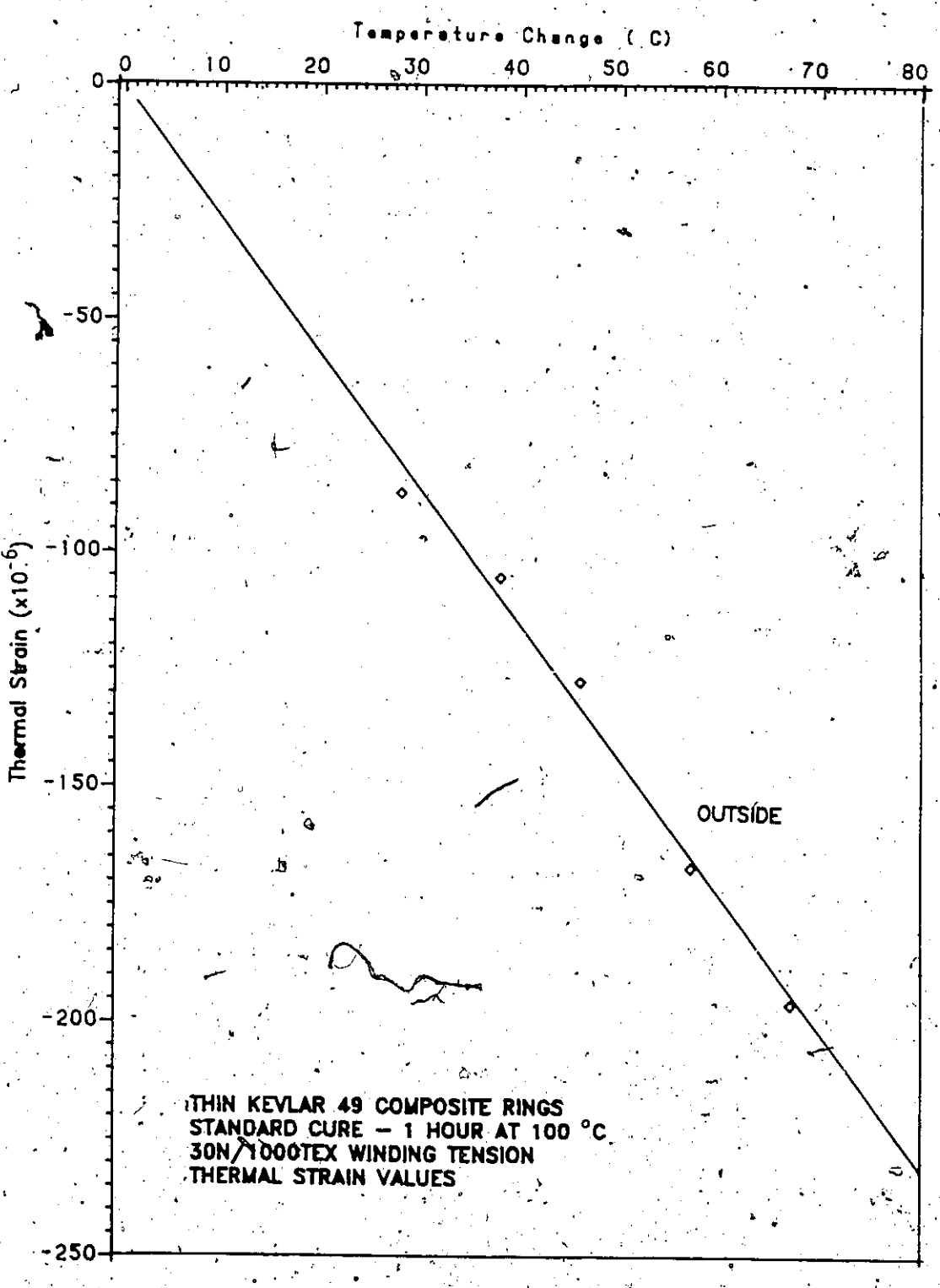

Figure D.9: Thermal strain as a function of temperature change. (thin Kevlar 49 composite ring with 30N/1000Tex winding tension).

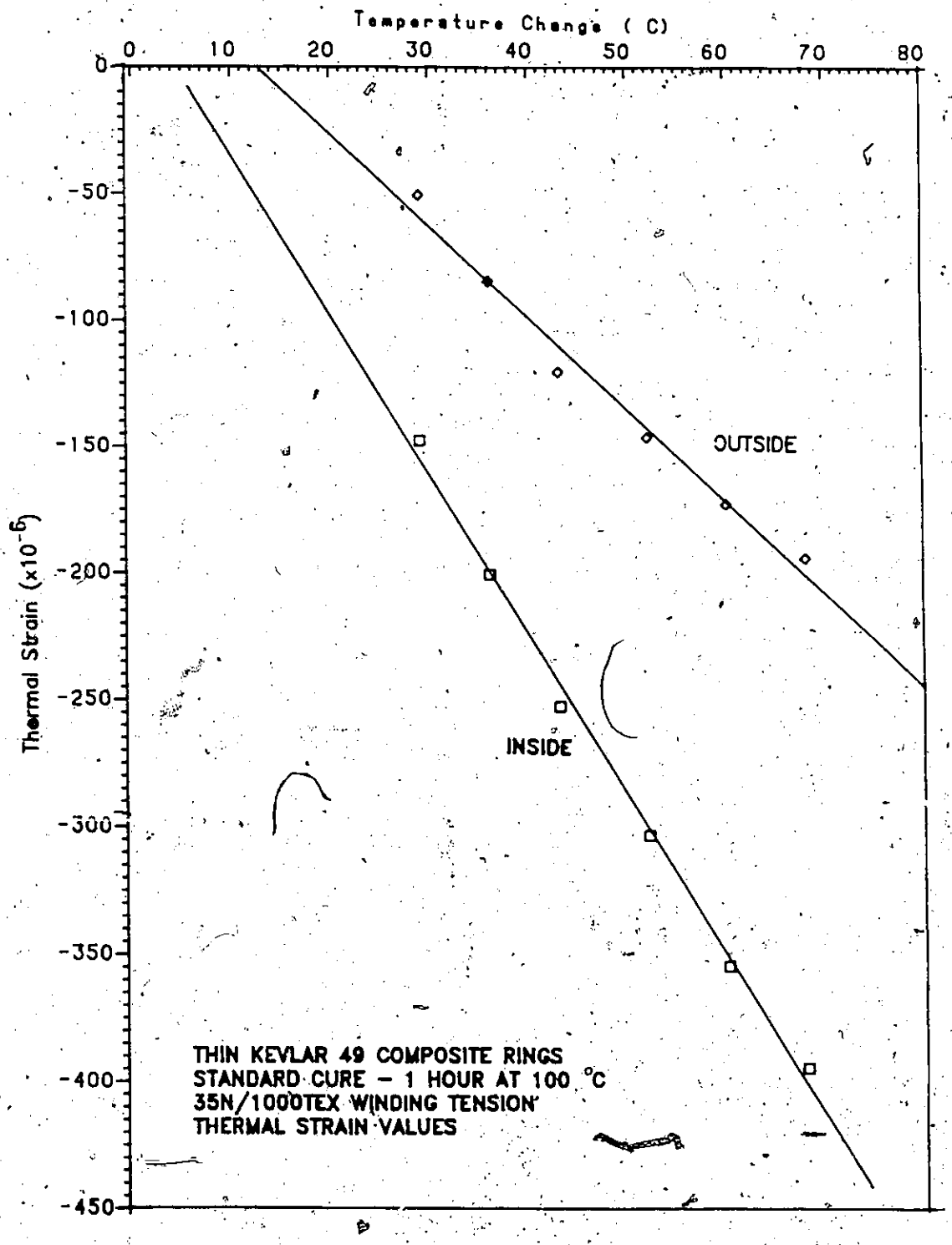

Figure D.10: Thermal strain as a function of temperature change. (thin Kevlar 49 composite ring with 35N/1000Tex winding tension).

Appendix E.

LISTING OF COMPUTER PROGRAM 'THEMOCOE'.

```
C
C*****************************************************************
C
C   PROGRAM NAME: THEMOCOE
C
C   FUNCTION : INPUT INSIDE AND OUTSIDE STRAIN, THEN
C
C              CALCULATES THERMAL COEFFICIENTS & STRESSES
C
C
C      VALID AS OF DATE MAR-2-82
C
C     (UPDATED ON JUNE 7,1983 BY J. WONG)
C
C*****************************************************************
      IMPLICIT REAL*8(A-H,O-Z)
      REAL*8 K ,NK
C
C
C      R = RADIAL POSITION
C
C      U = RADIAL DISPLACEMENT
C
C      RADS, TANS = RADIAL AND TANGENTIAL STRESS
C
C      TORADS, TOTANS = TOATL RAD. AND TAN. STRAIN
C
C      RIRADS, RITANS = RISIDUAL RAD. AND TAN. STRAIN
C
C      RN, UN, RADSN, TANSN = NON-DIMENSIONALIZED VARIABLE
C
C
C
      DIMENSION R(300,5),U(300,5),RADS(300,5),TANS(300,5),
     &RN(300,5),UN(300,5),RADSN(300,5),TANSN(300,5),
     &TOTANS(300,5),TORADS(300,5),RITANS(300,5),
     &RIRADS(300,5),NK(10)
      REAL NYA1,NYA2,NXA,NXA2
      DIMENSION NYA1(300,5),NYA2(300,5),NXA(300,5),
     &NXA2(300,5),XARRAY(350),YARRAY(350),XCOM1(900),
     &YCOM1(900),YCOM2(900)
```

```
      INTEGER CHY11(20),CHY21(20),CHX(20),CHY12(20),
     &CHY22(20),CHY13(20),CHY23(20),CHY14(20),CHY24(20)
      REAL XCOM11,XCOM12,YCOM11,YCOM12,YCOM21,YCOM22
C
C
C*************************************************************
C
C     INPUT :
C
C      CARD 1-9     CHARACTER AND NUMERIC(IGNORED)
C
C      CARD 10    (FORMAT 10I3)
C
C              KPLT = 0 -> NO PLOT REQ.
C                   = 1 -> PLOT REQ.
C              N    = NO. OF POINTS THE RING TO BE DIVIDED
C       CARD 11   (FORMAT 8F10.4)
C
C                  NK(I)= SQRT. OF (ET/ER)
C
C       CARD 12   (FORMAT 8E10.1)
C                   STRNI,STRNO = INSIDE AND OUTSIDE STRAIN
C                               ER  = TRANSVERSE MODULUS
C       CARD 13   (FORMAT 8F10.5)
C                   A,B   = INSIDE AND OUTSIDE RADII OF RING
C                     T   = CHANGE OF TEMPERATURE
C                           (NEGATIVE FOR COOL DOWN)
C                   VT    = POISSON RATIO IN LONGITUDINAL DIR
C
C*************************************************************
C
C
      READ(5,55)CHY11
      READ(5,55) CHY21
      READ(5,55) CHX
      READ(5,55) CHY22
      READ(5,55)CHY13
      READ(5,55) CHY23
      READ(5,55) CHY14
      READ(5,55) CHY24
   55 FORMAT(20A4)
      READ(5,56)NCHY11,NCHY21,NCHX,NCHY22,NCHY13,
     &NCHY23,NCHY14,NCHY24
      READ(5,56) KPLT,IK,N
      READ(5,57)(NK(I),I=1,IK)
   57 FORMAT(8F10.4)
      READ(5,58) STRNI,STRNO,ER
   58 FORMAT(8E10.1)
   56 FORMAT(10I3)
      READ(5,54) A,B,T,VT
   54 FORMAT(8F10.5)
      DO 70 II = 1,IK
      C = A/B
      CP = B/A
```

```
      K = NK(II)
      CONST1= (1-C**(-K-1))/(1-C**(-2*K))*(K-VT)
      CONST2= (1-C**(K-1))/(1-C**(2*K))*(K+VT)
      CONST3 = (CONST1 - CONST2 +(VT-1.))/A
      CONST4 = (CONST1*(CP**K)-CONST2*(CP**(-K)))/B
     &+(VT-1.)/A
      DIFF = (1.0-K**2)*(STRNI-STRNO)/(A*T*(CONST3-CONST4))
      ALPT = ((1-K**2)*STRNI/(A*T)-DIFF*CONST3)*A/(1-K**2)
      ALPR = ALPT - DIFF
      WRITE(6,80) ALPT,ALPR,STRNI,STRNO
   80 FORMAT('  ALPT = ',E12.3,' ALPR = ',E12.3,2(2X,D12.3))
      DELR = (B-A)/(N-1)
      VR=VT/(K**2)
      CN = ER*ALPR*T/(1-VR*VT)
      DO 10 I = 1,N
      R(I,II) = A + (I-1)*DELR
      ALPDIF = ALPT - ALPR
      C = A/B
      RA = R(I,II)/A
      RB = R(I,II)/B
      FRAC1 = (1-C**(-K-1))/(1-C**(-2*K))
      FRAC2 = (1-C**(K-1))/(1-C**(2*K))
      C1 = ER*(K**2-VT**2)*ALPDIF/((1-VT*VR)*(1-K**2))
      U(I,II)=(A*T/(1.-K**2))*(ALPDIF*(K-VT)*FRAC1*(RA**K)
     &-ALPDIF*(K+VT)*FRAC2*(RA**(-K))
     &+((VT*ALPDIF+ALPR-K**2*ALPT)*RA))
      RADS(I,II) = C1*T*(FRAC1*RA**(K-1)+FRAC2*RA**(-K-1)-1)
      TANS(I,II) = C1*T*(K*FRAC1*RA**(K-1)
     &-K*FRAC2*RA**(-K-1)-1)
      RN(I,II) = R(I,II)/A
      UN(I,II) = U(I,II)/(A*ALPR*T)
      RADSN(I,II) = RADS(I,II)/CN
      TANSN(I,II) = TANS(I,II)/CN
      TOTANS(I,II) = TANS(I,II)/(K**2*ER)-VR*RADS(I,II)
     &/ER+ALPT*T
      TORADS(I,II) = RADS(I,II)/ER-VT*TANS(I,II)
     &/(K**2*ER)+ALPR*T
      RITANS(I,II) = TOTANS(I,II)-ALPT*T
      RIRADS(I,II) = TORADS(I,II)-ALPR*T
   10 CONTINUE
   70 CONTINUE
      WRITE (6,20)
   20 FORMAT('1',///,8X,'RADIUS',16X,'TANGENTIAL STRESS',
     &5X,'RADIAL STRESS',10X,'DISPLACEMENT',//)
      WRITE(6,30)((R(I,II),TANS(I,II),RADS(I,II),U(I,II),
     &I=1,N),II=1,IK)
   30 FORMAT(4(6X,E16.8))
      WRITE(6,40)
   40 FORMAT('1',////,20X,'NON-DIMENSIONALISED RESULT')
      WRITE(6,50)
   50 FORMAT(///,8X,'RADIUS',16X,'TANGENTIAL STRESS',5X,
     &'RADIAL STRESS',10X,'DISPLACEMENT',//)
      WRITE (6,30)((RN(I,II),TANSN(I,II),RADSN(I,II),
     &UN(I,II),I=1,N),II=1,IK)
```

```
      WRITE(6,61)
   61 FORMAT('1',////,20X,'TOTAL STRAINS AND
     &RESIDUAL STRAINS')
      WRITE(6,62)
   62 FORMAT(///,4X,'TOT RAD STR',16X,'TOTAL TANG STRAIN',
     &5X,'RISD RAD STR ',10X,'RISD TAN STR',//)
      WRITE (6,30)((TORADS(I,II),TOTANS(I,II),RIRADS(I,II),
     &RITANS(I,II),I=1,N),II=1,IK)
   60 STOP
      END
/*GO.SYSIN  DD  *
RADIAL STRESS
TANGENTIAL STRESS
RADIUS
RADIAL DISPLACEMENT
TOTAL RADIAL STRAIN
TOTAL TANGENTIAL STRAIN
RESIDUAL RADIAL STRAIN
RESIDUAL TANGENTIAL STRAIN
 13 17  6 19 19 23 22 26
  0  1 51
 3.959       3.0       10.0
-144.0D-06 -34.0D-06  1.182D06
  5.10500   5.33609 -70.00000   0.29000
/*
```

Appendix F

LISTING OF COMPUTER PROGRAM 'THEMOSUP'.

```
C
C*************************************************************
C
C  PROGRAM NAME : THEMOSUP
C
C  FUNCTION : INPUT TANGENTIAL AND RADIAL THERMAL
C             COEFFICIENTS, THEN CALCULATES RESIDUAL
C             THERMAL STRAINS AND STRESSES.
C
C      AS OF DATE MAR-2-82
C
C     (UPDATED ON JUNE 7, 1983 BY J. WONG.
C
      IMPLICIT REAL*8(A-H,O-Z)
      REAL*8 K,NK
C
C   R = RADIAL POSITION
C
C   U = RADIAL DISPLACEMENT
C
C   RADS, TANS = RADIAL AND TANGENTIAL STRESS
C
C   TORADS, TOTANS = TOTAL RAD. AND TAN. STRAIN
C
C   RIRADS, RITANS = RESIDUAL RAD. AND TAN. STRAIN
C
C   RN, UN, RADSN, TANSN = NON-DIMENSIONALIZED VARIABLES
C
C
      DIMENSION R(300,5),U(300,5),RADS(300,5),TANS(300,5),
     &RN(300,5),UN(300,5),RADSN(300,5),TANSN(300,5),
     &TOTANS(300,5),TORADS(300,5),RITANS(300,5),
     &RIRADS(300,5),NK(10)
      INTEGER CHY11(20),CHY21(20),CHX(20),CHY12(20),CHY22(20),
     &CHY13(20),CHY23(20),CHY14(20),CHY24(20)
C
C*************************************************************
C
C    INPUT:
C
C    CARD 1-9    CHARACTER AND NUMERIC. (IGNORED)
```

```
C
C    CARD_10      (FORMAT 10I3)
C
C              KPLT = 0 -> NO PLOT REQ.
C                   = 1 -> PLOT REQ.
C              N = NO. OF POINTS THE RING TO BE DIVIDED
C
C    CARD 11      (FORMAT 8F10.4)
C              NK(I)= SQRT. OF (ET/ER)
C
C    CARD 12      (FORMAT 8E10.1)
C   ALPT, ALPR = TANGENTIAL AND RADIAL THERMAL COEFFICIENTS
C           ER = TRANSVERSE MODULUS
C
C    CARD 13      FORMAT(8F10.5)
C        A,B =  INSIDE AND OUTSIDE RADII OF RING
C          T =  CHANGE OF TEMPERATURE
C               (NEGATIVE FOR COOL DOWN)
C         VT =  POISSON RATIO IN LONGITUDINAL DIR.
C
C*****************************************************************
C
C
      READ(5,55) CHY11
      READ(5,55) CHY21
      READ(5,55) CHX
      READ(5,55) CHY22
      READ(5,55) CHY13
      READ(5,55) CHY23
      READ(5,55) CHY14
      READ(5,55) CHY24
   55 FORMAT(20A4)
      READ(5,56) NCHY11,NCHY21,NCHX,NCHY22,NCHY13,NCHY23,
     &NCHY14,NCHY24
      READ(5,56) KPLT,IK,N
      READ(5,57) (NK(I),I=1,IK)
   56 FORMAT(10I3)
   57 FORMAT(8F10.4)
      READ(5,58) ALPT,ALPR,ER
   58 FORMAT(8E10.1)
      READ(5,54) A,B,T,VT
   54 FORMAT(8F10.5)
      DO 70 II=1,IK
      DELR = (B-A)/(N-1)
      K= NK(II)
      VR=VT/(K**2)
      CN=ER*ALPR*T/(1-VR*VT)
      DO 10 I=1,N
      R(I,II)=A+(I-1)*DELR
      ALPDIF=ALPT-ALPR
      C=A/B
      RA=R(I,II)/A
      RB=R(I,II)/B
      FRAC1=(1-C**(-K-1))/(1-C**(-2*K))
```

```
      FRAC2=(1-C**(K-1))/(1-C**(2*K))
      C1=ER*(K**2-VT**2)*ALPDIF*(K-VT)*FRAC1*(RA**K)-ALPDIF
     &*(K+VT)
      U(I,II)=(A*T/1.-K**2))*(ALPDIF*(K-VT)*FRAC1*(RA**K)-
     &ALPDIF*(K+VT)*FRAC2*(RA**(-K))+((VT*ALPDIF+ALPR-K
     &**2*ALPT)*RA))
      RADS(I,II)= C1*T*(FRAC1*RA**(K-1)+FRAC2*RA**(-K-1)-1)
      TANS(I,II)= C1*T*(K*FRAC1*RA**(K-1)-K*FRAC2
     &*RA**(-K-1)-1)
      RN(I,II)=R(I,II)/A
      UN(I,II)=U(I,II)/(A*ALPR*T)
      RADSN(I,II)=RADS(I,II)/CN
      TANSN(I,II)=TANS(I,II)/CN
      TOTANS(I,II)=TANS(I,II)/(K**2*ER)-VR*RADS(I,II)
     &/ER+ALPT*T
      TORADS(I,II)=RADS(I,II)/ER-VT*TANS(I,II)/(K**2*ER)
     &+ALPR*T
      RITANS(I,II)=TOTANS(I,II)-ALPT*T
      RIRADS(I,II)=TORADS(I,II)-ALPR*T
   10 CONTINUE
   70 CONTINUE
      WRITE(6,20)
   20 FORMAT('1',///,8X,'RADIUS',16X,'TANGENTIAL STRESS',
     &5X,'RADIAL STRESS',10X,'DISPLACEMENT',//)
      WRITE(6,30)((R(I,II),TANS(I,II),RADS(I,II),U(I,II),
     &I=1,N),II=1,IK)
   30 FORMAT(4(6X,E16.8))
      WRITE(6,40)
   40 FORMAT('1',////,20X,'NON-DIMENSIONALISED RESULT')
      WRITE(6,50)
   50 FORMAT(///,8X,'RADIUS',16x,'TANGENTIAL STRESS',5X,
     &'RADIAL STRESS',10X,'DISPLACEMENT',//)
      WRITE(6,30)((RN(I,II),TANSN(I,II),RADSN(I,II),
     &UN(I,II),I=1,N),II=1,IK)
      WRITE(6,61)
   61 FORMAT('1',////,20X,'TOTAL STRAINS AND RESIDUAL STRAINS')
      WRITE(6,62)
   62 FORMAT(///,4X,'TOT RAD STR',16X,'TOT TAN STRAIN',5X,
     &'RESID RAD STR',10X,'RESID TAN STR',//)
      WRITE(6,30)((TORADS(I,II),TOTANS(I,II),RIRADS(I,II),
     &RITANS(I,II),I=1,N),II=1,IK)
      IF (KPLT.EQ.0) GO TO 60
   60 STOP
      END
//GO.SYSIN  DD *
RADIAL STRESS
TANGENTIAL STRESS
RADIUS
RADIAL DISPLACEMENT
TOTAL RADIAL STRAIN
TOTAL TANGENTIAL STRAIN
RESIDUAL RADIAL STRAIN
RESIDUAL TANGENTIAL STRAIN
 13 17 6 19 19 23 22 26
```

```
 0 1 51
3.959     — 3.0       10.0          f
-0.700D-06 -30.0D-06    1.182D06
5.10500    5.33609  -70.00000  0.29
/*
```

Appendix G

LISTING OF COMPUTER PROGRAM 'FTENSION'.

```
C
C
C     ***************************************************************
C     *
C     *    FTENSION - WINDING TENSION FROM LIU & CHAMIS
C     *
C     *          WITH ROTATIONAL AND INTERFACIAL PRESS
C     *
C     ***************************************************************
C
C          UPDATED JUNE 7, 1983 BY J. WONG

      IMPLICIT REAL*8(A-H,O-Z)
      REAL K
      REAL*4 XARRAY(310),YARRAY(310)
      DIMENSION AP(100,2)
      DIMENSION NYA1(300,9),NYA2(300,9),NXA(300,9),
      GRA1(300,2),GRA2(300,2),GRA3(300,2)
      DIMENSION R(20),VR(20),VT(20),ET(20),ER(20),
     &D(20),K(20)
C
C     READ DATA
C
C***************************************************************
C
C     INPUT  :
C
C      CARD 1   (FORMAT  6I5)
C               NUM1 = 0 -> NO PLOT REQ.
C                    = 2 -> PLOT REQ.
C      CARD 2   (FORMAT 8F10.5)
C
C               R(M) = OUTSIDE RADIUS OF RING
C
C      CARD 3   (FORMAT 8F10.5)
C
C               VR(1) = RADIAL POISSON RATIO OF RING
C
C       CARD 4  (FORMAT 8F10.5)
C
```

```
C                D(1) = DENSITY OF RING
C
C       CARD 5  (FORMAT 8F10.0)
C
C                   ER(1) = RADIAL MODULUS OF RING
C       CARD 6  (FORMAT 8F10.3)
C
C               RO = INSIDE RADIUS OF RING
C               A = INSIDE RADIUS OF STEEL MANDREL
C
C       CARD 7  (FORMAT 8F10.0)
C
C                   ET(1) = TANGENTIAL MODULUS OF RING
C
C       N.B.  MODULUS OF STEEL MANDREL,EM = 30.E06
C             (EM IS INSIDE THE PROGRAM)
C
C
C*****************************************************************
C
C
      READ(5,1)NL,INC,KOUNT,M,JA,NUM1
    1 FORMAT(6I5)
      READ(5,2)R(M)
      MMM=M-2
    2 FORMAT(8F10.5)
      READ(5,4)VR(1)
    4 FORMAT(8F10.5)
      READ(5,6)D(1)
    6 FORMAT(8F10.5)
      READ(5,5)ER(1)
    7 FORMAT(8F10.0)
      DO 1117 I=2,M
      VR(I)=VR(1)
      D(I)=D(1)
      ER(I)=ER(1)
 1117 CONTINUE
      READ(5,8)PO,PM,OME,RO,G,A
    8 FORMAT(6F10.3)
      RDEL = (R(M)-RO)/M
      R(1) = RO + RDEL
      DO 1116 I = 2,M
      R(I) = R(I-1) + RDEL
 1116 CONTINUE
      FACTOR=1.0
      READ(5,5)ET(1)
      DO 1115 II=1,KOUNT
      IF(II.GT.1)D(6)=0.036
    5 FORMAT(8F10.0)
      DO 1118 I=2,M
      ET(I)=ET(1)
 1118 CONTINUE
      DO 1001 I=1,M
      K(I)=DSQRT(ET(I)/ER(I))
```

```
      VT(I)=VR(I)*((K(I))**2)
 1001 CONTINUE
      NP=300/M
      NNP=NP/6
      NP=NNP*6+1
      NG=M*NP
      IF(NG.GT.300)NP=(NNP-1)*6+1
      NL=NP
      ML=NL
      N3=1
      NN3=1+N3*(NP-1)
      NG=M*NP
      NA=KOUNT
      WRITE(6,1119)II
 1119 FORMAT('1',///,20X,'STIMULATED RESULTS
     &AT CONDITION',3X,I2)
      DO 1002 NN=1,INC
      WRITE(6,15)
   15 FORMAT(///,20X,'RADIUS',7X,'VR',11X,'VT',11X,
     &'DENSITY',6X,'K',12X,'ER',15X,'ET')
      DO 13 I=1,M
      WRITE(6,14) I,R(I),VR(I),VT(I),D(I),K(I),ER(I),ET(I)
   14 FORMAT('0',5X,'RING',I3,5(6X,F7.4),2(6X,F10.0))
   13 CONTINUE
      WRITE(6,1111)PO
 1111 FORMAT(///,6X,'INTERNAL PRESSURE,PO=',F8.2,'PSI')
      WRITE(6,1112)PM
 1112 FORMAT('0',5X,'EXTERNAL PRESSURE,PM=',F8.2,'PSI')
      WRITE(6,1113)RO
 1113 FORMAT('0',5X,'INTERNAL RADIUS,RO=',F6.2,'IN.')
      WRITE(6,1114)OME
 1114 FORMAT('0',5X,'ANGULAR VELOCITY,OME=',F8.1,'RPM')
      CALL STRESS(R,VR,VT,ER,ET,D,K,N3,NN3,ML,INC,M,NG,NA,
     &GRA1,GRA2,GRA3,AP,PO,PM,OME,RO,G,NL,A)
      OME=OME+0
 1002 CONTINUE
      STOP
      END
      SUBROUTINE STRESS(R,VR,VT,ER,ET,D,K,N3,NN3,ML,INC,
     &M,NG,NA,GRA1,GRA2,GRA3,AP,PO,PM,OME,RO,G,NL,A)
      IMPLICIT REAL*8(A-H,O-Z)
      REAL MAXX,MINX,MAXY,MINY
      REAL K
      REAL N
      DOUBLE PRECISION MNSTT,MXSTT
      DIMENSION GRA1(300,2),GRA2(300,2),GRA3(300,2)
      DIMENSION P(20),R(20),VR(20),VT(20),ET(20),D(20),
     &K(20),DEL(20)
      DIMENSION ERRM(20,60),STTM(20,60),R1(20,60),
     &UM(20,60),AP(100,2)
      DIMENSION MAXX(20),MINX(20),MAXY(20),MINY(20)
      DIMENSION MXSTT(20),MNSTT(20)
      DIMENSION H(20,20),C(20),Q(20),ER(20),UUM(20,60)
      OME1=OME
```

```
      OME=(OME*2*3.1415926)/60
C     M IS THE NUMBERS OF RING OF THE FLYWHEEL
C     CALCULATE THE COEFFICIENT OF THE MATRIX A
      M1=M-1
      M=M-1
      DO 9 I=1,M
      DO 19 J=1,M
      H(I,J)=0
   19 CONTINUE
    9 CONTINUE
      M=M-1
      DO 29 I=2,M
      BETA1=(VT(I)-K(I)*(1+(R(I-1)/R(I))**(2*K(I)))/
     &(1-(R(I-1)/R(I))**(2*K(I))))/ET(I)
      BETA2=(VT(I+1)+K(I+1)*(1+(R(I)/R(I+1))**(2*K(I+1)))/
     &(1-(R(I)/R(I+1))**(2*K(I+1))))/ET(I+1)
      H(I,I)=H(I,I)+R(I)*(BETA1-BETA2)
      H(I,I-1)=H(I,I-1)+R(I-1)*2*K(I)*(R(I-1)/R(I))**K(I)/
     &(ET(I)*(1-(R(I-1)/R(I))**(2*K(I))))
      H(I,I+1)=H(I,I+1)+R(I+1)*2*K(I+1)*(R(I)/R(I+1))**K(I+1)
     &/(ET(I+1)*(1-(R(I)/R(I+1))**(2*K(I+1))))
   29 CONTINUE
      H(1,1)=H(1,1)+R(1)*((VT(1)-K(1)*(1+(RO/R(1))**(2*K(1)))
     &/(1-(RO/R(1))**(2*K(1))))/ET(1)-(VT(2)+K(2)
     &*(1+(R(1)/R(2))**(2*K(2)))/(&1-(R(1)/R(2))**(2*K(2))))
     &/ET(2))
      H(1,2)=H(1,2)+R(2)*2*K(2)*(R(1)/R(2))**K(2)/(ET(2)
     &*(1-(R(1)/R(2))**(2*K(2))))
      M=M+2
C M BECOMES THE NUMBER OF RINGS
      H(M-1,M-2)=H(M-1,M-2)+R(M-2)*2*K(M-1)*(R(M-2)
      /R(M-1))**K(M-1)/
     &(ET(M-1)*(1-(R(M-2)/R(M-1))**(2*K(M-1))))
      H(M-1,M-1)=H(M-1,M-1)+R(M-1)*((VT(M-1)-K(M-1)
     &*(1+(R(M-2)/R(M-1))**(2*K(M-1)))/(1-(R(M-2)/R(M-1))
     &**(2*K(M-1))))/ET(M-1)-(VT(M)
     &+K(M)*(1+(R(M-1)/R(M))**(2*K(M)))/(1-(R(M-1)/R(M))
     &**(2*K(M))))/ET(M))
C     READ VECTOR Q
      M=M-1
C    M BECOMES THE NUMBERS OF INTERFACES
      DO 30 I1=1,M
      I=I1
      DC1=D(I)/(9-K(I)**2)
      DC2=(1+3*VR(I))/ER(I)
      DC3=(3+VT(I))*K(I)/ET(I)
      IF(I.EQ.1)GO TO 500
      DC4=(1-2*(R(I-1)/R(I))**(K(I)+3)+(R(I-1)/R(I)).
     &**(2*K(I)))/(1-(R(I-1)/R(I))**(2*K(I)))
  600 DC11=DC1
      DC21=DC2
      DC31=DC3
      DC41=DC4
      I=I+1
```

```
      DC1=D(I)/(9-K(I)**2)
      DC2=(1+3*VR(I))/ER(I)
      DC3=(3+VT(I))*K(I)/ET(I)
      DC5=(1-2*(R(I-1)/R(I))**(K(I)-3)+(R(I-1)/R(I))
     &**(2*K(I)))/(1-(R(I-1)/R(I))**(2*K(I)))
      I=I-1
      DEL(I)=DC11*(DC21-DC31*DC41)-DC1*(DC2+DC3*DC5)
      IF(I.EQ.1)GO TO 300
      IF(I.EQ.M1)GO TO 400
      Q(I)=OME**2*R(I)**3*DEL(I)/G
      GO TO 30
  300 Q(1)=OME**2*R(1)**3*DEL(1)/G-PO*RO**2*K(1)
     &*(RO/R(1))**K(1)/(ET(1)*(1-(RO/R(1))**(2*K(1))))
      GO TO 30
  400 Q(M)=OME**2*R(M)**3*DEL(M)/G-PM*R(M+1)**2*K(M+1)
     &*(R(M)/R(M+1))**
     &K(M+1)/(ET(M+1)*(1-(R(M)/R(M+1))**(2*K(M+1))))
      GO TO 30
  500 DC4=(1-2*(RO/R(I))**(K(1)+3)+(RO/R(1))**(2*K(1)))
     &/(1-(RO/R(1))**(2*K(1)))
      GO TO 600
   30 CONTINUE
      CALL MATINV(H,M)
      DO 16 I=1,M
      C(I)=0
   16 CONTINUE
      DO 17 L=1,M
      DO 18 J=1,M
      C(L)=C(L)+H(L,J)*Q(J)
   18 CONTINUE
   17 CONTINUE
      M=M+1
C      M BECOMES THE NUMBER OF RINGS
C      CALCULATE ALL THE STRESS IN EACH RING
      DO 701 I1=1,M
      N=K(I1)
      IF(I1.EQ.1)W=RO
      IF(I1.EQ.1)PA=PO
      IF(I1.EQ.1)GO TO 704
      W=R(I1-1)
      PA=C(I1-1)
  704 B=R(I1)
      IF (I1.EQ.M)PB=PM
      IF (I1.EQ.M)GO TO 705
      PB=C(I1)
  705 RAD=W
      X=(B-W)/(NL-1)
      J=1
  702 RA=RAD/W
      RB=RAD/B
      R1(I1,J)=RAD
      F=W/B
      Z=B/W
      A1=ER(I1)*(N+VT(I1))/(1-VR(I1)*VT(I1))
```

```
      A2=ER(I1)*(-N+VT(I1))/(1.-VR(I1)*VT(I1))
      A3=(3.+VT(I1))*D(I1)/((9.-N**2.)*G)
      DIV=W**(N-1)*B**(-N-1)-W**(-N-1)*B**(N-1.)
      C1=A3*OME**2*(W**2*B**(-N-1)-W**(-N-1)*B**2.)/(A1*DIV)
     &-(PA*B**(-N-1)-PB*W**(-N-1))/(A1*DIV)
      C2=A3*OME**2*(W**(N-1)*B**2.-W**2.*B**(N-1))/(A2*DIV)
     &+(PA*B**(N-1)-PB*W**(N-1))/(A2*DIV)
      U=C1*RAD**N+C2*RAD**(-N)-D(I1)*OME**2.*(1-VR(I1)
     &*VT(I1)) *RAD**3./(ER(I1)*G*(9.-N**2))
      BAC=(K(I1)-VT(I1))*(1-F**(K(I1)+3))*(RB**K(I1))
     &/(1 -F**(2*K(I1)))-(K(I1)+VT(I1))*(1-F**(K(I1)-3))*F
     &**(K(I1)+3)*RB**(-K(I1))/(1-F**(2*K(I1)))
      BAC1=(3+VT(I1))*BAC-(K(I1)**2-VT(I1)**2)*RB**3
      BAC2=(K(I1)-VT(I1))*RB**K(I1)+(K(I1)+VT(I1))
     &*RB**(-K(I1))
      BAC3=(K(I1)-VT(I1))*RB**K(I1)+(K(I1)+VT(I1))*F
     &**(2*K(I1))*RB**(-K(I1))
      UU=D(I1)*OME**2*B**3*BAC1/(G*ET(I1)*(9-K(I1)**2))
     &+PA*B*F**(K(I1)&+1)*BAC2/(ET(I1)*(1-F**(2*K(I1))))
     &-PB*B*BAC3/(ET(I1)*(1-F**(2*&K(I1))))
      DENO=(W/B)**(-N-1)-(W/B)**(N-1)
      E1=(RA**(-N-1)-RA**(N-1))/DENO
      E2=(RB**(-N-1)-RB**(N-1))/DENO
      F1=(RA**(-N-1)+RA**(N-1))/DENO
      F2=(RB**(-N-1)+RB**(N-1))/DENO
      X1=(3+VT(I1))*D(I1)*(OME**2)*(B**2)/((9.-(N**2))*G)
      X2=(1.-(F**(N+3)))/(1.-(F**(2*N)))
      X3=(1.-(F**(-N+3)))/(1.-(F**(-2*N)))
      XN=(N**2+3*VT(I1))/(3+VT(I1))
      ERR=PB*(Z**2)*E1-PA*E2-X1*(RB**2-X2*(RB**(N-1))-X3
     &*(RB**(-N-1)))
      STT=N*PA*F2-N*PB*(Z**2)*F1-X1*((RB**2)*XN-N*X2
     &*(RB**(N-1))+N*X3*(RB**(-N-1)))
      AP(J,2)=ERR
      UM(I1,J)=U
      UUM(I1,J)=UU
      EM=30.0E6
      VM=0.3
      B1=(ET(I1)/(EM*(RO**2-A**2)))*((1.-VM)*(RO**2)
      +(1.+VM)*(A**2))
      CALL RESTEN(A,RO,B1,R(M),RAD,VT(I1),K(I1),
     &RTEERR,RTESTT)
      ERRM(I1,J)=ERR+RTEERR
      STTM(I1,J)=STT+RTESTT
      RAD=RAD+X
      J=J+1
      IF(J.LE.ML)GO TO 702
C     WRITE AND PLOT RESULTS
      J=ML
      I=I1
      DO 901 I4=1,J
      AP(I4,I)=R1(I,I4)
  901 CONTINUE
C      COMPUTE THE MAXIMUM OF ERR
```

```
      MAXY(I)=ERRM(I,1)
      DO 806 J=1,ML
      IF(ERRM(I,J).LE.MAXY(I))GO TO 806
      MAXY(I)=ERRM(I,J)
  806 CONTINUE
C COMPUTE THE MINUMUM OF ERR
      MINY(I)=ERRM(I,1)
      DO 807 J=1,ML
      IF(ERRM(I,J).GT.MINY(I))GO TO 807
      MINY(I)=ERRM(I,J)
  807 CONTINUE
C     COMPUTE THE MAXIMUM OF STT
      MXSTT(I)=STTM(I,1)
      DO 810 J=1,ML
      IF(STTM(I,J).LE.MXSTT(I))GO TO 810
      MXSTT(I)=STTM(I,J)
  810 CONTINUE
C     COMPUTE THE MINIMUM OF STT
      MNSTT(I)=STTM(I,1)
      DO 811 J=1,ML
      IF(STTM(I,J).GT.MNSTT(I))GO TO 811
      MNSTT(I)=STTM(I,J)
  811 CONTINUE
      XMAX=R1(I,ML)
      XMIN=R1(I,1)
      YMAX=MAXY(I)
      YMIN=MINY(I)
      S=I
  701 CONTINUE
C
C
      SUBROUTINE RESTEN(A,B,B1,C,R,VT,S,RAS,HOS)
C
C
C
C*************************************************************
C
C      A = INSIDE RADIUS OF THE MANDREAL
C
C      B = INSIDE RADIUS OF THE RING
C
C      B1= BETA (A CONSTANT)
C
C      C = OUTSIDE RADIUS OF THE RING
C
C      R = RADIAL POSITION OF A CERTAIN POINT
C
C     VT = POISSON RATIO OF COMPOSITE RING IN TANGENTIAL
C
C          DIRECTION
C
C      S = SQUARE ROOT OF (E11/E22)
C
```

```
C     RAS = RESIDUAL STRESS IN RADIAL DIRECTION AFTER
C
C           TAKEN AWAY FROM MANDREAL
C
C     HOS = RESIDUAL STRESS IN TANGENTIAL DIRECTION AFTER
C
C           TAKEN AWAY FROM MANDREAL
C
C
C*************************************************************
C
C
      IMPLICIT REAL*8(A-H,O-Z)
      REAL S
      RO=B
      N=400
      AT=S-VT-B1
      BT=S+VT+B1
      CALL SIMPSO(FB,N,B,C,AT,BT,S,R0)
      CALL SIMPSO(FR,N,R,C,AT,BT,S,RO)
      SAR=2*S*(B**(2*S))*(C**(S-1))*FB/((C**(2*S))
     &-(B**(2*S)))
      SAT=2*(S**2)*(B**(2*S))*(C**(S-1))*FB/((C**(2*S))
     &-(B**(2*S)))
      RAS=SAR*((C/R)**(S+1)-(R/C)**(S-1))-B**(S-1)
     &*((AT*((B/R)**(S+1)))+BT*((R/B)**(S-1)))*FR
      HOS=T(R)-SAT*((C/R)**(S+1)+(R/C)**(S-1))+S
     &*(B**(S-1))*(AT*((B/R)**(S+1))-BT*((R/B)**(S-1)))*FR
      RETURN
      END
       SUBROUTINE SIMPSO(SI,N,A,C,AT,BT,S,RO)
       IMPLICIT REAL*8(A-H,O-Z)
      REAL S
       INTEGER N2,N,I
           N2 = 2*N
           H = (C-A)/N2
           I = 2
           SUMEVN = 0.0
           SUMODD = F(A+H,AT,BT,S,RO)
30         IF(I.LE.N2-2) GO TO 10
               GO TO 20
10             X = A+I*H
               SUMEVN = SUMEVN+F(X,AT,BT,S,RO)
               SUMODD = SUMODD+F(X+H,AT,BT,S,RO)
               I = I+2
               GO TO 30
20         SI = (F(A,AT,BT,S,RO)+F(C,AT,BT,S,RO)
     &+4.0*SUMODD+2.0*SUMEVN)*H/3.0
       RETURN
       END

C
C
```

```
      FUNCTION F(X,AT,BT,S,RO)
      IMPLICIT REAL*8(A-H,O-Z)
      REAL S
      F=((X**S)*T(X))/(BT*(X**(2*S))+AT*(RO**(2*S)))
      RETURN
      END
C
C
C
      FUNCTION T(X)
      IMPLICIT REAL*8(A-H,O-Z)
      T=1000.
      RETURN
      END
//GO.SYSIN  DD  *
   50    1    1   06    1    0
   5.33290
   0.02411
   0.05000
 00841000.
 000          00    00000       5.105      386.       4.855
012905000.         0
/*
```

Appendix H

LISTING OF COMPUTER PROGRAM 'OVERLAP'.

```
C
C     COMPUTER PROGRAM 'OVERLAP' USED TO CALCULATE THE
C
C     RESIDUAL STRESS IN FILAMENT WOUND FIBRE COMPOSITE
C
C                    RINGS.
C
C                 (J. Wong, 1982)
C
      IMPLICIT REAL * 8(A-H,O-Z)
      DOUBLE PRECISION KK
      DIMENSION R(5,5,100),RRADS(5,5,100),RTANS(5,5,100),
     &RM(5,5),RM1(5,5),AM(5,5),BM(5,5),DIFF(5,5),
     &STAN(5,5,100),U(5,5,100),RRADSA(5,5,100),
     &RTANSA(5,5,100),RMA(5,5),DIFFA(5,5),STANA(5,5,100),
     &UA(5,5,100),ZM(5,5),SRADA(5,5,100)
      REAL NYA1,NYA2,NXA,NXA2
      DIMENSION NYA1(150,5),NYA2(150,5),NXA(150,5),
     &NXA2(150,5),XARRAY(350),YARRAY(350),XCOM1(900),
     &YCOM1(900),YCOM2(900)
      INTEGER CHY11(20),CHY21(20),CHX(20),CHY12(20),CHY22(20)
      REAL XCOM11,XCOM12,YCOM11,YCOM12,YCOM21,YCOM22
      READ(5,55)CHY11
      READ(5,55) CHY21
      READ(5,55) CHX
      READ(5,55)CHY12
      READ(5,55) CHY22
   55 FORMAT(20A4)
      READ(5,56)NCHY11,NCHY21,NCHX,NCHY12,NCHY22
   56 FORMAT(5I3)
      READ(5,51) NA,NB,NPT,NZ,KRLT
      READ(5,52) AO,BO,DELA,DELB,Z,VT,STANI
      READ(5,53) ET,ER
   51 FORMAT(5I3)
   52 FORMAT(8F10.4)
   53 FORMAT(8F10.1)
      STANI = STANI/1000000.
      PRIM=3.1416
      KK=DSQRT(ET/ER)
      VR = VT*ER/ET
      DO 30 I = 1,NA
```

```
      A= AO+(I-1)*DELA
      DO 10 J=1,NB
      B=(A+(BO-AO))+(J-1)*DELB
      C=A/B
      RNA=(A+B)/2.
      IF(NZ.EQ.1) GO TO 100
      COEF2 = (1.-C**(KK+1.))*(A/B)**(KK-1.)/(1.-C**(2*KK))
      COEF3 = (1.-C**(KK-1.))*C**(KK+1.)*(B/A)**(KK+1.)/(1.
     &-C**(2*KK))
      Z=2.*PRIM*(1.-KK**2)*RNA*STANI/((1.-KK*COEF2+KK*COEF3)
     &-VT*(1.-COEF2-COEF3))
  100 RM(I,J)=Z*ET*((B**2-A**2)**2-4.*(A**2)*(B**2)*
     &(DLOG(B/A))**2)
     &/(16.*PRIM*RNA*(B**2-A**2))
      RG = (1.-C**2)/2.-KK*(1.-C**(KK+1))**2/((KK+1.)*
     &(1.-C**(2*KK)))
     &+KK*C**2*(1.-C**(KK-1.))**2/((KK-1.)*(1.-C**(2*KK)))
      RMA(I,J)=B**2*RG*ET*Z/(2.*PRIM*(1.-KK**2)*RNA)
      RM1(I,J)=ET*Z*(B-A)**3/(24.*PRIM*RNA**2)
      DIFF(I,J) = (RM(I,J)-RM1(I,J))*100./RM(I,J)
      DIFFA(I,J)=(RMA(I,J)-RM(I,J))*100./RMA(I,J)
      DELR=(B-A)/(NPT-1)
      AM(I,J) = A
      BM(I,J) = B
      ZM(I,J) = Z
      DO 20 K =1, NPT
      R(I,J,K) = A+(K-1)*DELR
      RK       = R(I,J,K)
      RRADS(I,J,K) =Z*ET*(A**2*B**2*(DLOG(B/A))/RK**2
     &+B**2*DLOG(RK/B)+A**2*DLOG(A/RK))/
     &(4.*PRIM*RNA*(B**2-A**2))
      RTANS(I,J,K) = Z*ET*(-A**2*B**2*(DLOG(B/A))/RK**2
     &+B**2*DLOG(RK/B)+A**2*DLOG(A/RK)+B**2-A**2)/
     &(4.*PRIM*RNA*(B**2-A**2))
      STAN(I,J,K) = (RTANS(I,J,K)-VR*RRADS(I,J,K))/ET
      U(I,J,K)    = STAN(I,J,K)*RK
      COEF1 = (ET*Z)/(2.*PRIM*(1.-KK**2)*RNA)
      COEF2 = (1.-C**(KK+1.))*(RK/B)**(KK-1.)/(1.-C**(2*KK))
      COEF3 = (1.-C**(KK-1.))*C**(KK+1.)*(B/RK)**(KK+1.)/
     &(1.-C**(2*KK))
      RRADSA(I,J,K) = COEF1*(1.-COEF2-COEF3)
      RTANSA(I,J,K) = COEF1*(1.-KK*COEF2+KK*COEF3)
      STANA(I,J,K) = RTANSA(I,J,K)/ET-VR*RRADSA(I,J,K)/ER
      UA(I,J,K)    = STANA(I,J,K)*RK
      SRADA(I,J,K) = RRADSA(I,J,K)/ER-VT*RTANSA(I,J,K)/ET
   20 CONTINUE
      IF(KPLT.EQ.0) GO TO 10
      KCOUNT = 0
      CALL ARRANG(RRADSA,RTANSA,R,I,J,NPT,1,NYA1,NYA2,NXA)
      CALL GENPT2(NYA1,NYA2,NXA,NXA,20.0,16.0,NPT,1,1,1.0,
     &0.0,1,0.0,XCOM11,XCOM12,YCOM11,YCOM12,YCOM21,YCOM22,
     &1.0,1.0,CHY11,NCHY11,CHY21,NCHY21,CHX,NCHX,KPLT,KCOUNT)
      CALL ARRANG (SRADA,STANA,R,I,J,NPT,1,NYA1,NYA2,NXA)
      CALL GENPT2(NYA1,NYA2,NXA,NXA,20.0,16.0,NPT,1,1,1.0,
```

```
     &0.0,1,0.0,XCOM11,XCOM12,YCOM11,YCOM12,YCOM21,YCOM22,
     &1.0,1.0,CHY12,NCHY12,CHY22,NCHY22,CHX,NCHX,KPLT,KCOUNT)
  10 CONTINUE
  30 CONTINUE
     WRITE(6,61)((AM(I,J),BM(I,J),RM(I,J),RMA(I,J),RM1(I,J)
    &,DIFF(I,J),DIFFA(I,J),ZM(I,J),J=1,NB),I=1,NA)
  61 FORMAT(5(3X,F10.5),3X,F5.2,2X,F5.2,2X,F5.2)
     DO 70 I=1,NA
     DO 80 J=1,NB
     WRITE(6,62) AM(I,J),BM(I,J),RM(I,J),ZM(I,J)
     WRITE(6,64) ET,ER,VT,NZ
  64 FORMAT(5X,'ET= ',F12.1,5X,'ER= ',F12.1,5X,'VT= ',F7.3,
    &5X,'NZ= ',   I2,//)
  62 FORMAT('1',5X,'A=',F10.5,5X,'B=',F10.5,5X,'MOMENT=',
    &F10.5,5X,'OVERLAP=',F10.5,//)
     DO 90 K=1,NPT
     WRITE(6,63)R(I,J,K),RRADS(I,J,K),RTANS(I,J,K),
    &STAN(I,J,K),U(I,J,K),
    &RRADSA(I,J,K),RTANSA(I,J,K),STANA(I,J,K),SRADA(I,J,K)
  63 FORMAT(2X,F10.5,2(F10.1,2X),2(E12.5,2X),2(F10.1,2X),
    &2(E12.5,2X))
  90 CONTINUE
  80 CONTINUE
  70 CONTINUE
     STOP
     END
//GO.SYSIN  DD  *
RADIAL STRESS
TANGENTIAL STRESS
RADIUS
RADIAL STRAIN
TANGENTIAL STRAIN
 13 17  6 13 17
  1  1 20  1  0
 5.2595     7.7398   1.0   0.2   -0.17279  0.300    788.
19434936.  1240065.
/*
```

Appendix I.

TRANSVERSE SENSITIVITY CALCULATIONS.

I.1 Radially thick S2-glass and E/XAS carbon composite rings.

Equations 4.2 and 4.3 of section 4.2.2 were utilized with strain readings generated as described in section 4.4.2 and repeated here:

$$\epsilon_r = \frac{1-\nu_o K}{1-K^2}(\epsilon_r' - K\epsilon_\theta') \tag{4.2}$$

$$\epsilon_\theta = \frac{1-\nu_o K}{1-K^2}(\epsilon_\theta' - K\epsilon_r') \tag{4.3}$$

The required inputs are tabulated in Table I.1

Table I.1: Inputs for Transverse Sensitivity Equations.

Ring Number	Transverse Sensitivity of Gauge (%)	Poisson's Ratio	Apparent Strains ($\times 10^{-6}$)	
S2-TK-8-35	-0.4	0.285	-206.21	226.40
XAS-TK-2-25	-0.4	0.285	-19.55	904.09

Substituting values for E/XAS carbon:

$$\epsilon_\theta = \frac{1-0.285(-0.004)}{1-(-0.004)^2}[-19.55\times10^{-6} - (-0.004)(904.09\times10^{-6})]$$

$$\epsilon_\theta = -15.95\times10^{-6}$$

$$\epsilon_r = \frac{1-0.285(-0.004)}{1-(-0.004)^2}[904.09\times10^{-6} - (-0.004)(-19.55\times10^{-6})]$$

$$\epsilon_r = 905.06\times10^{-6}$$

and for S2-glass:

$$\epsilon_\theta = \frac{1 - 0.285(-0.004)}{1 - (-0.004)^2}[-206.21 \times 10^{-6} - (-0.004)(226.40 \times 10^{-6})]$$

$$\epsilon_\theta = -205.54 \times 10^{-6}$$

$$\epsilon_r = \frac{1 - 0.285(-0.004)}{1 - (-0.004)^2}[226.40 \times 10^{-6} - (-0.004)(-206.21 \times 10^{-6})]$$

$$\epsilon_r = 225.84 \times 10^{-6}$$

I.2 S2-glass-E/XAS carbon biannular composite ring.

As mentioned in Section 5.3 the effect of transverse sensitivity was verified with the use of 0/90° rosette gauges mounted on a biannular ring. Figure I.1 shows the orientation of these gauges as applied to the ring.

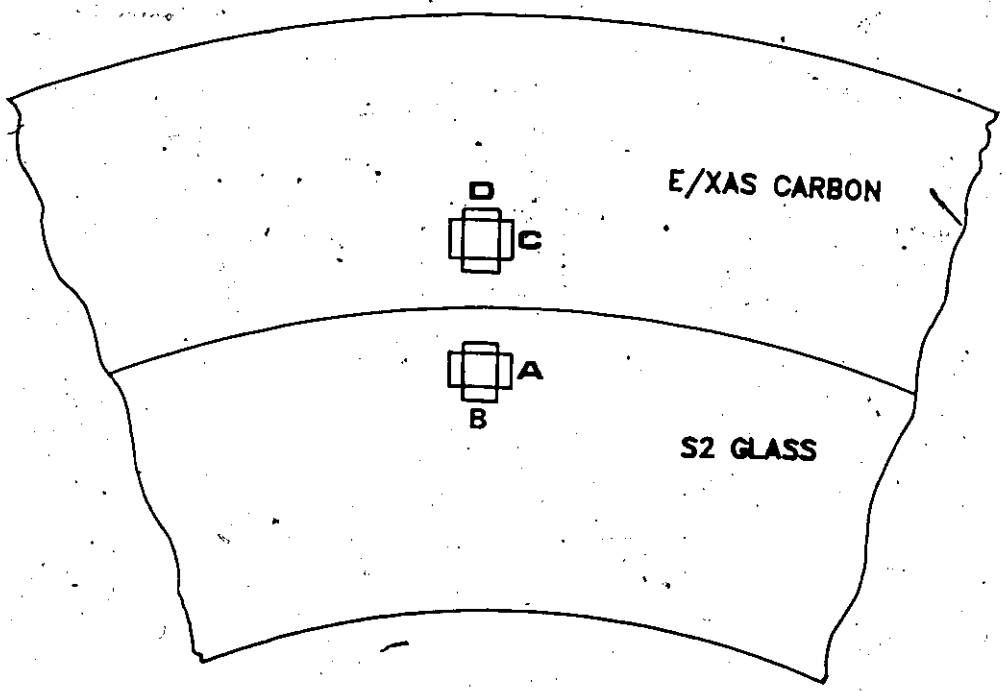

Figure I.1: Location and orientaion of rosette gauges.

Table I.2 presents the data obtained from the gauges when the ring was radially cut.

Table I.2: Strain Readings from Biannular Ring.

Gauge	Strain Reading ($\times 10^{-6}$)
A	216
B	661
C	-103
D	1139

As before this data was substituted into equations 4.2 and 4.3 resulting in S2-glass results:

$$\epsilon_\theta = \frac{1-0.285(-0.008)}{1-(-0.008)^2}[216\times10^{-6} - (-0.008)(661\times10^{-6})]$$
$$\epsilon_\theta = 222\times10^{-6}$$

$$\epsilon_r = \frac{1-0.285(-0.008)}{1-(-0.008)^2}[661\times10^{-6} - (-0.008)(216\times10^{-6})]$$
$$\epsilon_r = 664\times10^{-6}$$

with the E/XAS carbon given as,

$$\epsilon_\theta = \frac{1-0.285(-0.008)}{1-(-0.008)^2}[1139\times10^{-6} - (-0.008)(-103\times10^{-6})]$$
$$\epsilon_\theta = 1141\times10^{-6}$$

$$\epsilon_r = \frac{1-0.285(-0.008)}{1-(-0.008)^2}[-103\times10^{-6} - (-0.008)(1139\times10^{-6})]$$
$$\epsilon_r = -94\times10^{-6}$$